Simone Franziska Neuhold, BSc

Mechanism of the “self-reduction“ of Eu^{3+} in binary and ternary glasses

MASTER’S THESIS

to achieve the university degree of

Diplom-Ingenieurin

Master’s degree programme: Advanced Materials Science

submitted to

Graz University of Technology

Supervisor

Ao.Univ.-Prof. Dipl.-Ing. Dr.techn.

Karl Gatterer

Institute of Physical and Theoretical Chemistry

Graz, November 2015

AFFIDAVIT

I declare that I have authored this thesis independently, that I have not used other than the declared sources/resources, and that I have explicitly indicated all material which has been quoted either literally or by content from the sources used. The text document uploaded to TUGRAZonline is identical to the present master‘s thesis dissertation.

Date

Signature

EIDESSTATTLICHE ERKLÄRUNG

Ich erkläre an Eides statt, dass ich die vorliegende Arbeit selbstständig verfasst, andere als die angegebenen Quellen/Hilfsmittel nicht benutzt, und die den benutzten Quellen wörtlich und inhaltlich entnommenen Stellen als solche kenntlich gemacht habe. Das in TUGRAZonline hochgeladene Textdokument ist mit der vorliegenden Masterarbeit identisch.

Datum

Unterschrift

Acknowledgment

I want to thank,

Professor Gatterer for all the support, advices, motivation, enthusiasm, etc. and for the great working atmosphere.

Professor Arafa for sharing his many years of experience on glass making with me and for all the helpful input and thinking impulses.

Professor Mautner for the X-ray measurements.

Binder + Co for providing the LS55 and L950 instruments.

Especially my family and friends for making my life worth living.

Abstract

Rare-earth doped glasses are important materials in optoelectronic applications (lasers, LED's, etc.). In the frame of this master's thesis a number of Europium doped glasses have been prepared and characterized by spectroscopic methods. The glasses were from the binary sodium borate and the ternary sodium boroaluminate systems. While Europium normally enters solids in the form of Eu^{3+} ions, it is known that in such glasses Europium can also exist in the divalent Eu^{2+} state, even though the glasses are prepared under oxidizing conditions. This behaviour is called "self-reduction" and its mechanism for glass systems is not yet completely understood. The aim of the thesis is to clarify the mechanism that leads to this unusual property. This was done by investigating the influence of the preparation conditions (melting temperature, melting time, quenching method as well as post-quenching sample treatment) and the glass composition on the final products. The glasses were studied with spectroscopic methods (luminescence and absorption) since the optical properties of Eu^{3+} and Eu^{2+} ions are considerably different. It was found that the main influence on the "self-reduction" in these glasses originates in the composition and the corresponding structural changes that take place in the glass matrix.

Kurzfassung

Seltenerd-dotierte Gläser spielen eine wichtige Rolle für optoelektronische Anwendungen, wie zum Beispiel Laser, LEDs, u.v.m. Im Zuge dieser Diplomarbeit wurde eine Reihe von Europium dotierten Gläsern hergestellt und spektroskopisch untersucht. Die hergestellten Proben waren binäre Natriumborat- und ternäre Natrium-Boraluminat-Gläser. Obwohl Europium normalerweise als Eu^{3+} Ion in einen Festkörper eingebaut wird, ist bekannt, dass Europium in den oben erwähnten Gläsern auch als Eu^{2+} vorkommt, obwohl die Gläser unter oxidierender Atmosphäre hergestellt wurden. Dieses Verhalten wird als „Selbst-Reduktion“ bezeichnet und ist bei Gläsern noch nicht vollständig verstanden. Ziel dieser Arbeit war es, den Mechanismus für dieses ungewöhnliche Verhalten aufzuklären. Dafür wurden sowohl die Einflüsse der Präparationsbedingungen (Schmelztemperatur, Schmelzzeit, Abschreckmethode und Nachbehandlung der Proben) als auch die Einflüsse der Zusammensetzung der Endprodukte untersucht. Da die optischen Eigenschaften der Eu^{3+} und der Eu^{2+} Ionen signifikante Unterschiede aufweisen, wurden die Gläser spektroskopisch untersucht (Lumineszenz, Absorption). Es konnte herausgefunden werden, dass die Zusammensetzung der Gläser und die daraus resultierenden strukturellen Änderungen der Glasmatrix den größten Einfluss auf den Mechanismus der „Selbst-Reduktion“ haben.

Table of Contents

1 INTRODUCTION 8

2 GLASSES 10

2.1 General concepts 10

2.2 Binary alkali borate glasses 13

2.3 Ternary boroaluminate glasses 15

3 RARE EARTH IONS 17

3.1 Properties of rare earth ions 17

3.2 Russell-Saunders-Terms 18

3.3 Europium 20

3.3.1 Europium as a structural probe 22

3.3.2 Europium in glasses 25

3.3.2.1 Mode of incorporation 25

3.3.2.2 Inhomogeneous broadening 26

4 EXPERIMENTAL 29

4.1 Glass preparation 29

4.1.1 Influences of the preparation parameters 29

4.1.2 Influence of the Na_2O content in binary glass 32

4.1.3 Influence of the Al_2O_3 content in ternary glass 32

4.2 Spectroscopy 34

4.2.1 Luminescence spectroscopy 34

Spectrometer 34

Procedure 36

Measurements 38

4.2.2 Absorption 40

Spectrometer 40

Procedure 42

Measurements 42

4.2.3 X-ray Diffraction (XRD) analysis 43

5 RESULTS AND DISCUSSION 46

5.1 Influences of the preparation parameters 46

5.2 Influence of the Na_2O content in binary glass 52

5.3 Influences of the Al_2O_3 content in ternary glass 53

5.4 Europium as a structural probe in glass 58

5.4.1 Symmetry of surrounding 58

5.4.2 Nephelauxetic effect 59

5.5 Reabsorption mechanism 61

5.6 Discussion 67

5.6.1 Optical basicity 68

5.6.2 Glass structure 71

Binary glass 72

Ternary glass 73

5.7 "Self-reduction" mechanism 75

6 CONCLUSION AND OUTLOOK 79

7 REFERENCES 81

8 LIST OF FIGURES 86

9 LIST OF TABLES 93

10 APPENDIX 94

1 Introduction

Rare-earth (RE) elements (i.e., elements with atomic numbers 57 to 71) have found numerous applications in diverse optoelectronic devices such as lasers, scintillators, waveguides, displays, amplifiers for optical fibres, LEDs (light-emitting diodes). [1-12] Their usefulness lies in their unique optical properties. These are essentially determined by the existence of an unfilled 4f-electron shell, which is shielded from external fields by filled outer lying electron shells. The RE elements enter solid materials as positively charged cations. The host materials containing one type of RE ion or a combination of several of them may be single crystals (e.g., Nd:YAG a common laser material), polycrystalline materials (e.g., Eu:Y_2O_3 an efficient red phosphor) or amorphous materials (e.g., the Eu-doped glasses presented in this thesis). [13,14] Among the host materials for RE ions glasses are the most versatile, because they can be produced in a wide compositional range. It was found that gradual changes of the glass composition lead to changes of physical properties of the doped materials. [15] Hence a "chemical tailoring" of materials to meet the needs of a desired application is best achieved with glasses. Therefore, it is no surprise that for all the applications mentioned above glasses are either used already or are in the list of possible candidates. The large number of potential applications, as well as the chemical versatility of RE doped glasses, makes these materials attractive for basic research investigations as well.

The predominant oxidation state of RE ions in solids is 3+. RE^{2+} and RE^{4+} species are unstable. Notable exceptions are Eu^{2+} and Ce^{4+} which have found applications as phosphors because of their broad emission bands. [13,14] In the RE^{3+} species the electronic transitions giving rise to emission bands in the visible range are all intra-configurational $4f^n \rightarrow 4f^n$ transitions (n is the number of electrons in the 4f-shell). This means that they take place between discrete energy levels within the unfilled 4f-shell. Due to the shielding effect mentioned above the emission consists of relatively narrow bands. In Ce^{4+} and Eu^{2+}, however, the transitions in the visible range are inter-configurational $4f^{n-1}5d^1 \rightarrow 4f^n$ transitions. Here the involvement of outer lying d-orbitals leads to a considerable broadening of the observed transitions bands. [16]

In the preparation of RE containing glasses the source for the RE ions is normally the corresponding RE oxide. In the case of Cerium the oxides CeO_2 (containing Ce^{4+}) and Ce_2O_3 (containing Ce^{3+}) as well as Ce_3O_4 (containing Ce^{3+} and Ce^{4+} at the same time) are available. In contrast, the only commercially available oxide of Europium is the Eu^{3+} containing Eu_2O_3. Hence, in order to obtain Eu^{2+} in glasses reducing conditions have to be established during the preparation. This is usually achieved by melting the constituents of the glass in an oven where the normal atmosphere is replaced by a reducing atmosphere (e.g., Nitrogen/Hydrogen gas mixtures). However, some research groups have discovered that in certain materials, including glasses, Eu^{3+} is reduced to Eu^{2+} even under atmospheric preparation conditions. This phenomenon is called "self-reduction" and was observed in crystals and in glasses which contain borate. [1-12] The detailed mechanism of the "self-reduction" of Eu^{3+} is still not clarified completely.

The "self-reduction" in mostly ionic bound crystalline materials (e.g., $Sr_4Al_{14}O_{25}$) is somehow driven by the need of charge compensation, because divalent host ions (e.g., Sr^{2+}) are replaced by trivalent RE^{3+} ions. [7,8,11,12] In such cases four general rules have been established, which have to be fulfilled for the reduction of RE ions in solids to take place under atmospheric conditions at high temperatures [8]:

I) no oxidizing ions are present in the host compound
II) a trivalent RE^{3+} ion (dopant) replaces a divalent cation in the host
III) the substituted dopant cation and the host cation have similar radii
IV) the host material contains tetrahedral negatively charged groups (e.g., BO_4^-, SO_4^-)

However, the situation for mostly covalently bound amorphous materials like glasses is not so clear and many different explanations have been proposed in the literature. [1-6]

The aim of this master thesis is to clarify the mechanism of the "self-reduction" of Europium in binary sodium borate glasses and in ternary sodium boroaluminate glasses (NABAL-glasses). The influence of the preparation conditions (melting temperature, melting time, quenching method as well as post-quenching sample treatment) and the composition on the self-reduction is investigated by analysing the final glasses with luminescence and absorption spectroscopy.

2 Glasses

Glasses are formed from super cooled liquids without crystallization. This leads to an amorphous system which has short-range order but no long-range order in contrast to crystalline solids. Another difference is the melting behaviour. Heating glasses leads to a continuous softening of the glass and not to a discrete melting temperature as for crystals. Oxides which possess the ability to form glasses are SiO_2, B_2O_3, GeO_2, P_2O_5 and As_2O_5. Additionally glasses can be formed by mixing two (binary glass) or three (ternary glass) components. The composition of ternary glasses is given by the following notation: $xNa_2O - yB_2O_3 - zAl_2O_3 : Eu$. Here the coefficients indicate the amounts in mol% and Eu indicates the doping material Eu_2O_3. [17]

2.1 General concepts

The process of glass formation and the resulting structure have been described by several theories, based on different approaches. Sun's single bond strength criterion assumes that the glass formation is a consequence of the inability of a system to rearrange the bonds during the transition from the liquid phase to the crystalline phase. The bond strength is a direct measure for the glass forming ability of an oxide. Dietzel's field strength criterion on the other hand proposes that the amount of the field strength of a cation and its size are the driving forces for a disordered arrangement. The field strength of a cation depends on the valency of the cation and the ionic radii of the cation and the oxide and is high for network forming cations and low for modifiers. [15]

In this thesis, however, only Zachariasen's "random network theory" will be explained further, as it had the most prominent influence on the ideas of glass structure and formation. Zachariasen defined a glass as a "substance (that) can form extended three-dimensional networks lacking periodicity with an energy content comparable with that of the corresponding crystal network." [18] His argumentation was based on the fact that the mechanical properties of crystals and the corresponding glasses are similar and hence the atomic forces must be of the same order. He proposed further that a glass and a crystalline system of comparable composition are both composed of similar structural units but with the main difference that the glass is less ordered (short-range order of small structural units

linked together randomly) than the crystal (long-range periodicity). The disorder in the glass is merely due to the changes in bond angles and bond lengths between the cation in the centre of a structural unit and the oxide ions surrounding it. This leads to distorted polyhedra forming a "random network". As a consequence the glass has a slightly higher internal energy than the crystal but not high enough to serve as the driving force towards crystallization. The differences and the similarities between the glass structure and the crystal structure are shown below in Figure 1, which represents a system composed of AO_3 units (A is the cation). [15]

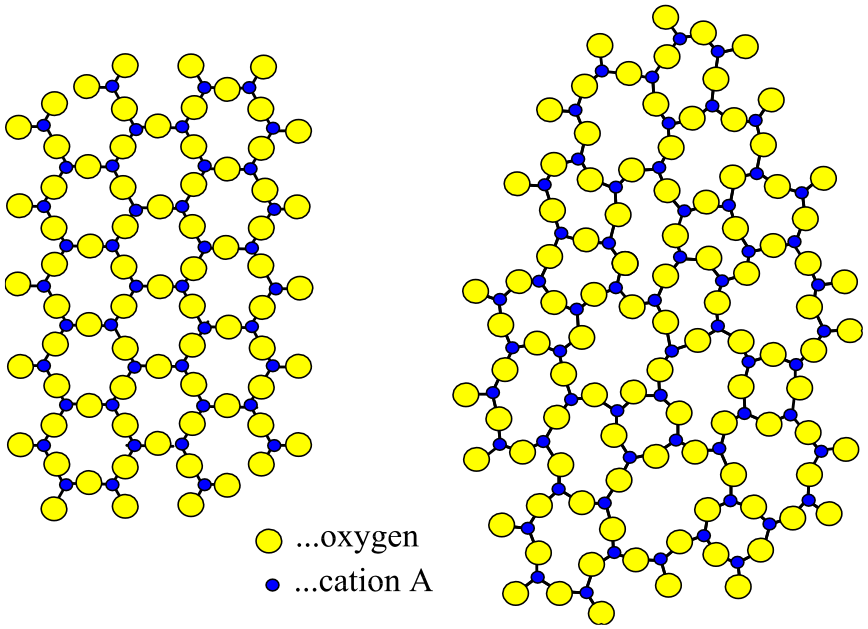

Figure 1: Differences and similarities between crystal structure (left) and glass structure (right). [19]

The following four rules for glass formation for a compound with the composition A_mO_n were established by Zachariasen:

- an oxygen atom O is linked to no more than two A-atoms
- an atom A is coordinated by a small number of oxygen atom (e.g.: 3 or 4)
- the coordination polyhedra share only corners (not edges or faces)
- at least three corners are shared

If all of these four rules are fulfilled glass formation is the favoured process. [15]

For glass systems with more than one component the concept of *network formers* and *network modifiers* was introduced. As the names indicate, the network formers build up the random network of the glass by forming bridging oxygens (BO) between the cations, while the network modifiers modify the network in three possible ways (shown in Figure 2). [19]

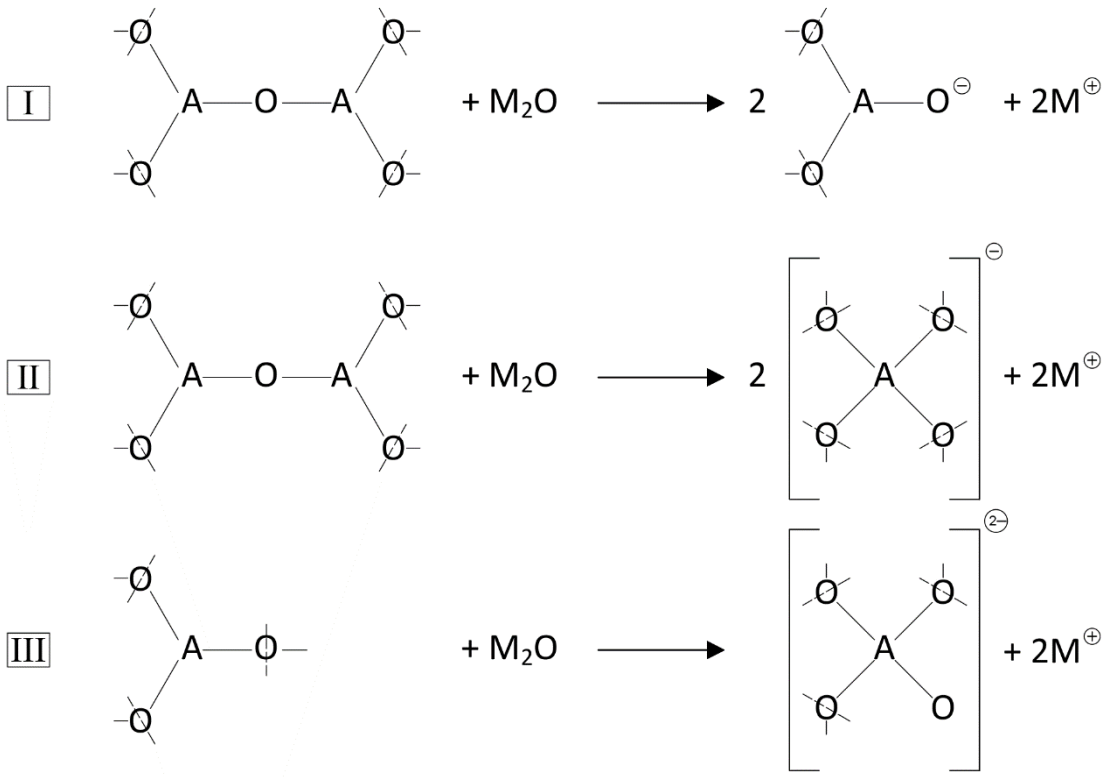

Figure 2: Possible actions of the modifier (M_2O) in a glass network. Adopted from [19].

The first path shows the conversion of one BO into two non-bridging oxygens (NBO). For convenience BOs are written as Ø and the NBOs are written as O in this thesis. The second path shows the increase of the oxygen coordination of the cation A. The main difference between these two actions is that the formation of NBOs leads to a less rigid glass structure while the increase of the cation coordination leads to a more rigid structure. The third possibility is a combination of the other two. In all cases the introduced negative charges are compensated by the modifier cations. [19]

Apart from network formers (e.g.: SiO_2, B_2O_3, GeO_2) and network modifiers (e.g.: Na_2O, K_2O) there are also so called intermediates (e.g.: Al_2O_3, PbO) which can act as both, formers or modifiers, depending on the glass composition and the nature of their partners. [19]

2.2 Binary alkali borate glasses

Binary alkali borate glasses constituted attractive materials for structural investigations for two reasons. First the occurrence of all three modifications of the glass system by addition of a modifier (see Figure 2) and second the non-monotonic variation of most physical properties with a monotonic variation of the composition, which is known as “boron anomaly” in glasses. [15,20]

Although there were a lot of assumptions and theories which tried to explain these anomalies with the compositional change of the ratio of BO_3-units and BO_4-units, the first structural elucidation was achieved by the NMR work of Bray and co-workers. [21] With NMR - using the ^{11}B isostope as the structural probe - it has been possible to determine experimentally the fraction of BO_4-units in the glass in dependence of the alkali content. The trend showed an increase of the higher coordination with increasing modifier up to approximately 45 mol% and a decrease of the formation of BO_4-units until an alkali content of ~ 70 mol% has reached. [20,21]

Other important contributions to elucidate the structure of binary glasses came from Krogh-Moe who related IR and Raman spectra of crystalline materials to those of binary glasses with comparable compositions. One of the main results of these studies was, that Krogh-Moe proposed that binary glasses consist of well-defined and stable substructures composed of BO_3- and BO_4-subunits, so called polyborate groupings (which are also formed in crystalline materials of the same composition) and not just of randomly attached BO_3- and BO_4-units linked via corners. Some of these polyborate groupings and their subunits are shown in Figure 3 and Figure 4. [22]

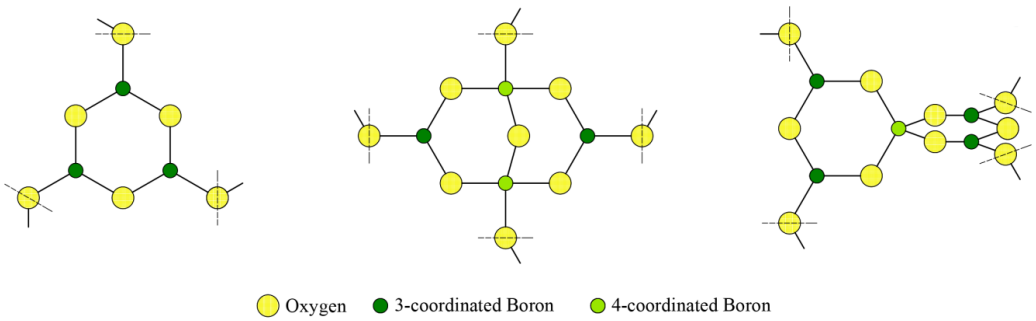

Figure 3: Schematical drawing of polyborate groupings from left to right: boroxol ring, diborate and pentaborate. Adapted from [20,22].

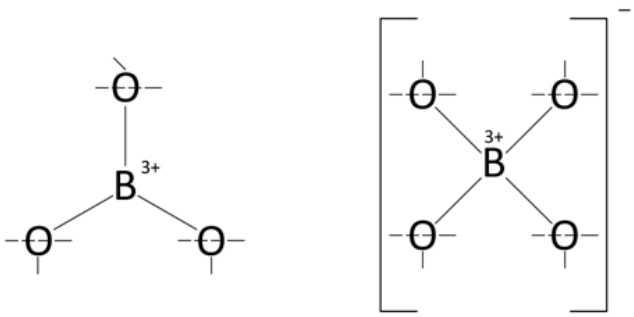

Figure 4: Polyborate subunits BO_3 (planar) and BO_4 (tetrahedral).

The existence of these polyborate groupings which were confirmed by the NMR data for the fraction of four-coordinated boron atoms in the glasses finally yielded the Krogh-Moe structural model for binary alkaliborate glasses shown in Figure 5. [22]

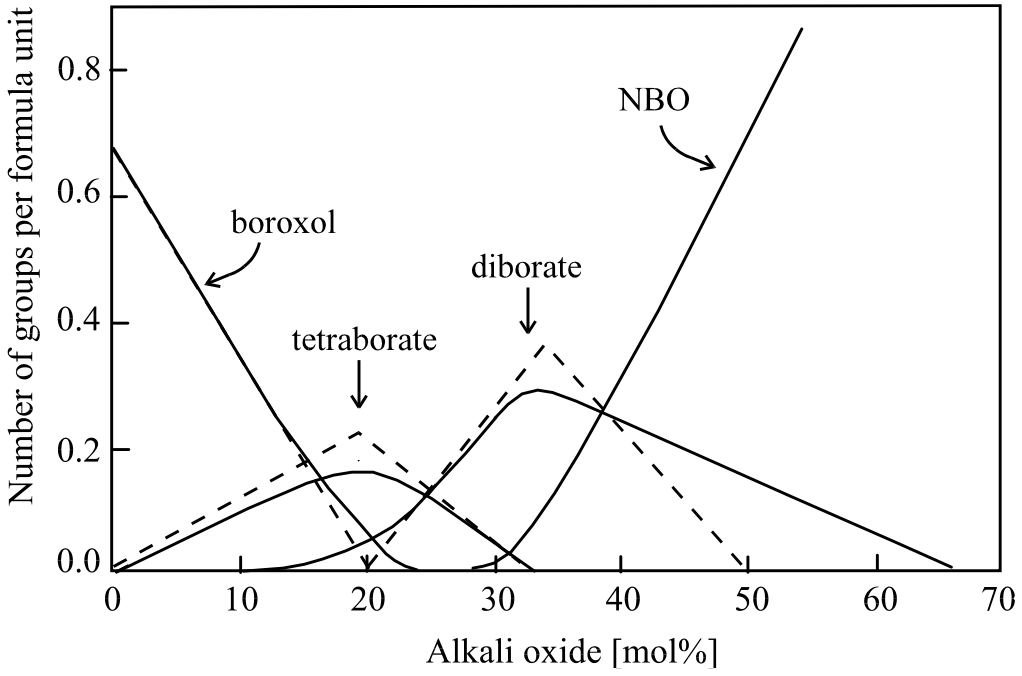

Figure 5: Predicted Krogh-Moe model (dashed line) and experimental data (solid line) for the structural dependence of the binary glasses on the alkali amount in mol%. [22,23]

This model until today serves as a guide for experimental data, although some of the details of the model are still arguable.

The main conclusions of most of the investigations on binary glass systems are:

Without modifier, pure borate glass consists of boroxol rings, containing only $B\emptyset_3$-units.

An increasing addition of modifier first results in the formation of polyborate groupings with more and more $B\emptyset_4$-units. Where pentaborate is the grouping with the lowest amount of $B\emptyset_4$-units and diborate is one of the groupings with the highest amount of $B\emptyset_4$-units. If the modifier concentration reaches a value of ~30 mol% the formation of NBOs starts in the binary glass and the number of $B\emptyset_4$-units decreases. It has to be noted that NBOs can only be formed in borate systems by BO_3-units (notation $B\emptyset_2O^-$) and not by $B\emptyset_4$-units. [1-3,20,21,24]

2.3 Ternary boroaluminate glasses

Ternary boroaluminate glasses have a few advantages compared to binary alkali borate glasses. The addition of Al_2O_3 increases the mechanical stability of the glasses and it increases also the stability of the glasses with respect to atmospheric conditions (not hygroscopic in comparison to the binary glasses), to variations in temperature (minimization of the coefficient of expansion) and additionally it minimizes the devitrification tendency of the glass. The structural investigation of ternary glass with Al_2O_3 is particularly interesting as Al_2O_3 is an intermediate which can serve as network former and as network modifier. [17]

Gresch and Müller-Warmuth [25] investigated Na_2O-B_2O_3-Al_2O_3 (NABAL) glasses via NMR studies to elucidate the structural dependence on the composition. The studies indicate that the alkaline oxide acts as a modifier with both, the boron oxide and the aluminium oxide to form BO_4 and AlO_4 tetrahedra. The results indicate furthermore, that there is a trend in the development of the two competing processes. Since the amount of the fraction of four-coordinated boron atom decreases with increasing Al_2O_3 content it is assumed, that the formation of AlO_4 tetrahedra is favoured in this glass system. This means that with higher Al_2O_3 content polyborate groupings with a higher amount of BO_3–units are the predominant structural subunits in the glass. It is also stated that there is an avoidance of BO_4 – AlO_4 linkages in the glass structures. [24]

Doweidar and co-workers [24] proposed that there are structural changes around 15 mol% Al_2O_3 in the glasses due to the fact that there are significant changes in some properties of NABAL glasses at this composition. It is assumed that these structural changes are

correlated to the formation of so called triclusters (composed of three tetrahedral BO_4- and/or AlO_4-units having one oxygen atom in common). It is also stated that not only AlO_4- but also AlO_6-units could be present in the glasses. [24]

3 Rare earth ions

The metal ions of the Lanthanide series which include the 15 elements from Lanthanum to Lutetium are called “rare earth ions” and have the electron configuration $[Xe]4f^n5d^25p^6$. Along the series the 4f-shell gets filled successively, while there is an energetical preference towards the configurations of the half-filled ($4f^7$)- and completely-filled ($4f^{14}$)- shells. RE ions are always found in combination with each other in minerals such as monazite ($MePO_4$; Me = La, Ce, Nd, Sm), bastnaesite ($MeCO_3F$; Me = Ce, La, Nd, Y) or fluorite ($MeCaF_2$; Me = Eu, Sm). There are many applications where RE ions are used such as fabrication of coloured glass (e.g.: Nd), for permanent magnets (e.g.: Sm), as phosphors in optical devices such as LEDs, as light amplifiers in glass fibres (e.g.: Er), as lasers, etc. [13,14]

3.1 Properties of rare earth ions

All RE ions exist predominately in the oxidation state 3+. The oxidation states 2+ and 4+ are stable only for some Lanthanides (e.g. Eu^{2+}, Yb^{2+}, Ce^{4+}, Nd^{4+}). Due to the high number of unpaired electrons most of the RE ions are paramagnetic, which means that they possess permanent magnetic moments and a magnetic susceptibility: $\chi > O$. The addition of electrons in the inner f-shell of the Lanthanides causes a stepwise decrease of the ion radius, called Lanthanide-contraction. This leads to an almost continuous change of the properties of the ions with increasing filling. For example the basicity (i.e. electron donating power) of the ions decreases as the atomic number increases. For some properties, however, there are exceptions from the almost linear behaviour. Examples are the ions Eu^{3+} and Yb^{3+} which show maxima of their atomic radii and minima of their densities and melting temperatures. [13]

The fact that an inner f-shell is filled rather than an outer d-shell is one of the most important differences to the d-elements, as their optical behaviour changes significantly, which is what makes RE ions so suitable for optical devices. The reasons for these differences are discussed in section 3.3.

3.2 Russell-Saunders-Terms

To describe the energy levels of atoms or ions with more than one electron, one uses the Russell-Saunders term symbols which are defined by the quantum numbers S, L and J and written as $^{2S+1}L_J$, with 2S+1 as the spin multiplicity. [26]

The quantum number S is derived from the coupling of the *spins* $\vec{s}$ of all individual electrons in an atom/ion to the *total spin* $\vec{S}$. The coupling leads to a z-component of the total spin M_S which is the sum of the z-components of the electron spins m_s and has the values:

$$M_S = \Sigma\, m_s = S, S\text{-}1, S\text{-}2, \ldots, -S.$$

Likewise, the quantum number L is derived from the coupling of the *orbital angular momenta* $\vec{l}$ of all single electrons in an atom/ion to the *total orbital angular momentum* $\vec{L}$ with:

$$M_L = \Sigma\, m_l = L, L\text{-}1, L\text{-}2, \ldots, -L.$$

The letter code used for the quantum number L is analogous to the notation for the single electrons with:

S (L = 0) P (L = 1) D (L = 2) F (L = 3) G (L = 4) H (L = 5)

The *total angular momentum* with the quantum number J is derived from the coupling of the spin and orbit angular momenta and is given by:

$$J = L + S, L + S\text{ -}1, L + S\text{ -}2, \ldots, |L - S|$$

As a consequence of this spin-orbit coupling, each Russell-Saunders term ^{2S+1}L is split into a corresponding number of $^{2S+1}L_J$ "multiplets". In a free ion (i.e. without external fields) each multiplet is (2J+1)-fold degenerate. [26]

The ground state (according to Hund's rules) has to have the maximum spin multiplicity (2S+1). If there are states with the same multiplicity the state with the highest L value is lowest in energy. And in the case of spin-orbit coupling it is then the largest value of J (for more than half-filled shells) or the smallest value of J (for less than half-filled shells) that corresponds to the ground state. [14,26]

It is easy to identify the ground state multiplet for each configuration of f-electrons by using a graphical ("orbital graph" [14]) which is shown for Eu^{3+} ($4f^6$) in Figure 6.

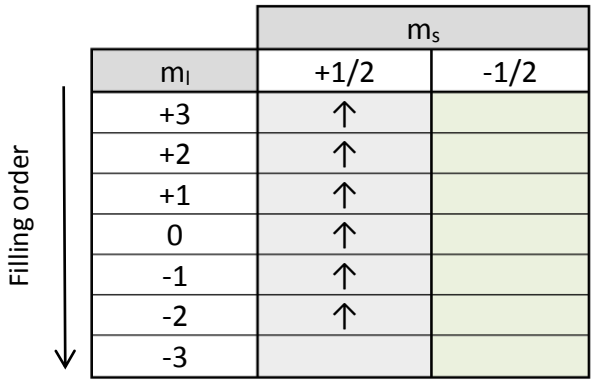

Figure 6: Orbital graph of the $4f^6$ configuration of Eu^{3+}.

In this graph every row represents an orbital consisting of two boxes, to allow for the presence of two electrons with opposite spin. In accordance to Hund's rules the corresponding number of electrons is filled into the boxes starting in the left column from the top. The identification of the ground state for Eu^{3+} is shown below.

The f-shell of Eu^{3+} has an l-value of 3 and therefore m_l values of +3, +2, +1, 0, -1, - 2, -3. Filling of the boxes with 6 electrons leads to a maximum value for M_S and the quantum number S of:

$$M_{S,max} = S = 6 * ½ = 6/2 = 3 \quad \text{and a spin multiplicity of : } 2S+1 = \underline{\mathbf{7}}$$

Summation of all occupied boxes yields the maximum value for M_L and the quantum number L:

$$M_{L,max} = L = 3 + 2 + (-2) + 1 + (-1) + 0 = 3 \quad \text{and a the state: } L = 3 : \underline{\mathbf{F}}$$

Summation and subtraction of the quantum numbers L and S yields J = L +S = 6 and J = |L -S| = **0**. And as for the less than half-filled shell the quantum number J has to be lowest the Russell-Saunders term for the ground state multiplet of the Eu^{3+} ion is $^7\mathbf{F_0}$. This ground state has a J-value of zero and its degeneracy (2J+1) is 1. Therefore it cannot be split any further by external fields (e.g., crystal fields).

3.3 Europium

As mentioned above Europium behaves differently than the other Lanthanides in some respect. For this thesis the occurrence of the trivalent and the divalent Europium ions was of the most importance, since the two ions show totally different spectroscopic behaviour when they are incorporated in a material [16]

- the Eu^{2+} ion shows a blue/violet emission and the Eu^{3+} ion shows a red/orange emission in the investigated glasses (in other materials the Eu^{2+} emission can be in the green and even in the red part of the visible spectral range (see Figure 8))
- Eu^{2+} shows broad emission/absorption bands while Eu^{3+} shows narrow lines (in glasses however they are inhomogeneously broadened as explained below)
- the number of peaks is higher for Eu^{3+} than for Eu^{2+}
- the Eu^{3+} emission/absorption spectrum resembles almost the spectrum of the free ion
- the emission of the excited Eu^{2+} ion decays faster than that for the Eu^{3+} ion.

Figure 7 shows the typical emission spectra for both ions in glasses.

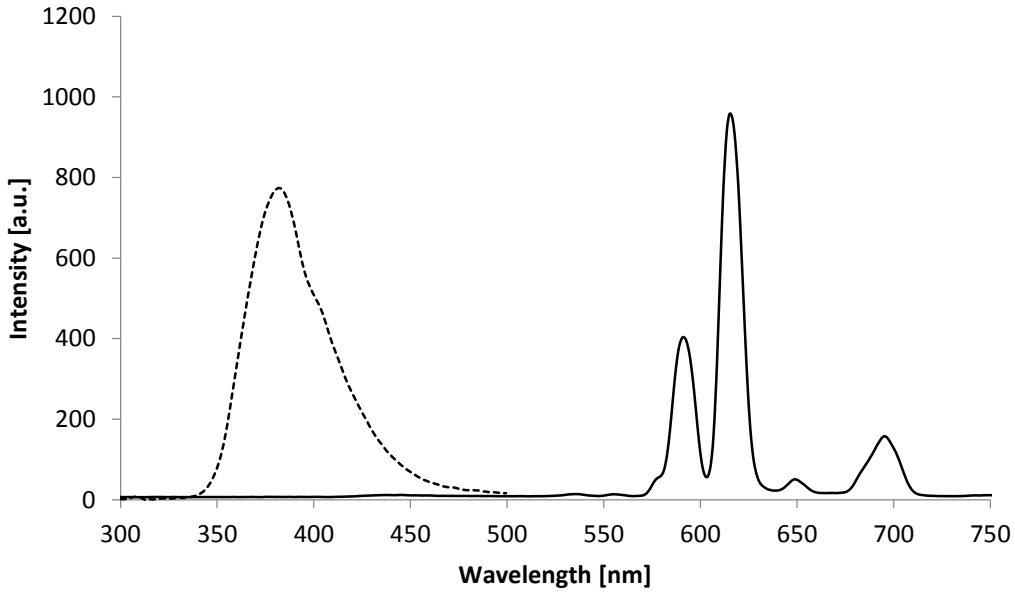

Figure 7: Emission spectra of Eu^{2+} (dashed line) and of Eu^{3+} (solid line). The spectra were recorded after excitation with 396 nm and have been arbitrarily picked from the produced glass samples.

The reason for the different shapes and numbers of the peaks is that different energy levels are involved in the transitions. While the Eu^{3+} emission is a $4f^n \rightarrow 4f^n$ transition, the Eu^{2+} emission is an interconfigurational transition $4f^{n-1}5d^1 \rightarrow 4f^n$ which leads to completely different optical behaviour. The d-shell is an outer shell and is therefore sensitive to the surrounding. The crystal field of the ligands causes a high splitting of the 5d-energy levels which can be seen below in Figure 8. The 4f-shell, in contrast, is an inner shell, shielded by the filled outer shells 5s and 5p and hence it is not sensitive to the surrounding and shows little crystal field splitting. This leads to broad bands for the Eu^{2+} ion emission/absorption and narrow bands for the Eu^{3+} ion emission/absorption in the spectrum. [16]

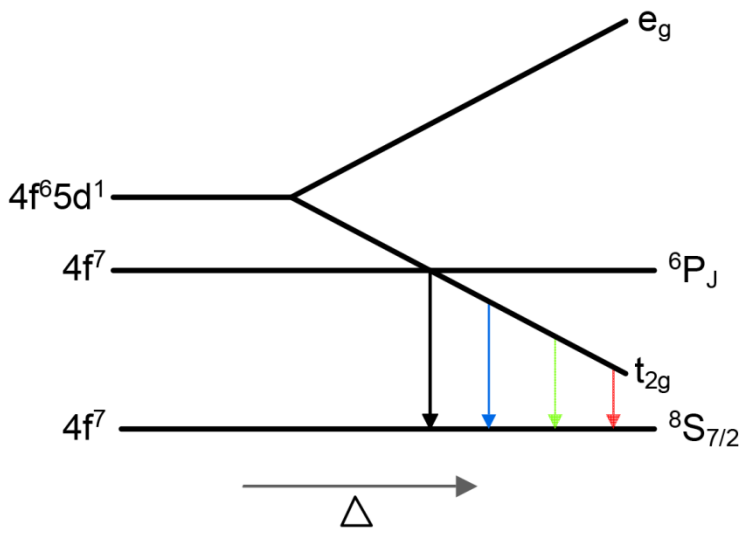

Figure 8: Splitting of the 5d-energy levels of the Eu^{2+} ion with increasing crystal field strength Δ and its according emission (from left to right: UV, blue, green, red), adapted from [27].

A second important difference between the optical properties of Eu^{3+} and Eu^{2+} are the different decay times for the emission. As the transition of the excited state in Eu^{2+} to the ground state is parity allowed the excited state has a much shorter lifetime. In contrast the Eu^{3+} transition from the excited state to the ground state is parity forbidden and the excited state has a longer lifetime. [28]

Some important spectroscopic differences for the two ions are listed in Table 1.

Table 1: Comparison of the two Europium ions with respect to their electron configuration, transition and ground state.

	Eu^{3+}	Eu^{2+}
electron configuration	$[Xe]4f^6$	$[Xe]4f^7$
transition (emission)	$4f^6 \rightarrow 4f^6$	$4f^65d^1 \rightarrow 4f^7$
ground state	$^7F_0$	$^8S_{7/2}$

3.3.1 Europium as a structural probe

The optical investigations on trivalent RE ions can also be used to clarify the surrounding of the RE ions in different materials. For that it is necessary to be able to assign the different peaks in the spectra to the corresponding transitions.

As mentioned above the valence electrons of the trivalent RE ions are shielded by the electrons of the filled outer 5s and 5p shell and are therefore little affected by the crystal field. And as the energy levels of the RE^{3+} ions are very similar to the energy levels of the free ion, the optical spectra of RE^{3+} ions incorporated into different solids consist of band always found close to their free-ion position. This makes it possible to assign all transitions in an optical spectrum by comparing with the Dieke diagram (Figure 9), which shows the energy of the $^{2S+1}L_J$ multiplets for the trivalent RE ions in the crystal $LaCl_3$. [16]

Two transitions of Eu^{3+} are particularly used as structural probes, first the so called hypersensitive transitions and second the $^7F_0 \rightarrow {}^5D_0$ transition as a measure for the so called nephelauxetic effect.

The phenomenon of **hypersensitive transitions** has been investigated by Judd and Jørgensen [30] and shows a significant change of the intensity of the $^7F_0 \rightarrow {}^5D_2$ peak in absorption spectra and the $^5D_0 \rightarrow {}^7F_2$ peak in emission spectra of the Eu^{3+} ion depending on the properties of the surrounding ligands (such as symmetry of the environment, polarizability of the ligands, crystal field strength, …). [31] One significant property of the hypersensitive peak is that it vanishes completely when the ion is located at an inversion centre and that it has a high intensity when little changes from the inversion centre occur. [29]

The **nephelauxetic effect** is generally speaking a measure for the covalent character of the ion-ligand interaction in a material. In optical spectra the nephelauxetic effect leads to a shift of transitions towards lower energies, where a high shift means a high nephelauxetic effect. An explanation has been given by Jørgensen [32] who states that in Lanthanides an expansion of the partly filled f-shell towards the ligands takes place and therefore the ion – ligand interaction has a higher covalent character. To avoid the influences of crystal field splitting effects, singlet to singlet transitions are used to show the nephelauxetic effect. In this thesis the position of the $^7F_0 \rightarrow {}^5D_0$ transition in the absorbance spectra of Eu^{3+} has been used (section 5.4.2) to investigate the nephelauxetic effect in the glasses. [29,33]

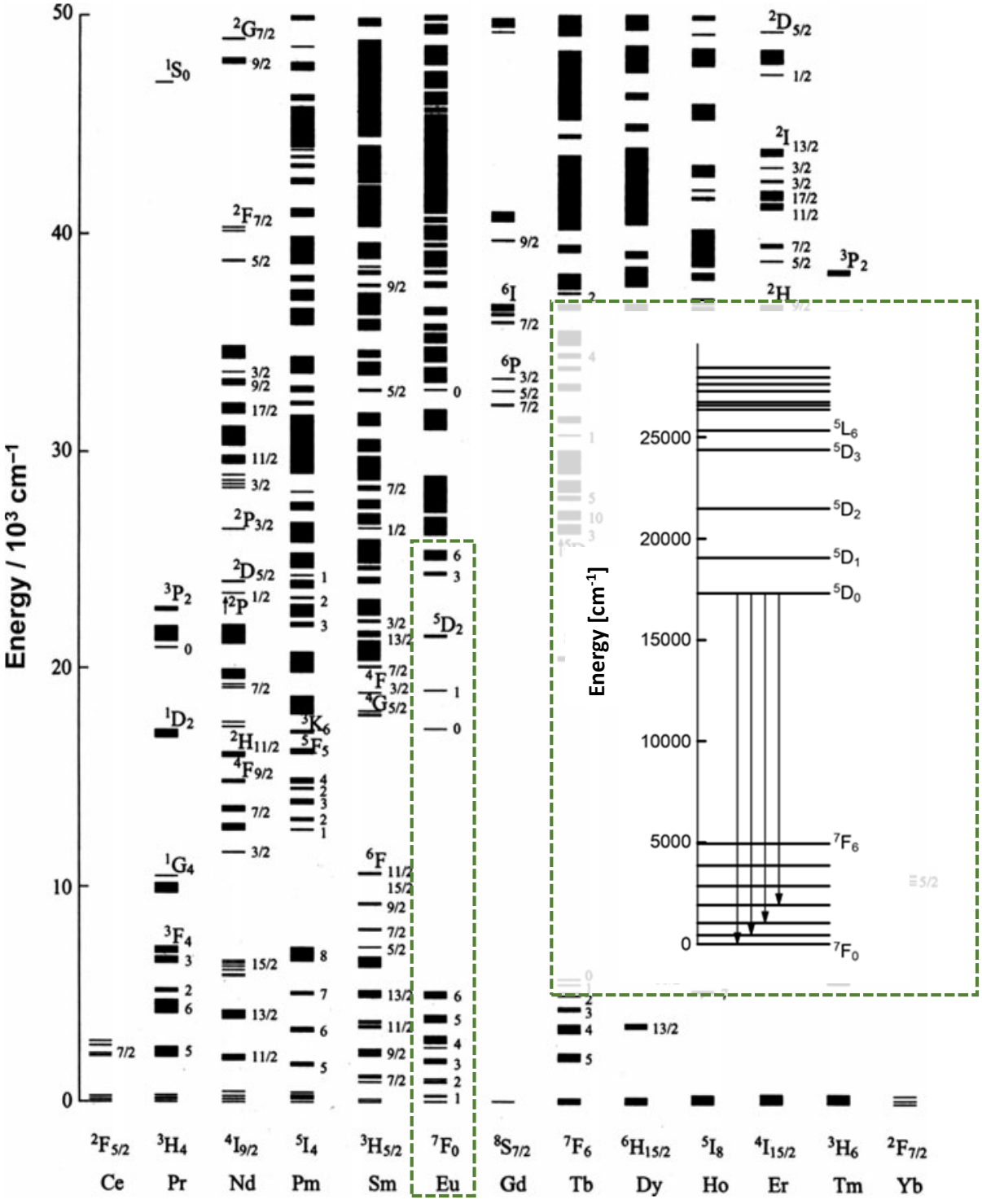

Figure 9: Dieke diagram [26] with magnification of the Eu^{3+} ion and some important emission transitions, adapted from [29].

3.3.2 Europium in glasses

3.3.2.1 Mode of incorporation

Four possible modes (see Figure 10) for the incorporation of RE ions into glasses have been discussed in the literature. These are, as molecular complexes, as quasi-molecular complexes, as network modifiers or as network formers. [29]

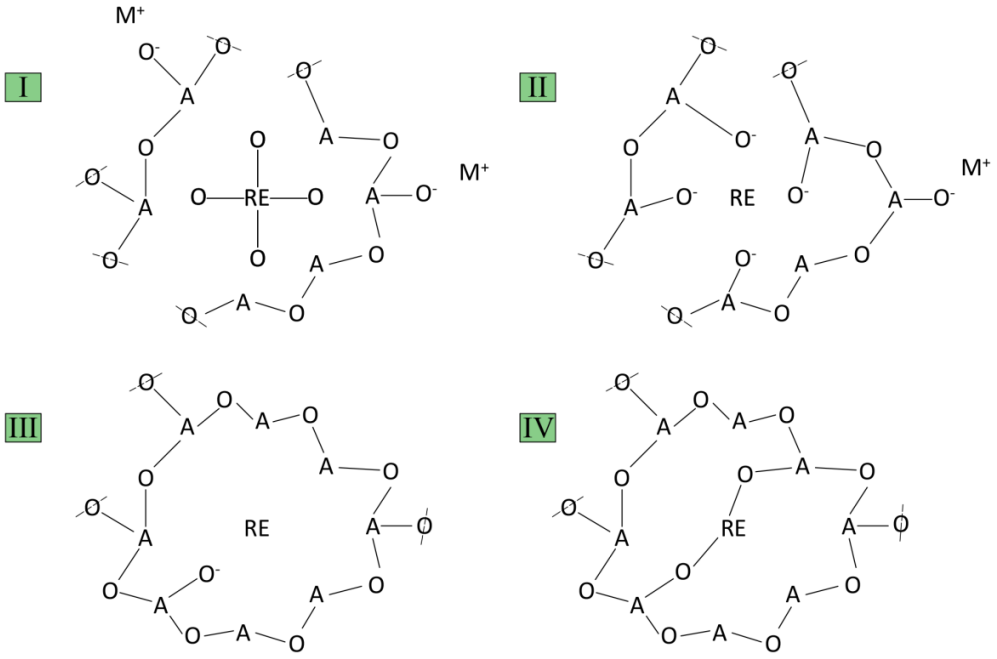

Figure 10: Schematical drawing of the different possible incorporations of RE ions into a glass network. I) molecular complex, II) quasi-molecular complex, III) network modifier and IV) network former. Adopted from [29,34].

The last two options can be easily refuted. On the one hand it is known from literature that it is impossible to include Eu_2O_3 into pure silica glass in the absence of a modifier which loosens the random network. [29,34] Additionally it was not possible to produce a homogeneous glass only containing B_2O_3 and Eu_2O_3 in the frame of this master's thesis, probably for the same reason. On the other hand it is known that RE oxides are glass formers only when they are present in considerably higher concentrations than the ones used for doping the glasses in this work. [29,34]

The idea of a molecular complex is, that the RE ion is not part of the random network but transfers its own oxide environment into the voids of the resulting glass. Besides the fact that the optical spectra of the glasses would be almost identical with the ones of crystalline Eu_2O_3 also investigations of doped borate glasses in this thesis (see section 4.2.3) have shown that the formation of molecular complexes can be excluded.

This leads to the assumption that Eu_2O_3 incorporates as quasi-molecular complexes, where the Europium ions are surrounded by NBOs. In fact, optical spectra in [29] indicate that for rare-earth concentrations in the 1 mol% range quasi-molecular complexes are the predominant species.

3.3.2.2 Inhomogeneous broadening

Since glasses do not have long-range periodicity as crystals, the surrounding of incorporated ions in glasses changes slightly from one ion to another and therefore every ion experiences a different crystal field which influences the crystal field splitting differently. This leads to an overlap of states for the different sites which cannot be resolved separately and hence to an inhomogeneous broadening of the peaks. This inhomogeneous broadening follows a Gaussian-profile additional to the homogeneous broadening (Lorentz-profile) dependent on the lifetime of the excited state. The combination of both broadenings leads to a Voigt - profile for each peak. The inhomogeneous broadening is measured by the FWHM (full width at half maximum) of a peak and is generally about 1 - 10 cm^{-1} in crystals and about 100 – 500 cm^{-1} in glasses. The effect of the inhomogeneous broadening is evident by comparing Figure 11 and Figure 12. [14]

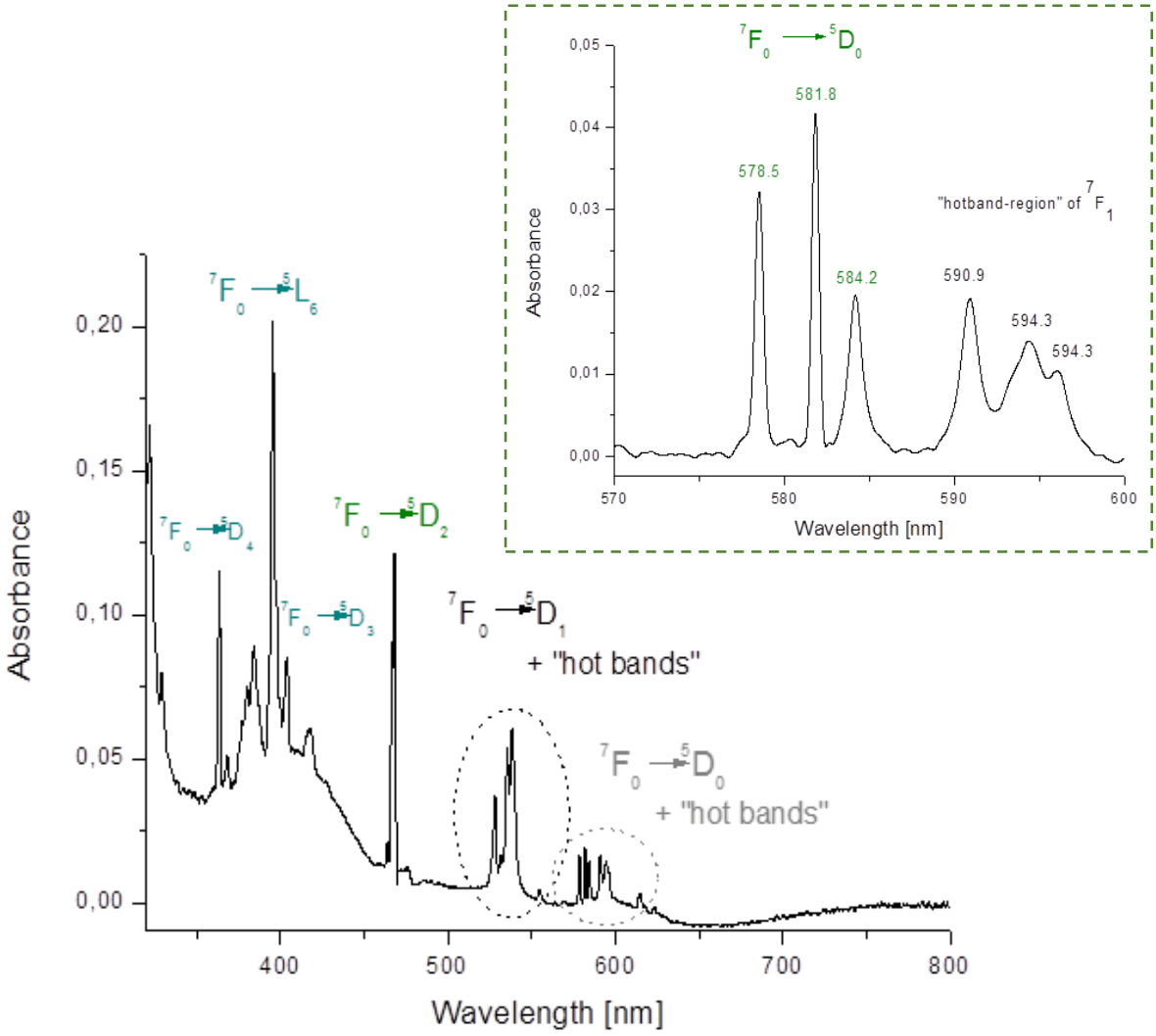

Figure 11: Absorbance spectrum of crystalline Eu_2O_3 with magnification of the $^7F_0 \rightarrow {}^5D_0$ transition.

As explained in section 3.3.1 the $^7F_0 \rightarrow {}^5D_0$ transition does not split in the presence of a crystal field. Nevertheless in the magnification of the absorbance spectrum in Figure 11 one can see three peaks for the $^7F_0 \rightarrow {}^5D_0$ transition. This can be explained by the fact that the Europium ions can incorporate at different sites in the crystal structure. This leads to a different symmetric surrounding of the ions and hence a different influence on the degeneracy of the energy levels and therefore to different transition energies. [35]

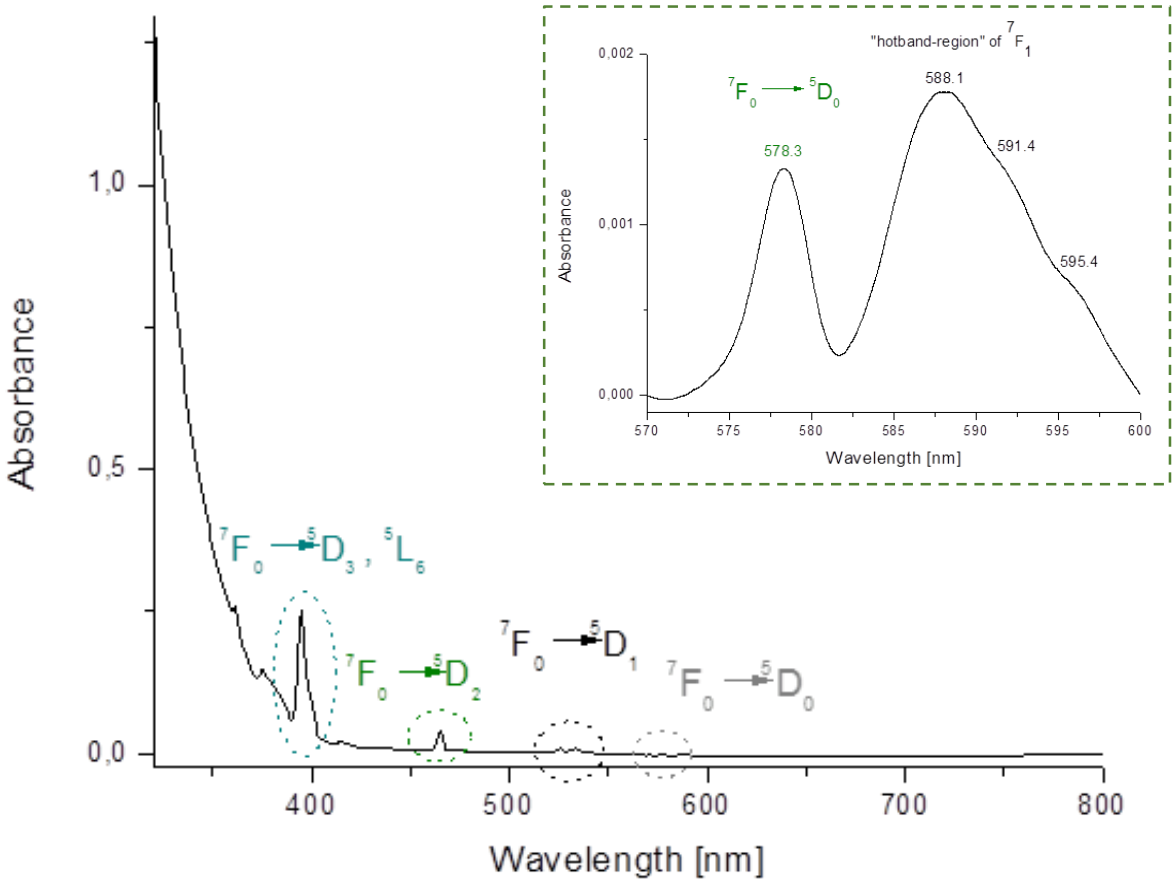

Figure 12: Absorbance spectrum of Eu_2O_3 incorporated in a ternary glass sample (9,4-84,6-6 AD1300) with magnification of the $^7F_0 \rightarrow {}^5D_0$ transition.

Another interesting phenomenon can be seen in the spectra above. The excitation of the Eu^{3+} ion does not solely start from the ground state $^7F_0$ but also from the first excited multiplet $^7F_1$ which only lies ~300 cm^{-1} above the ground state and is therefore occupied at room temperature. With increasing temperature these so called "hot bands" get more and more intense and even transitions from the second excited multiplet $^7F_2$ are possible. "Hot bands" can also be observed in the optical spectra of Nd^{3+} ions, but in this case they do not originate from the first excited multiplet but from the different levels of the crystal field split ground state multiplet. [14]

4 Experimental

4.1 Glass preparation

The glass making process on a laboratory scale, in general, consists of several steps:

a) weighing the glass components (oxides, carbonates)
b) mixing thoroughly in a mortar
c) transfer the mixture stepwise to the crucible at elevated temperature
d) melting for some time at high temperature
e) quenching the melt on a cold plate or mould
f) subsequent thermal treatment

4.1.1 Influences of the preparation parameters

Before the binary and ternary glass samples with different compositions were prepared to study the reaction mechanism, all possible parameters which may influence the glass forming process, and therefore also the "self-reduction" mechanism, were investigated. Hence it was necessary to find the optimal parameters for preparing the glass samples and to show their respective influences on the "self-reduction" mechanism.

The basic method used was the conventional melt-quench technique under atmospheric conditions in an oven *Nabertherm L5/R 1990*. The variable parameters were the following: the quenching method, the subsequent treatment (post-treatment), the melting time and the melting temperature. For this analysis a glass composition $10Na_2O\text{-}90B_2O_3\text{-}0.5Eu_2O_3$ (in mol%) was chosen, because it has been known from previous studies [36] that the "self-reduction" mechanism takes place in glasses with this composition.

All experiments and the associated parameters are listed below. For the influence of the melting time three series of glass samples were prepared.

A: Variation of the quenching method and post-treatment:

quenching method	air	air	air	ice	ice	ice
post-treatment	no treatment/ direct	annealing*	crystallization*	no treatment/ direct	annealing*	crystallization*

Constant parameters:

melting temperature	1000 °C
melting time	1 h

**Annealing: ~30 min at 450 °C - Crystallization: 24 h at 450 °C*

B: Variation of the melting time:

melting time	15 min	30 min	45 min	-	-	-	-	2 h
melting time	-	-	45 min	1 h	1 h 15 min	-	-	2 h
melting time	-	30 min	-	1 h	1 h 15 min	1 h 30 min	1 h 45min	2 h

Constant parameters:

melting temperature	1000 °C
quenching method	air
post-treatment	direct

C: Variation of the melting temperature:

melting temperature	1000 °C	1100 °C	1200 °C	1300 °C

Constant parameters:

melting time	1 h
quenching method	air
post-treatment	direct

For the glass production the analytical reagents Na_2CO_3, B_2O_3 and the high purity reagent Eu_2O_3 (99.99 %) were weighed and mixed with a mortar to get a fine and homogeneous powder. This powder was then added stepwise to a preheated platinum crucible at a constant temperature of 750 °C. The temperature program of the oven is given in Table 2. The preheating of the crucible and the stepwise addition was necessary because of the generation of gases (mainly CO_2 due to the conversion of $Na_2CO_3 \rightarrow Na_2O + CO_2$). Excessive gas formation could lead to a rising of the partially melted powder in the crucible and in the worst case to an overflow and therefore a material loss. After complete addition of the powder the oven was heated up to a preset temperature and was held at that temperature

for a fixed time. 15 minutes before the end of the melting time the crucible was swirled to avoid the formation of bubbles in the glass and to ensure that the glass was homogeneous. When the melting time was over, the crucible was again shortly swirled and the glass melt was poured into a copper mould on a copper plate (cooled by ice or cooled by air). Afterwards the glass samples were either directly stored or were placed in an oven for further heat treatment. Because it was not important to get large and totally perfect bricks, no efforts were made to avoid cracking at the edges or splitting of the samples into smaller pieces. This was not necessary because the samples could be placed in the spectrometer in such a way that the light struck the sample at a suitable face. All binary samples had to be stored in a desiccator for further investigations due to their hygroscopic behaviour.

Table 2: Temperature program for the glass production.

0 – 750 °C	00:30 h
750 – 750 °C	00:30 h
750 – 1000 °C	00:15 h
1000 – 1000 °C	01:00 h

Figure 13: Picture of the oven with magnifications of the crucible and the copper mould.

4.1.2 Influence of the Na_2O content in binary glass

After analysing the influences of the preparation conditions on the "self-reduction" mechanism and doing some literature search [1-3,5,36] for comparing the preparation parameters, glass samples with the composition xNa_2O-$(100-x)B_2O_3$-$0.5Eu_2O_3$ (x = 0, 5, 10, 15, 20, 30, 45) were prepared following exactly the same procedure as described in section 4.1.1 The adjustments for the preparation were the following:

Table 3: Preparation parameters for the binary glass production with different modifier content.

melting time	1 h
melting temperature	1000 °C
quenching method	Air
post-treatment	direct and annealing

4.1.3 Influence of the Al_2O_3 content in ternary glass

The first ternary glass samples were prepared based on the experiences made during the production of the binary glass samples. Therefore it was decided to set the ratio of Na_2O to B_2O_3 (R-value) as $R = 0.\dot{1}$, because the binary glass with the composition $10Na_2O$-$90B_2O_3$-$0.5EU_2O_3$ showed the best preparation characteristics and also clear evidence that the "self-reduction" mechanism had taken place. Therefore the mole fraction of Na_2O and B_2O_3 was calculated accordingly for glass samples with an Al_2O_3 content of 10 mol%, 15 mol% and 20 mol%.

For the glass production the analytical reagent Na_2CO_3, B_2O_3, Al_2O_3 and the high purity reagent Eu_2O_3 (99.99 %) were weighed and mixed with a mortar to get a fine and homogeneous powder. This time no temperature program was used and the oven was heated up to 1000 °C in 1 h. While heating the oven, the powder was added stepwise to a platinum crucible, ensuring that all powder was in the crucible when a temperature of 800 °C was reached. After finishing the addition and reaching the melting temperature, the same procedure as for the binary glass samples was performed. Although the ternary glass samples were not hygroscopic they were also stored in the desiccator.

Due to the fact that the melting temperature of 1000 °C was not sufficient for the samples with higher Al_2O_3 content than 10 mol%, the temperatures had to be varied during the

melting process up to 1400 °C. Additionally samples with melting times of 2h were prepared to test if there is also an effect of time on the “self-reduction” mechanism in ternary glasses.

After the produced glass samples were analysed, a literature search was again done and another series of ternary glass was fabricated, according to the composition and preparation conditions of one of the papers found. [4] As a result, two different glass families were prepared. One with a constant B_2O_3 amount of 85 mol% and the other with a constant R-value of $R = 0.\dot{1}$ mol% and an Al_2O_3 content of 5 mol%, 6 mol% and 10 mol% for each of the families.

The second series was prepared in the same way as the first series except for the melting temperature which was increased to 1300 °C for all samples. Furthermore the glass samples were not annealed and melted for only 1 h.

The compositions of all glass samples prepared in this thesis are pictured in the ternary phase diagram in Figure 14. The corresponding table and all original sample weights are attached in the appendix.

In the following a short-cut notation will be used for the glass composition, the quenching method (A: air, I: ice), the post-treatment (D: direct, A: annealing, C: crystallization) and the melting time. An example is given for better understanding:

The sample name **“9-81-10 AD1000”** corresponds to a glass with the composition $9Na_2O$-$81B_2O_3$-$10Al_2O_3$-$0.5Eu_2O_3$ in mol%, prepared at a melting time of 1000 °C, quenched on air and with no further heat treatment. Since all samples were doped with 0.5 mol% Eu_2O_3 it is not part of the short-cut notation.

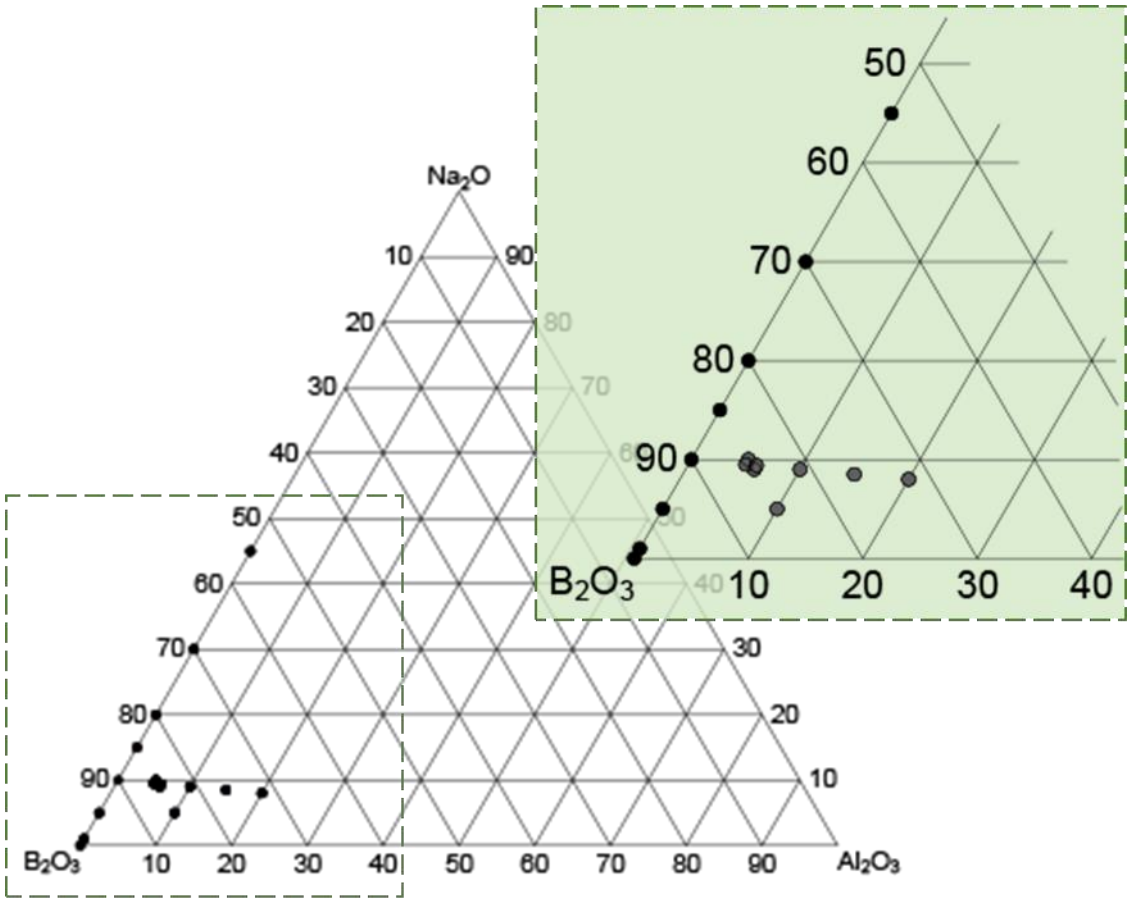

Figure 14: Ternary phase diagram with all glass sample compositions prepared in this thesis.

4.2 Spectroscopy

To elucidate the "self-reduction" mechanism, all prepared glass samples were optically investigated by recording their luminescence and for some samples also their transmission spectra were obtained.

4.2.1 Luminescence spectroscopy

Spectrometer

All luminescence spectra were recorded on a *Perkin Elmer LS55 fluorescence spectrometer (LS55)*, property of the company *Binder+Co AG*, which has been kindly provided for the investigations for this thesis.

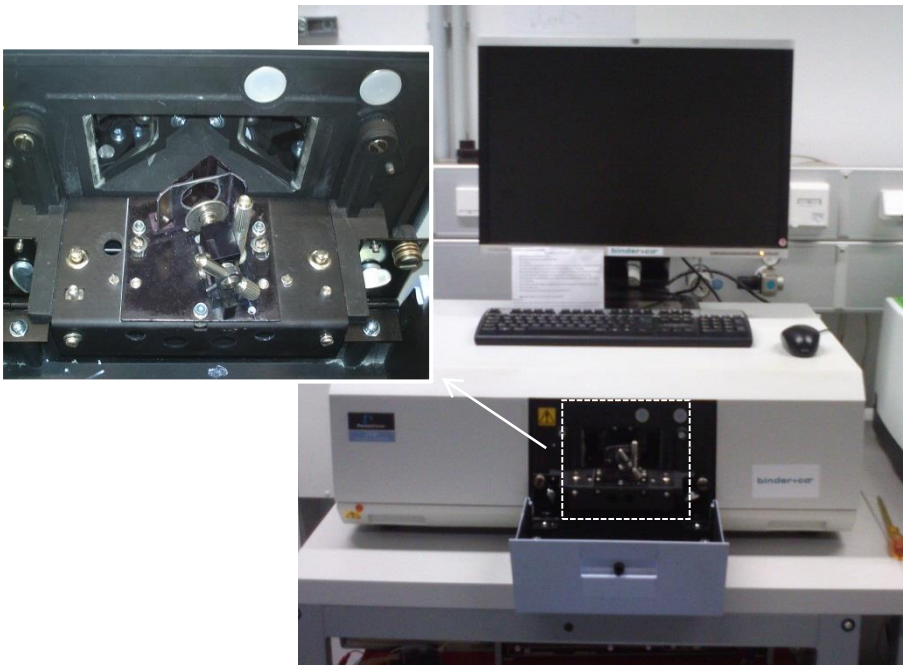

Figure 15: Picture of the LS55 with magnification of the specimen holder.

The LS55 is essentially equipped with a pulsed Xe-lamp as the light source, two monochromators (emission and excitation), selectable filters (on the emission and excitation side), a sample chamber and a detector (photomultiplier). [37] Many instrumental settings have to be chosen by the operator via the manual control window, displayed in Figure 16. The most important settings for the measurements in this thesis are listed below:

- Emission and excitation slit (2.5 – 20 nm / 2.5 – 15 nm [increments: 0.1])
- Detector gain (650 – 900 V [increment: 1)
- Delay time* (0.00 – x ms [increment: 0.01])
- Gate time* (0.00 – x ms [increment: 0.01])
- Adjustment of the sample

Asterisks indicate that these parameters are only adjustable for the phosphorescence mode. [37]

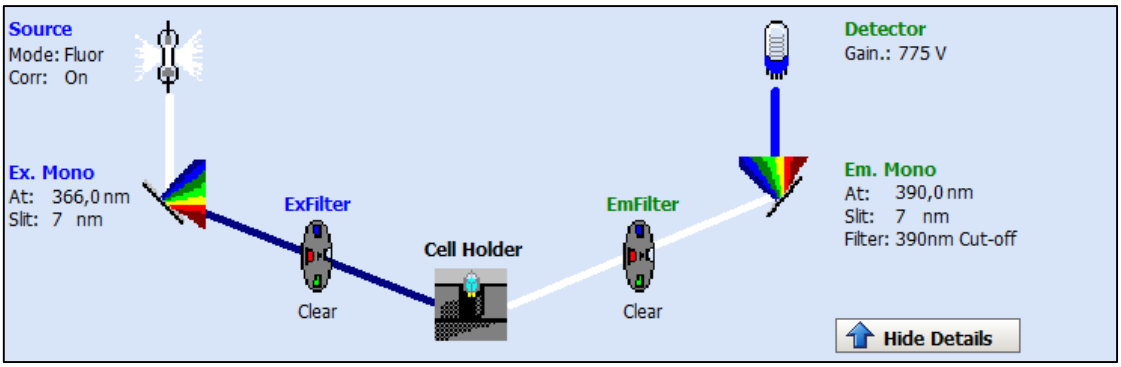

Figure 16: Screenshot of the manual control window of the LS55.

The LS55 can be operated in three different modes, the fluorescence mode, the phosphorescence mode and the chemiluminescence mode. [37] For this work only the fluorescence and the phosphorescence modes were of interest. The crucial difference between these two modes is the internal sequence of the measuring process.

The fluorescence mode is used to record short-lived luminescence. The detection of the emission starts at the peak of the excitation pulse. The lamp emission is subtracted from the signal as well as a dark current, which is measured after the excitation pulse is finished.

In phosphorescence mode data collection starts with a predefined delay after the excitation pulse and commences for a predefined time (gate). This is more suitable for materials with long-lasting luminescence investigated. [37]

Procedure

To get a first impression as to whether the “self-reduction” mechanism had taken place in the prepared glass samples, all samples were analysed under a UV lamp before they were investigated by the LS55. The UV lamp *VL-215-LC by Vilber* was used at the wavelengths 254 nm and 365 nm and the samples were placed on a non-luminescent foil *by Thorlabs*.

It turned out to be practical to record an emission spectrum with one of the predefined methods at the beginning of every new set of samples. Thereby some kind of overview, with respect to the position of the intensity maxima, was achieved.

Since none of the samples for this master's thesis showed any afterglow after the UV lamp excitation, it was assumed that the fluorescence mode would be the suitable one. As for

other solid state samples, measured in previous studies [38], it emerged, however, that the prompt dark current measurement, described above for the fluorescence mode, was also a problem for the glass samples. It is supposed that a slight afterglow causes a false dark current signal and therefore produces an incorrect spectrum in the fluorescence mode.

Thus although the luminescence of Europium in the investigated glass samples decays so quickly that there is no recognizable afterglow for the human eye, the phosphorescence mode was chosen for all measurements. To avoid signal loss due to the delay time, it was set to 0.0 ms for every cycle.

After finding a suitable mode for the gauging of the glass samples the most important thing was to place the sample properly into the excitation beam. One suitable method was to excite the sample at some short wavelength and observe the signal at the wavelength 615 nm, which corresponds to the maximum intensity of the Eu^{3+} peak, and then move the sample in the dark until the maximum intensity was reached. This method was used for every specimen to minimize error caused by intensity differences due to different placements.

Before the actual measurements started, excitation spectra for the Eu^{2+} and the Eu^{3+} emission were recorded to identify the optimum excitation wavelength for the emission spectra. From the emission spectrum one can identify the wavelengths where the maxima of the Eu^{2+} and Eu^{3+} peaks are located. In contrast to the emission spectrum, where the sample is excited at one wavelength and the emission is recorded over a defined wavelength range, for the excitation spectrum the sample is excited over a defined wavelength range and the emission of one wavelength is detected (namely the maximum value of the emission peak).

Finally the emission spectra for the specimen were recorded with the optimal wavelength from the excitation spectra.

All this time-consuming preliminary work was necessary since the emission spectra only provide qualitative information. Therefore one has to consider that if a set of samples are to be compared afterwards, all measurement conditions for this set of samples have to be exactly the same.

Measurements

The settings for the experiments with different glass compositions are listed below in Table 4, Table 5 and Table 6. Furthermore some samples were gauged to compare the decay times of the Eu^{2+} and Eu^{3+} emission and to show the reabsorption mechanism (Table 7). The tables for the preparatory studies (influences of the preparation parameters) are listed in the appendix.

Table 4: Parameters for the measurement of binary glass samples with varying modifier content.

measurement:	Na_2O variation	
sample name(s)		
0-100-0	AD/AA 1000	1h
5-95-0	AD/AA 1000	1h
10-90-0	AD/AA 1000	1h
15-85-0	AD/AA 1000	1h
20-80-0	AD/AA 1000	1h
30-70-0	AD/AA 1000	1h
45-55-0	AD/AA 1000	1h
fixed parameters		
method	phosphorescence	
λ_{exc} [nm]	254 and 366	
$slit_{em}$ [nm]	10	
$slit_{exc}$ [nm]	8	
detector gain [V]	775	
gate [ms]	0.4	
delay [ms]	0.0	

Table 5: Parameters for the first measurement of the ternary glass samples with varying Al_2O_3 amount (mol%).

measurement:	Al_2O_3 variation I	
sample name(s)		
10-90-0	AD/AA/AC 1000	1h/2h
9-81-10	AD/AA/AC 1000	1h/2h
8.5-76.5-15	AD/AA/AC 1400	1h/2h
8-72-20	AD/AA/AC 1400	1h/2h
fixed parameters		
method	phosphorescence	
λ_{exc} [nm]	254 and 396	
$slit_{em}$ [nm]	7	
$slit_{exc}$ [nm]	7	
detector gain [V]	760	
gate [ms]	0.4	
delay [ms]	0.0	

Table 6: Parameters for the second measurement of the ternary glass samples with varying Al_2O_3 amount (mol%).

measurement:	Al_2O_3 variation II	
sample name(s)		
10-85-5	AD1300	1h
9.5-85.5-5	AD1300	1h
9-85-6	AD1300	1h
9.4-84.6-6	AD1300	1h
9-81-10	AD1300	1h
5-85-10	AD1300	1h
fixed parameters		
method	phosphorescence	
$slit_{em}$ [nm]	7	
$slit_{exc}$ [nm]	7	
gate [ms]	0.4	
delay [ms]	0.0	
varied parameters		
λ_{exc} [nm] - detector gain [V]	254 - 775	
	320 - 710	
	366 - 750	
	382 - 750	
	396 - 750	

Table 7: Parameters for the measurement for the decay time (left) and for the reabsorption mechanism (right).

measurement:	delay variation
sample name(s):	10-90-0 AD1000 1h
fixed parameters	
method	phosphorescence
λ_{exc} [nm]	254
$slit_{em}$ [nm]	7
$slit_{exc}$ [nm]	7
detector gain [V]	775
gate [ms]	0.15 and 2.5
varied parameters	
	0.01-0.05 (increment: 0.01)
	0.1-0.2 (increment: 0.05)
delay [ms]	0.5-2.0 (increment: 0.5)
	3.0-5.0 (increment: 1.0)
	10.0

measurement:	reabsorption mechanism	
sample name(s)		
10-90-0	AD/AA/AC 1000	1h/2h
9-81-10	AD/AA/AC 1000	1h/2h
8,5-76,5-15	AD/AA/AC 1400	1h/2h
8-72-20	AD/AA/AC 1400	1h/2h
10-90-0	AD/AA/AC 1000	1h
10-90-0	ID/IA/IC 1000	1h
fixed parameters		
method	phosphorescence	
λ_{exc} [nm]	310 and 340	
$slit_{em}$ [nm]	7	
$slit_{exc}$ [nm]	7	
detector gain [V]	775	
gate [ms]	0.4	
delay [ms]	0.0	

4.2.2 Absorption

Spectrometer

To clarify the dependence of the reduction of Eu^{3+} to Eu^{2+} in glass on the structure, it was necessary to obtain some information about the surroundings of the Eu^{3+} ion in the glass. Therefore some samples were gauged on the *Perkin Elmer UV/VIS/NIR spectrometer Lambda950 (L950)* since it has a much better spectral resolution than the LS55. The L950 is also property of the company *Binder+Co AG* and has also been kindly provided for the investigations for this thesis.

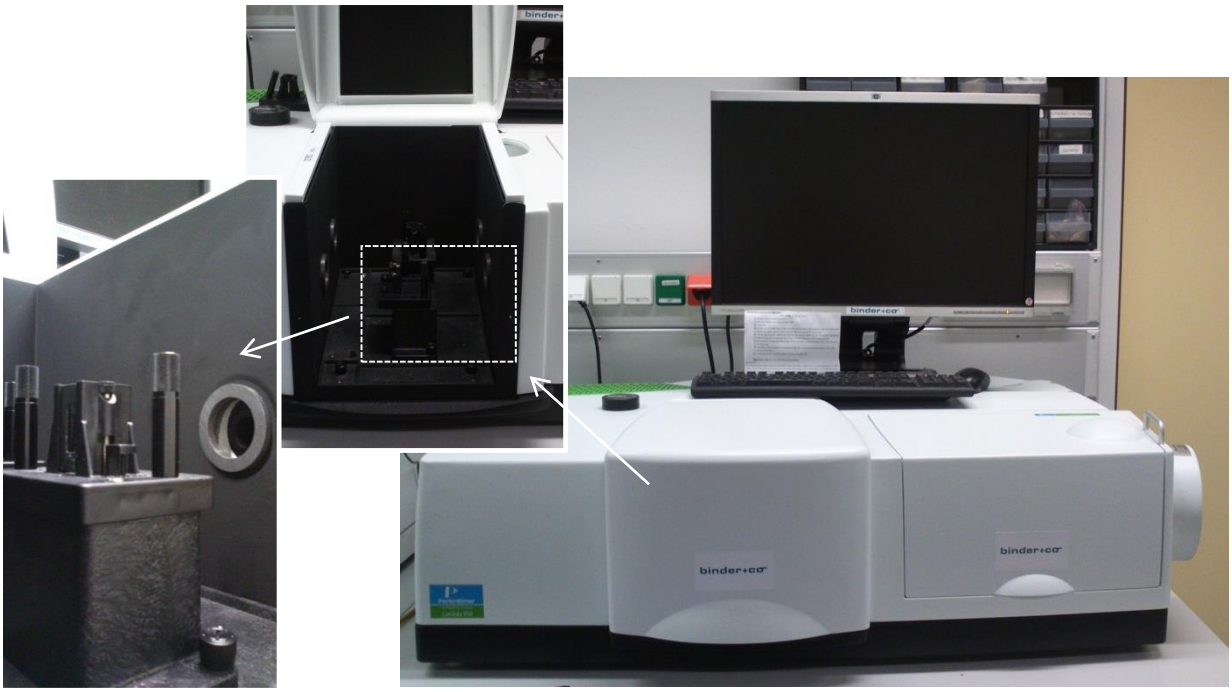

Figure 17: Picture of the L950 with the integrating sphere detector. The details show the opened sample chamber and a magnification of the specimen holder.

There are two different detection setups available for the L950. An integrating sphere (*150nm InGaAs Int. Sphere*) mainly used for the reflection mode and a *UV/VIS/NIR accessory 2D detector module* used for transmission/absorbance measurements. Both systems can be used in the range from UV (200nm-380 nm) to VIS (380-780 nm) and up to NIR (780-2500 nm), therefore two different light sources, a D_2-lamp for the UV region and the W-lamp for the VIS and NIR region, and two different detectors, a photomultiplier tube (PMT) for the UV/VIS range and a PbS (or InGaAs) detector for the NIR, are needed. The detector change at 810 nm is performed automatically but can sometimes cause steps in the plotted spectrum. [39]

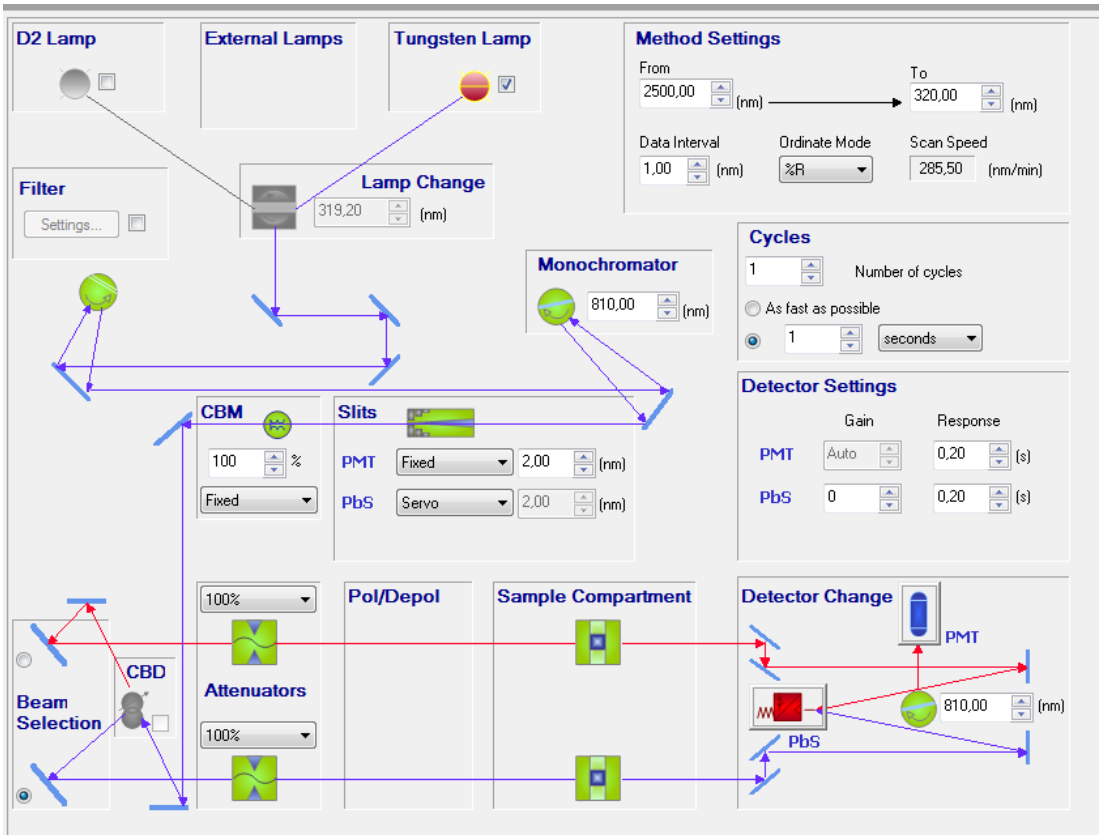

Figure 18: Screenshot of the control window of the L950.

Procedure

Before every set of scans, a baseline with the settings needed afterwards had to be recorded. For the integrating sphere a *certified reflectance standard by labsphere* was used. The baseline for the transmission/absorbance setup was recorded with air as a reference.

Since no satisfactory results could be achieved with the integrating sphere setup, only the 2D module for transmission was used for the glass samples. After some attempts to get even better plots by polishing the samples or adjusting various parameters, it was decided that all glass samples were to be measured as prepared since the effect was not significant. Only the step size and the slit width of the detector were adapted to enhance the resolution.

Measurements

Beside the glass samples, also pure crystalline Eu_2O_3 was investigated on the L950. In this case (non-transparent crystalline powder) the reflection set-up with the integrating sphere was used. To eliminate the water in the Eu_2O_3 powder it was tempered in a Pt crucible for

2 hours at 1200°C before the measurement. The performed measurements and settings are listed in the tables below.

Table 8: Parameters and wavelength range for the measurements of some binary and ternary glass samples.

	sample names	range / step size [nm]			slit (PMT) [nm]
binary	10-90-0	800 – 320 / 1	800 – 320 / 0.01	600 – 570 / 0.01	2
	15-85-0	800 – 320 / 1	-	600 – 570 / 0.01	2
	20-80-0	800 – 320 / 1	-	600 – 570 / 0.01	2
ternary	9.4-84.6-6	800 – 320 / 1	800 – 320 / 0.01	600 – 570 / 0.01	2
	9-85-6	800 – 320 / 1	-	600 – 570 / 0.01	2
	9-81-10	800 – 320 / 1	-	600 – 570 / 0.01	2
	5-85-10	800 – 320 / 1	-	600 – 570 / 0.01	2

Table 9: Parameters and wavelength range for the measurements of crystalline Eu_2O_3.

	crystalline Eu_2O_3					
range [nm]	2500 – 200	800 - 320	620 -570	560 - 520	500 - 450	430 - 350
step size [nm]	1	0.1	0.01	0.01	0.01	0.01
slit (PMT) [nm]	2	0.5	0.3	0.3	0.3	0.3

All other parameters were taken as originally set in the software (i.e. their default values).

4.2.3 X-ray Diffraction (XRD) analysis

During the preparation of the glass samples two interesting phenomena occurred which were investigated separately with X-Ray Diffraction (XRD) analysis by *Ao.Univ.-Prof. Dipl.-Ing. Dr.techn. Mautner*. The measurement parameters are listed in the appendix.

The first phenomenon was the occurrence of a milky white pure borate glass rather than the expected transparent one and the second phenomenon was the formation of crystals on the walls of the crucible for compositions with an Al_2O_3 amount of 15 mol% and 20 mol% in the investigated ternary glass samples. Both peculiarities are shown in Figure 19.

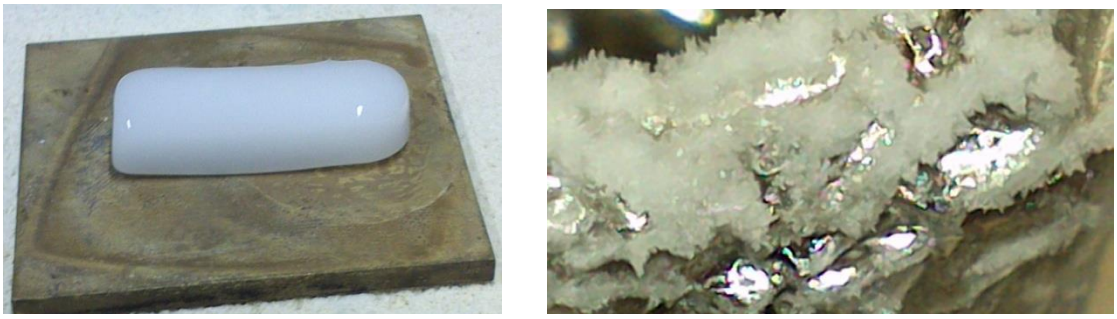

Figure 19: Photos of the pure borate glass (0-100-0 AD1300) [left] and the crystals on the crucible for the ternary glass 8.5-76.5-15 AD1400 [right].

Since no transparent pure borate glass with the composition 100 mol% B_2O_3 and 0.5 mol% Eu_2O_3 could be prepared even though the melting temperature had been elevated to 1300 °C, a glass with 1 mol% modifier with higher melting temperatures was prepared. But again a milky white "melt" and, after quenching the melt, a milky white "glass" was obtained. As an additional peculiarity the residual "glass" in the crucible dissolved easily in water. Since it was assumed that at this composition the glass formation does not take place completely, the samples 0-100-0 and 1-99-0 were powdered to fine grains and given to *Ao.Univ.-Prof. Dipl.-Ing. Dr.techn. Mautner* to analyze the powders with XRD. The results of the analysis in Figure 20 show that the samples have amorphous parts (broad features) but also crystalline Eu_2O_3 sites (sharp peaks).

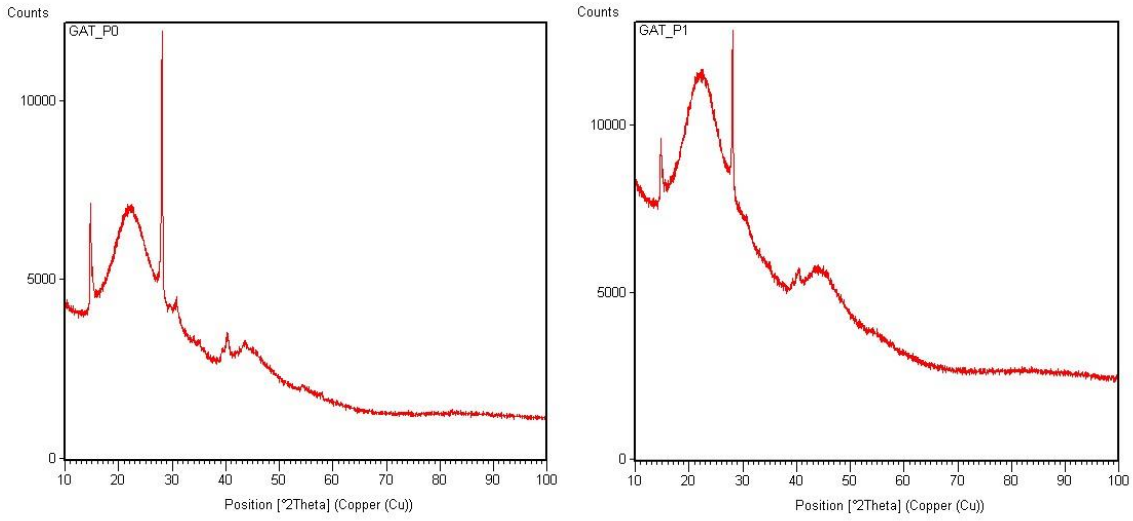

Figure 20: XRD spectra of the samples 0-100-0 (left) and 1-99-0 (right).

This indicates that the Eu_2O_3 crystals cannot dissolve in the glass melt without or too little amounts of modifier present. Due to the remaining crystallites of Eu_2O_3 the glass obtains its

milky white appearance because the crystallites scatter the visible light. To proof this assumption a pure borate glass without Eu_2O_3 was prepared and indeed a transparent glass was obtained. These experiments also helped to understand that Eu_2O_3 does not act as a modifier in the glass but can only be incorporated into the material when a modifier loosens the glass network.

Additional to the crystals at the edges of the crucibles, white inclusions were found in the glass samples poured out from these crucibles. Investigations under the light microscope showed that these white inclusions had the form of needles. To clarify their structure and composition the crystals from one crucible were collected and also investigated by *Ao.Univ.-Prof. Dipl.-Ing. Dr.techn. Mautner* with XRD.

The result in Figure 21 indicates the existence of pure single crystals with the proposed composition $Al_{20}B_4O_{36}$.

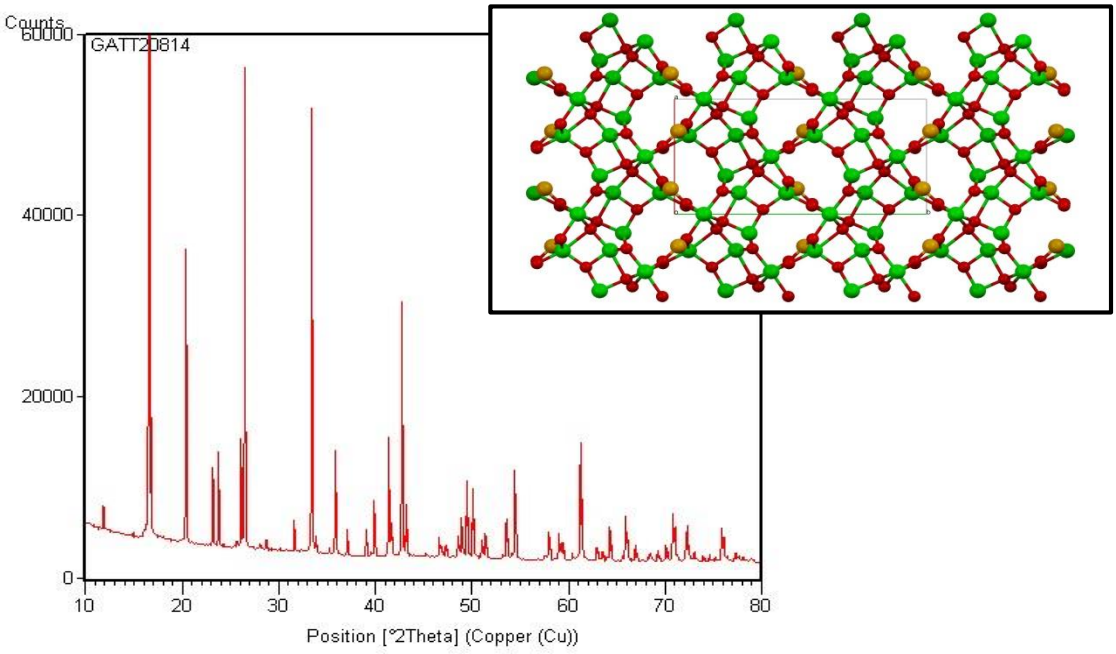

Figure 21: XRD spectrum of the needles of the sample 8.5-76.5-15 AD1400 and a simulation of the crystal structure (red spheres: Oxygen, green spheres: Aluminium and orange spheres: Boron).

A possible explanation for these needles could be the formation of triclusters (see section 2.3) since both, the needles and the triclusters are composed of BO_3-, BO_4-, AlO_4- and AlO_6-units. But due to the unsuitable melting temperature the triclusters might have had a higher tendency towards crystallization during the quenching of the melt. [24]

5 Results and discussion

5.1 Influences of the preparation parameters

As described in section 4.1 the four main parameters for the glass preparation were varied to make clear if they have any influence on the "self-reduction" mechanism. The results of the variation of the preparation conditions are presented and discussed below.

Figure 22, Figure 23 and Figure 24 show photos of some glass samples prepared with different **quenching methods and subsequent heat treatments.** The results of the luminescence measurements are plotted in Figure 25 and Figure 26.

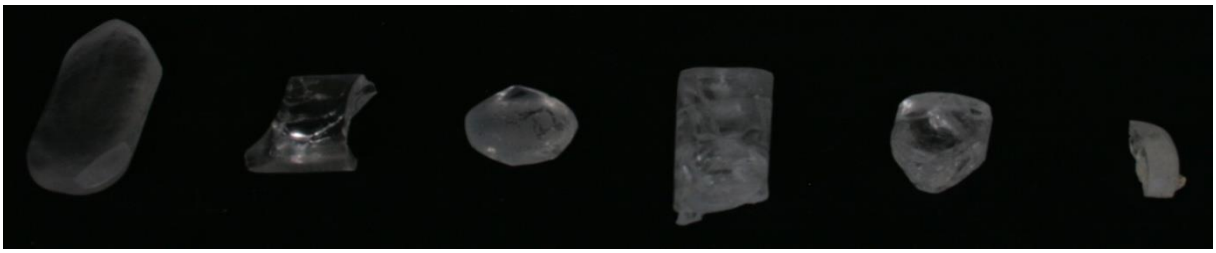

Figure 22: Glass samples with the composition 10-90-0 AD1000 and a melting time of 1 h, prepared with different quenching methods and post-treatments, photographed in daylight. The different preparation methods were, from left to right: AD, AA, AC, ID, IA, and IC.

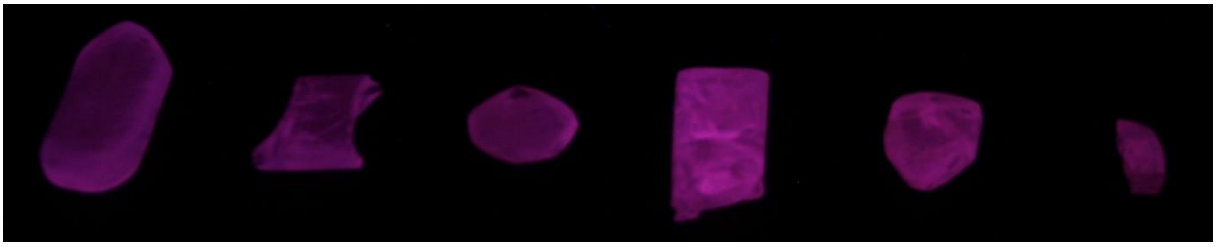

Figure 23: Glass samples with the composition 10-90-0 AD1000 and a melting time of 1 h, prepared with different quenching methods and post-treatments, photographed under UV light with a wavelength of 365 nm. The different preparation methods were, from left to right: AD, AA, AC, ID, IA, and IC.

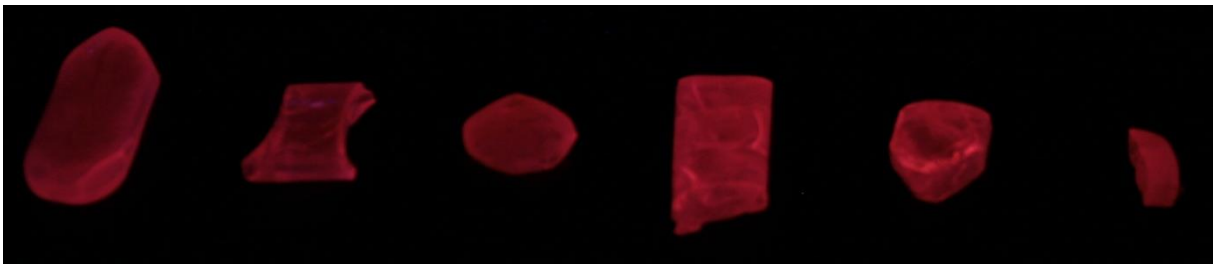

Figure 24: Glass samples with the composition 10-90-0 AD1000 and a melting time of 1 h, prepared with different quenching methods and post-treatments, photographed under UV light with a wavelength of 254 nm. The different preparation methods were, from left to right: AD, AA, AC, ID, IA, and IC.

As explained in section 3 the excitation of the Eu^{2+} ions in the glass leads to a blue/violet luminescence while a red/orange emission corresponds to the emission of the Eu^{3+} ions. The Eu^{2+} emission is more clearly visible by exciting the samples with the longer wavelength (365 nm) of the UV lamp, while the shorter wavelength (254 nm) excites the Eu^{3+} ions stronger. Therefore, the luminescence in Figure 23 indicates that the "self-reduction" mechanism took place in every sample. However, no noticeable difference between the glass samples themselves can be seen under the UV light. The emission spectra in Figure 25 confirm that in all glass samples a high proportion of the Eu^{3+} ions was reduced to Eu^{2+} ions.

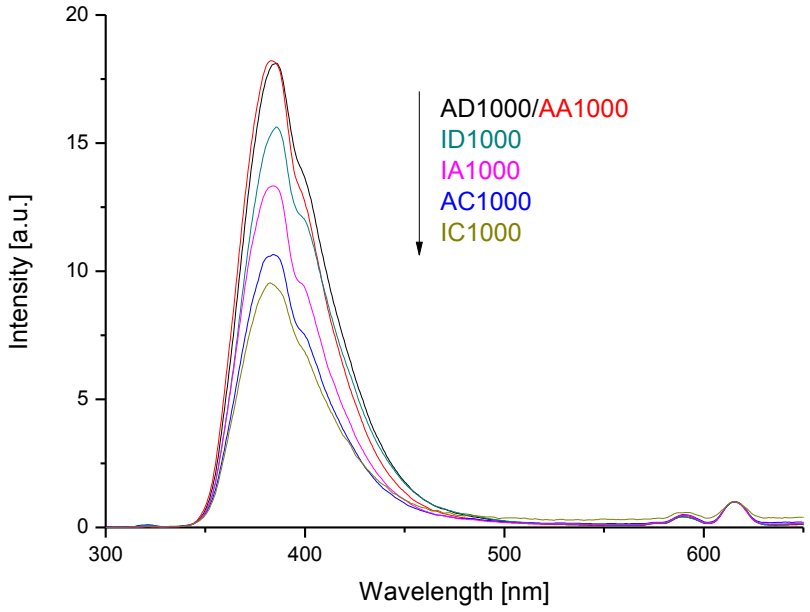

Figure 25: Emission spectra of the samples 10-90-0, melted at 1000 °C with different quenching methods and post-treatments. The excitation wavelength was 320 nm. All spectra were normalized to the value 1 for the Eu^{3+} maximum at 615 nm.

As there is still no evidence whether and how the different quenching methods and the post-treatments influence the reduction, the peaks for the original Eu^{2+} emission and the Eu^{3+} emission (without scaling) were integrated separately. From this the Eu^{2+}/Eu^{3+}ratio was obtained. Figure 26 shows that for both quenching methods (air and ice) the Eu^{2+} amount decreases as the duration of the heat treatment increases.

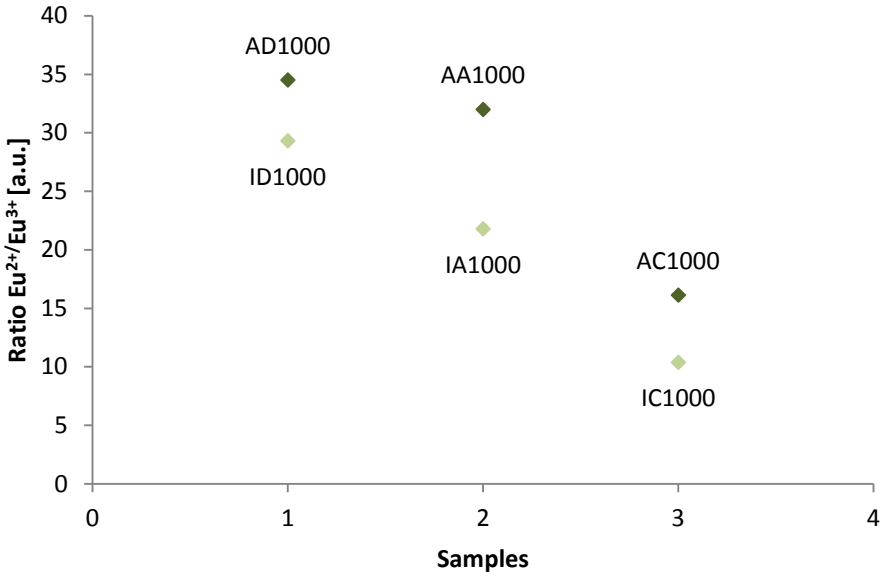

Figure 26: Ratio of the integrated Eu^{2+} peak and the integrated Eu^{3+} peak for the glass composition 10-90-0, melted at 1000 °C with different quenching methods and post-treatments. The peaks were integrated in the original emission spectra (excitation wavelength: 320 nm) without normalized Eu^{3+} peak.

To investigate the influence of the **melting time** further three sets of glass samples were prepared. The first samples (melting times: 15 min, 30 min, 45 min and 2 h) had white inclusions and therefore the emission spectra were not significant and they are not presented in this thesis. Under the UV lamp all samples showed red/orange luminescence at both wavelengths which indicates that no reduction took place. Since it was known from all the previous experiments that Eu^{3+} should be reduced to Eu^{2+} at this composition, the different results were ascribed to the inclusions. The second series had no peculiarities and there was evidence for a reduction under the UV lamp as well as in the emission spectra shown in Figure 27.

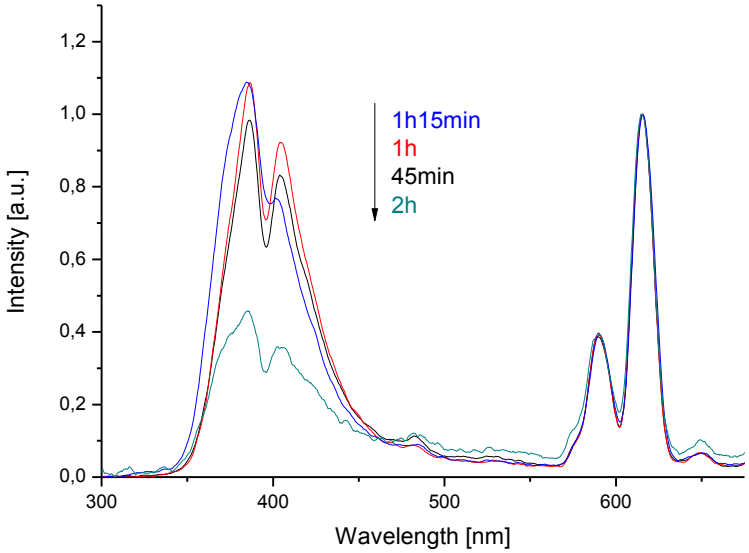

Figure 27: Emission spectra of the samples 10-90-0 AD1000 with melting times of 45 min, 1 h, 1 h 15 min and 2 h. The excitation wavelength was 254 nm. All spectra were normalized to the value 1 for the Eu^{3+} maximum.

To proof the reproducibility of the results on the time dependence the experiment was performed a third time with more glass samples. Again an influence of the melting time is already visible under the UV lamp (Figure 29) which is verified by the emission spectra shown in Figure 31.

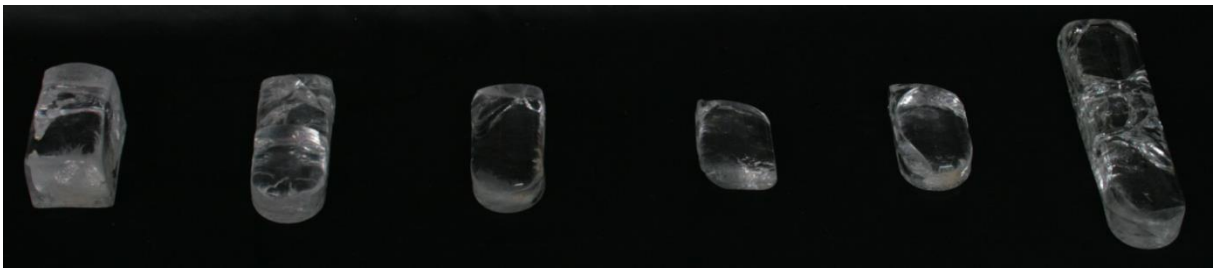

Figure 28: Glass samples with the composition 10-90-0 AD1000 prepared with different melting times, photographed at daylight. Melting times were, from left to right: 30 min, 1h, 1 h 15 min, 1 h 30 min, 1 h 45 min and 2 h.

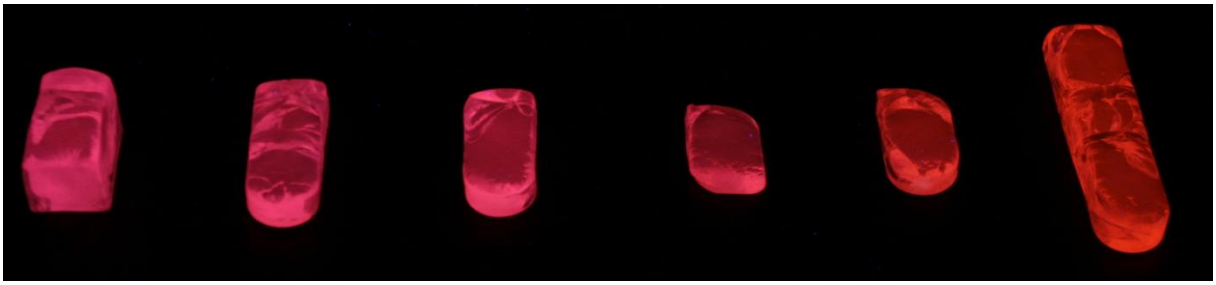

Figure 29: Glass samples with the composition 10-90-0 AD1000 prepared with different melting times, photographed under UV light with a wavelength of 365 nm. Melting times were, from left to right: 30 min, 1h, 1 h 15 min, 1 h 30 min, 1 h 45 min and 2 h.

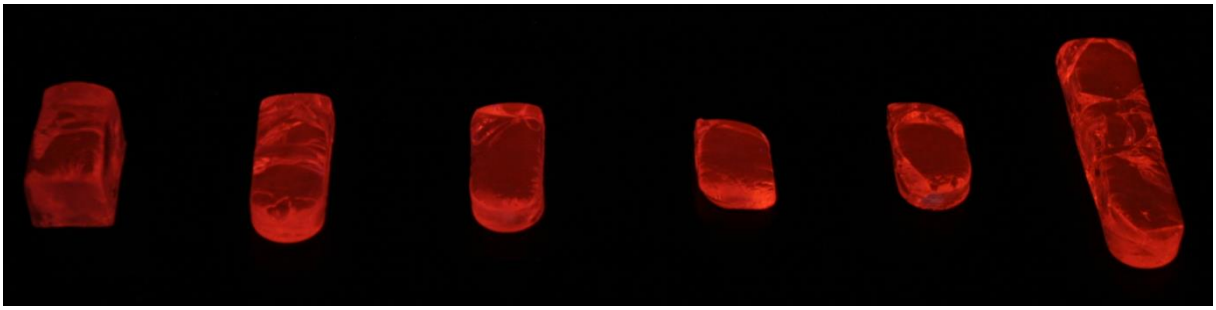

Figure 30: Glass samples with the composition 10-90-0 AD1000 prepared with different melting times, photographed under UV light with a wavelength of 254 nm. Melting times were, from left to right: 30 min, 1h, 1 h 15 min, 1 h 30 min, 1 h 45 min and 2 h.

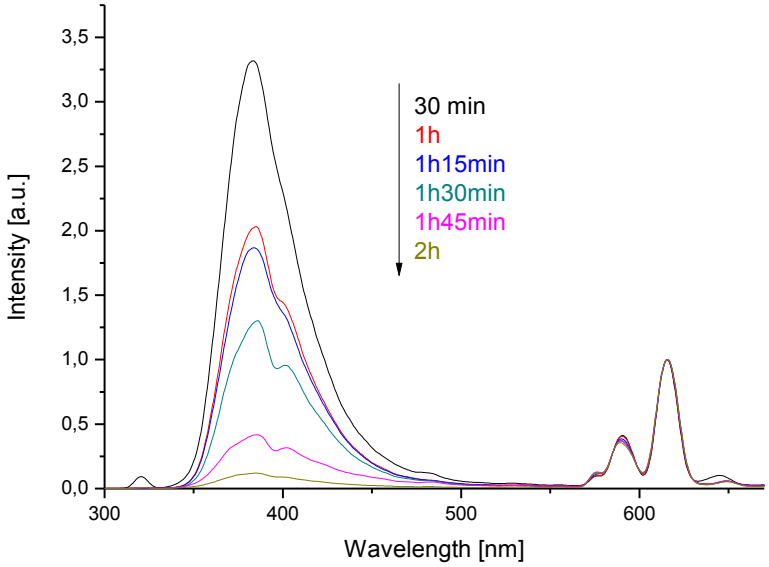

Figure 31: Emission spectra of the samples 10-90-0 AD1000 with melting times of 30 min, 1 h, 1 h 15 min, 1 h 30 min, 1 h 15 min and 2 h. The excitation wavelength was 320 nm. All spectra were normalized to the value 1 for the Eu^{3+} maximum.

To compare the trend for both series the Eu^{2+}/Eu^{3+} ratios were plotted versus the time. Unfortunately, it can be seen in Figure 32 that there is no uniform trend for the two different series which casts doubt on the reproducibility.

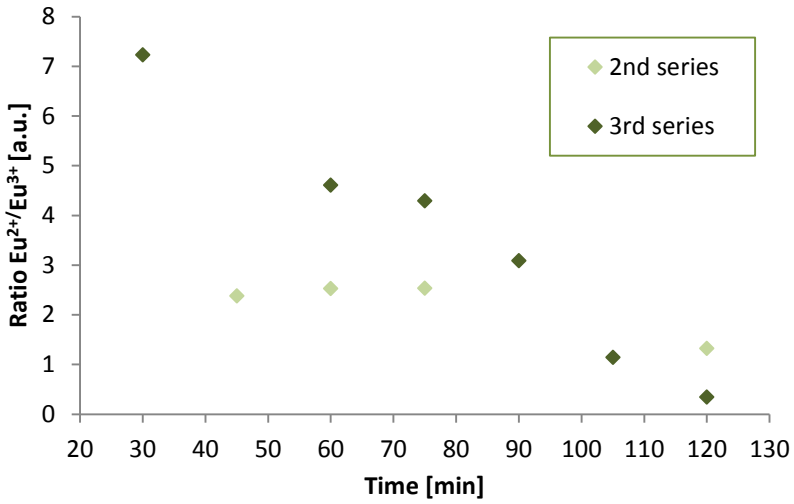

Figure 32: Ratio of the integrated Eu^{2+} peak and the integrated Eu^{3+} peak for the glass samples 10-90-0 AD1000 with melting times of 45 min, 1 h, 1 h 15 min and 2 h (2^{nd} series) and melting times of 30 min, 1 h, 1 h 15 min, 1 h 30 min, 1 h 15 min and 2 h (3^{rd} series). The peaks correspond to the original emission spectra without normalized Eu^{3+} peak.

While the trend for the second series indicates that first there is an increase of the reduction probability and afterwards a decrease with longer times for the glass melt in the oven, the trend for the third series shows that the probability that the "self-reduction" mechanism takes place decreases continuously with an increase in the melting time.

To investigate the **temperature dependence** of the self-reduction two sets of glass samples were prepared. Unexpectedly, however, the "self-reduction" could not be seen in any of the glasses, although the glass composition did not change. What would have been expected from the comparison of the data of ternary glasses shown in Figure 33 was that the probability for the "self-reduction" mechanism decreases with higher melting temperature.

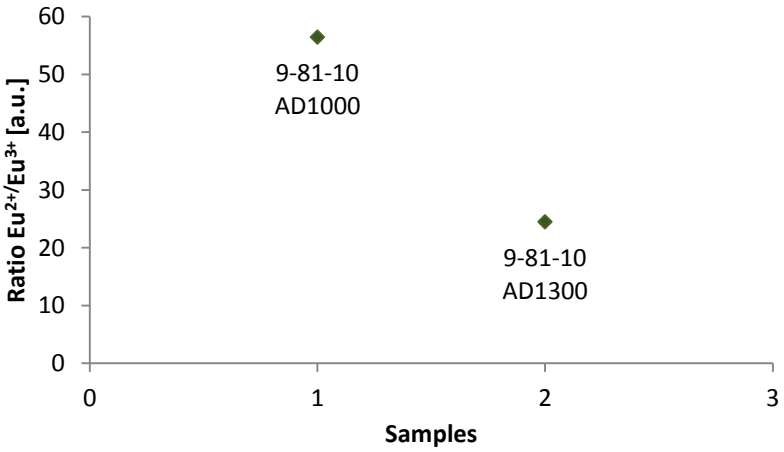

Figure 33: Ratio of the integrated Eu^{2+} peak and the integrated Eu^{3+} peak for the glass samples 10-90-0 AD1000 and AD1300 with a melting time of 1 h. The peaks correspond to the original emission spectra without normalized Eu^{3+} peak.

5.2 Influence of the Na_2O content in binary glass

The photos of the samples at daylight and under the UV lamp are shown below in Figure 34, Figure 35 and Figure 36. It can be seen in Figure 34 that the samples 0-100-0 and 45-55-0 are not transparent. The reason for the sample with 45 mol% Na_2O content is that the glass with that high modifier amount starts already to decompose. [20] An explanation for the pure, opaque borate glass has already been given in section 4.2.3.

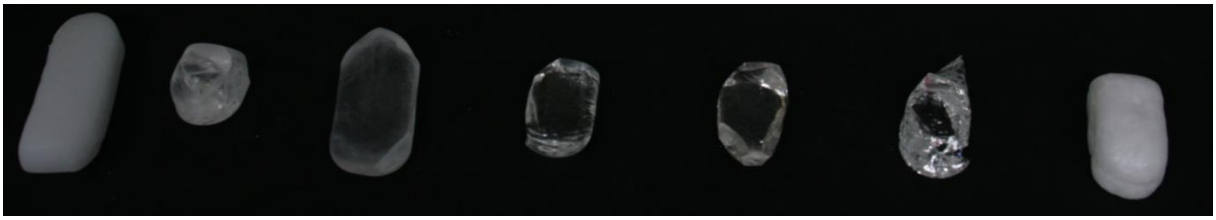

Figure 34: Glass samples with different amount of Na_2O, melted at 1000 °C for 1 h and quenched on air with no further heat treatment, photographed in daylight. The compositions were, from left to right: 0-100-0, 5-95-0, 10-90-0, 15-85-0, 20-80-0, 30-70-0 and 45-55-0. *0-100-0: after 1 h increase to 1200°C for 1 h.*

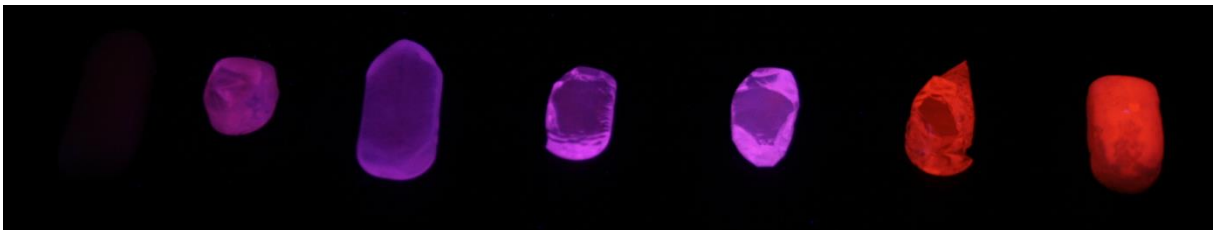

Figure 35: Glass samples with different amount of Na_2O, melted at 1000 °C for 1 h and quenched on air with no further heat treatment, photographed under UV light at a wavelength of 365 nm. The compositions were, from left to right: 0-100-0, 5-95-0, 10-90-0, 15-85-0, 20-80-0, 30-70-0 and 45-55-0. *0-100-0: after 1 h increase to 1200°C for 1 h.*

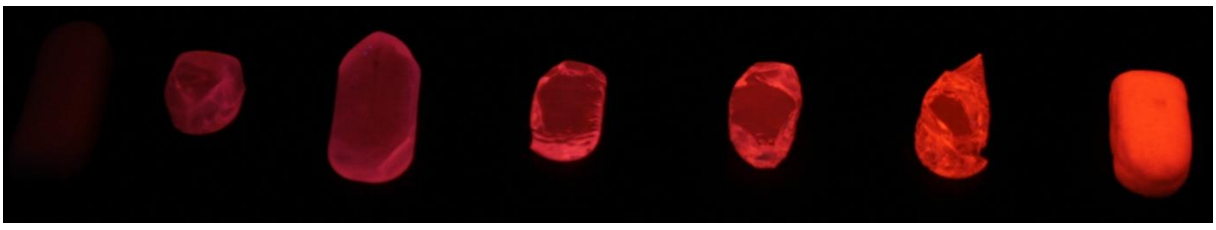

Figure 36: Glass samples with different amount of Na_2O, melted at 1000 °C for 1 h and quenched on air with no further heat treatment, photographed under UV light at a wavelength of 254 nm. The compositions were, from left to right: 0-100-0, 5-95-0, 10-90-0, 15-85-0, 20-80-0, 30-70-0 and 45-55-0. *0-100-0: after 1 h increase to 1200°C for 1 h.*

Due to Figure 35 it can be estimated that the probability that Eu^{3+} gets reduced decreases with increasing Na_2O amount. This trend can also be seen in the emission spectra shown in Figure 37.

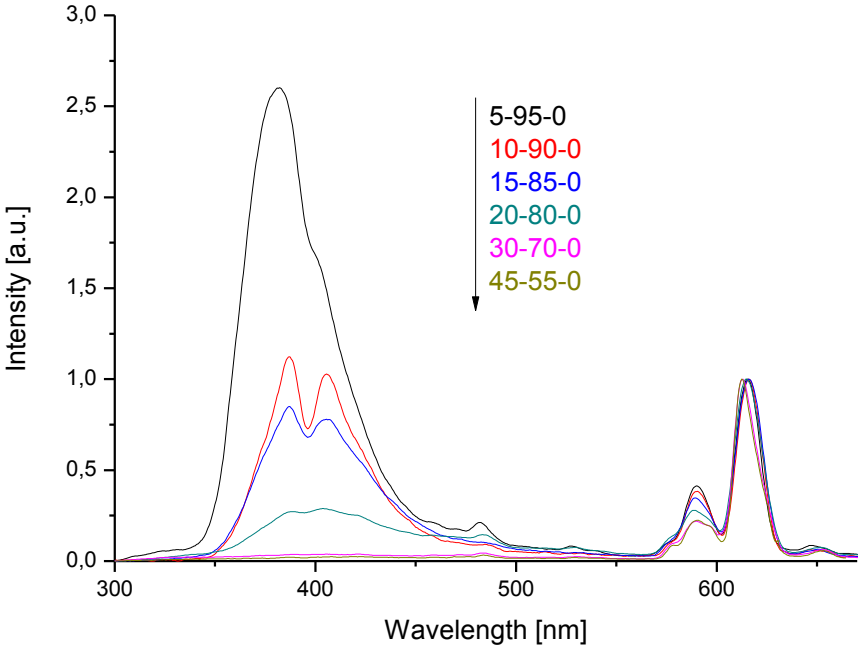

Figure 37: Emission spectra of the samples with different modifier content (5 mol%, 10 mol%, 15 mol%, 20 mol%, 30 mol% and 45 mol% Na_2O). All samples were melted at 1000 °C for 1 hour and were quenched on air with no further heat treatment. The excitation wavelength was 254 nm. All spectra were normalized to the value 1 for the Eu^{3+} maximum.

5.3 Influences of the Al_2O_3 content in ternary glass

The results for the first series of ternary glass samples are shown in the following figures.

Figure 38: Glass samples photographed in daylight. Top - from left to right: 10-90-0 AD1000 2 h, 9-81-10 AD1000 2 h, 8.5-76.5-15 AD1200 2 h and 8-72-20 AD1400 1 h 30 min. Bottom - from left to right: 10-90-0 AD1000 1 h, 9-81-10 AD1000 1 h, 8.5-76.5-15 AD1200 1 h, 8.5-76.5-15 AD1400 1 h and 8-72-20 AD1400 1 h.

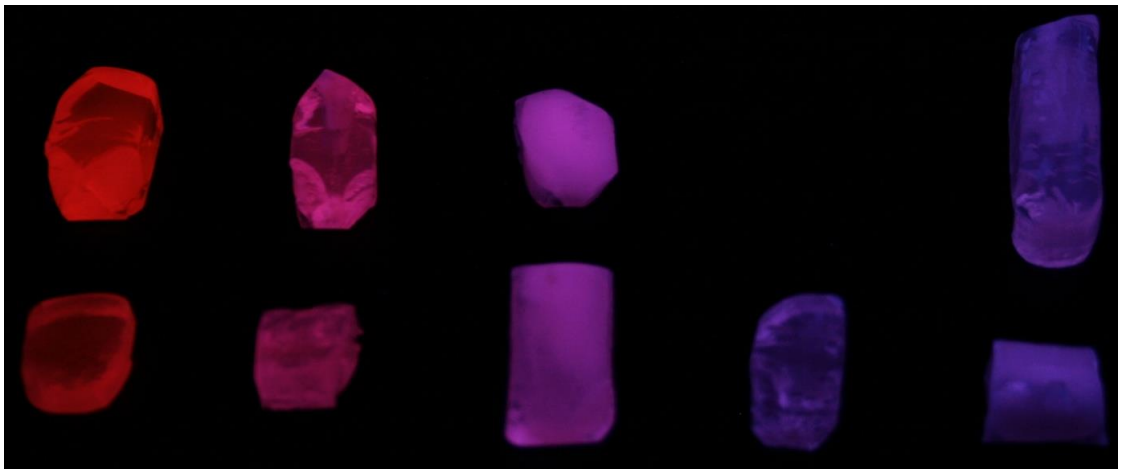

Figure 39: Glass samples photographed under UV light at a wavelength of 365 nm. Top - from left to right: 10-90-0 AD1000 2 h, 9-81-10 AD1000 2 h, 8.5-76.5-15 AD1200 2 h and 8-72-20 AD1400 1 h 30 min. Bottom - from left to right: 10-90-0 AD1000 1 h, 9-81-10 AD1000 1 h, 8.5-76.5-15 AD1200 1 h, 8.5-76.5-15 AD1400 1 h and 8-72-20 AD1400 1 h.

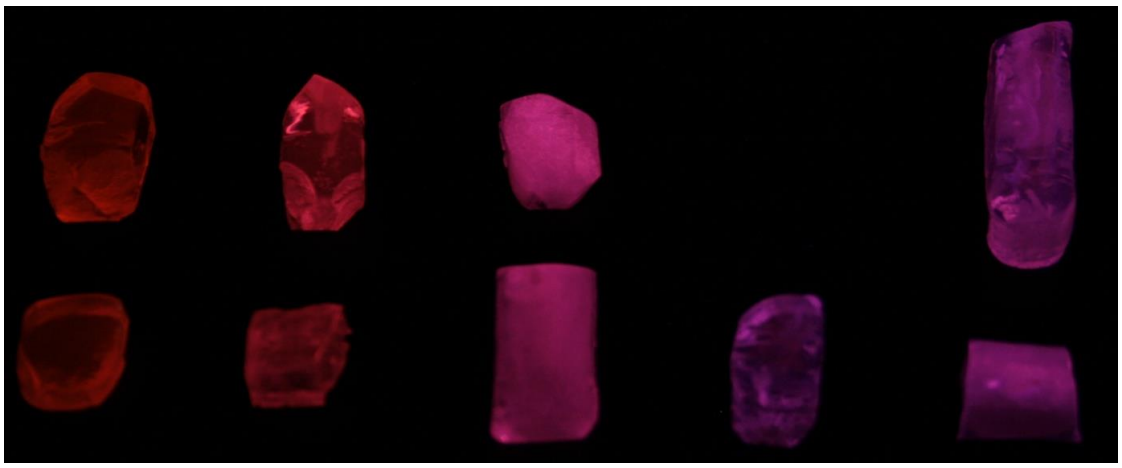

Figure 40: Glass samples photographed under UV light at a wavelength of 254 nm. Top - from left to right: 10-90-0 AD1000 2 h, 9-81-10 AD1000 2 h, 8.5-76.5-15 AD1200 2 h and 8-72-20 AD1400 1 h 30 min. Bottom - from left to right: 10-90-0 AD1000 1 h, 9-81-10 AD1000 1 h, 8.5-76.5-15 AD1200 1 h, 8.5-76.5-15 AD1400 1 h and 8-72-20 AD1400 1 h.

In Figure 38 one can recognize that there are white inclusions in some glass samples. This could be due to the fact that for some of the glass compositions the chosen melting temperatures were too low. But although the first attempt to prepare ternary glass samples was not that successful a trend for the reduction probability could already be estimated from the luminescence under the UV lamp, as well as from the emission spectra shown in Figure 41.

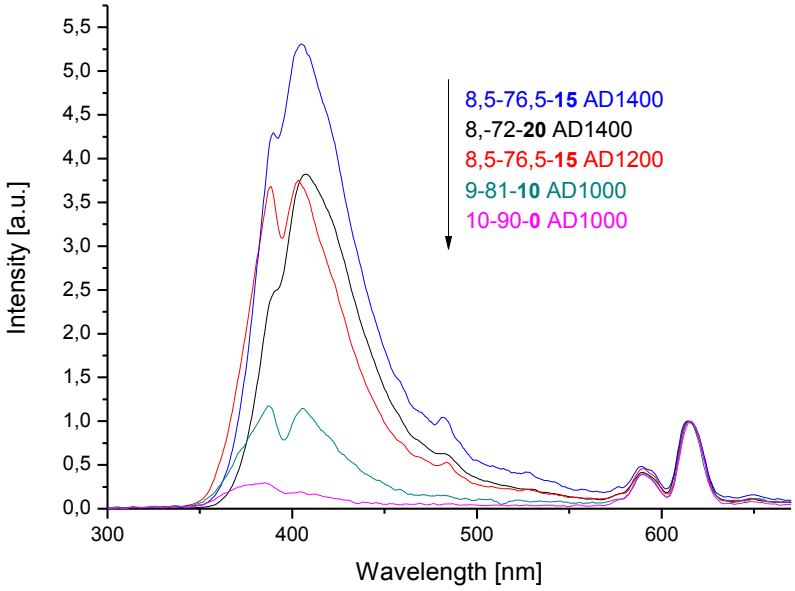

Figure 41: Emission spectra of the samples with different Al_2O_3 content (0 mol%, 10 mol%, 15 mol% and 20 mol%). The samples were melted for 1 hour and the melting temperatures varied with composition. The excitation wavelength was 254 nm. All spectra were normalized to the value 1 for the Eu^{3+} maximum.

Nevertheless it is difficult to separate between the influences from the composition and that of the melting temperature and melting time. Therefore the interpretation of the trend is only possible with the information gained from the second series of ternary glass samples.

After eliminating the problems of the different melting temperatures no white inclusions were visible anymore in the samples as shown in Figure 42.

Figure 42: Glass samples with the following compositions, melted at 1300 °C for 1 h and quenched on air with no further heat treatment, were photographed in daylight. Top - from left to right: 9.5-85.5-5, 9.4-84.6-6 and 9-81-10. Bottom - from left to right: 10-85-5, 9-85-6 and 5-85-10.

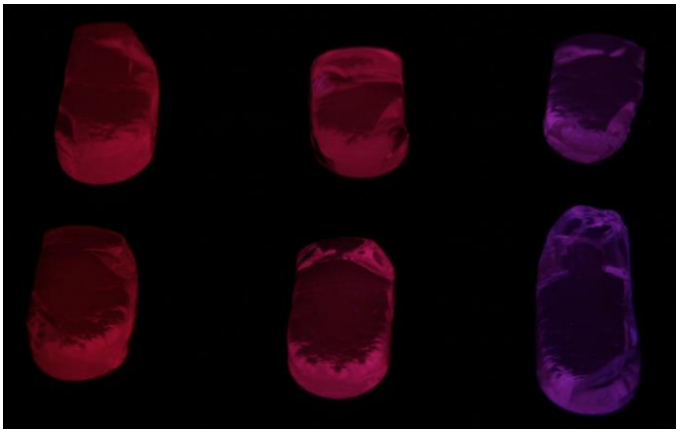

Figure 43: Glass samples with the following compositions, melted at 1300 °C for 1 h and quenched on air with no further heat treatment, were photographed under UV light at a wavelength of 365 nm. Top - from left to right: 9.5-85.5-5, 9.4-84.6-6 and 9-81-10. Bottom - from left to right: 10-85-5, 9-85-6 and 5-85-10.

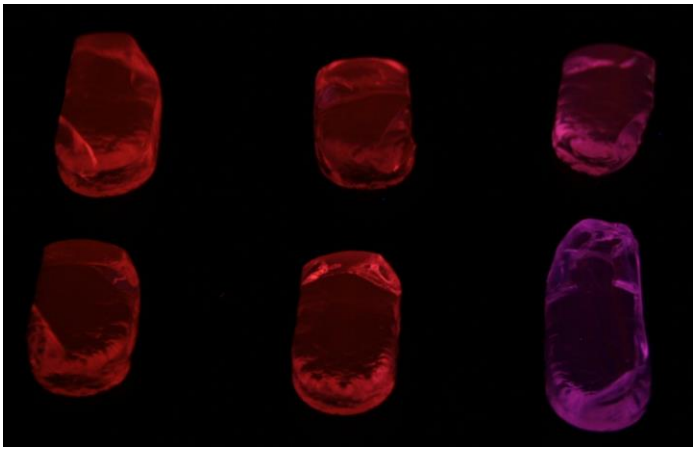

Figure 44: Glass samples with the following compositions, melted at 1300 °C for 1 h and quenched on air with no further heat treatment, were photographed under UV light at a wavelength of 254 nm. Top - from left to right: 9.5-85.5-5, 9.4-84.6-6 and 9-81-10. Bottom - from left to right: 10-85-5, 9-85-6 and 5-85-10.

Figure 43 indicates that the reduction probability depends on the composition in this set of glass samples, which could also be verified by the emission spectra in Figure 45.

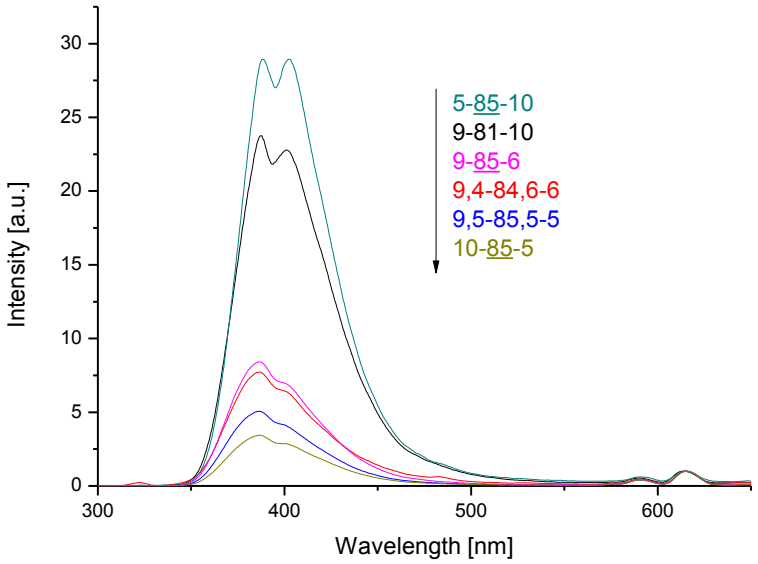

Figure 45: Emission spectra of the samples with different Al_2O_3 content (5 mol%, 6 mol% and 10 mol%) and either constant B_2O_3 amount or constant R-value (Na_2O/B_2O_3). The samples were melted for 1 hour at 1300 °C, quenched on air with no further heat-treatment. The excitation wavelength was 320 nm. All spectra were normalized to the value 1 for the Eu^{3+} maximum.

The plot of the Eu^{2+}/Eu^{3+} ratio in Figure 46 highlights the proportional dependence of the amount of Eu^{2+} ions on the Al_2O_3 content, although the compositions do not vary considerably.

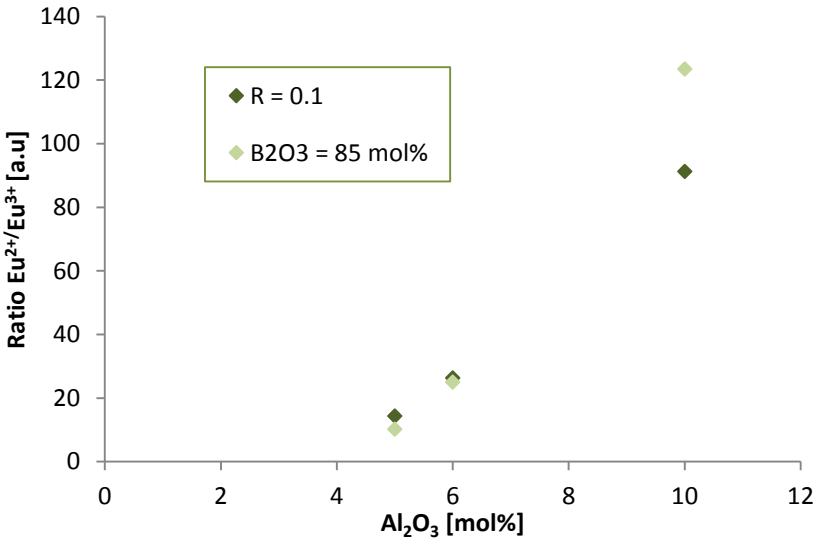

Figure 46: Ratio of the integrated Eu^{2+} peak and the integrated Eu^{3+} peak for the glass samples with different Al_2O_3 amount (5 mol%, 6 mol% and 10 mol%) and either constant R-value (Na_2O/B_2O_3) or constant B_2O_3 amount. The samples were melted for 1h at 1300 °C, quenched on air with no further heat-treatment. The peaks correspond to the original emission spectra (excitation wavelength: 320 nm) without normalized Eu^{3+} peak.

5.4 Europium as a structural probe in glass

5.4.1 Symmetry of surrounding

The ratio of the electric- dipole allowed transition $^5D_0 \rightarrow {}^7F_2$ (e) and the magnetic-dipole allowed transition $^5D_0 \rightarrow {}^7F_1$ (m) is a measure for the symmetry around the Eu^{3+} ion in the glass. [1] Therefore the fitted peaks (via *OriginLab software*) for the two transitions were integrated and their ratio demonstrates how the surrounding of the Eu^{3+} ion in the glass changes with different composition. The results for the two investigated glass families are plotted in Figure 47 and Figure 48.

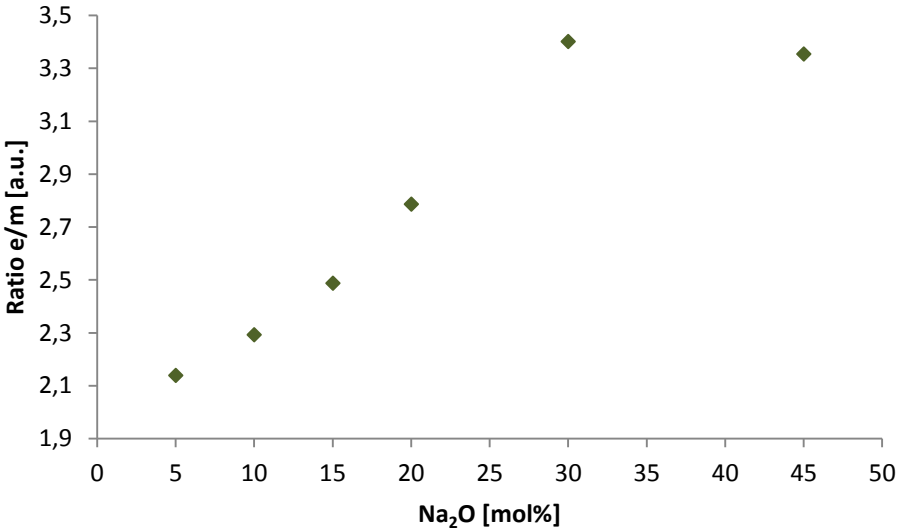

Figure 47: e/m ratio for the binary glass samples with different Na_2O amount.

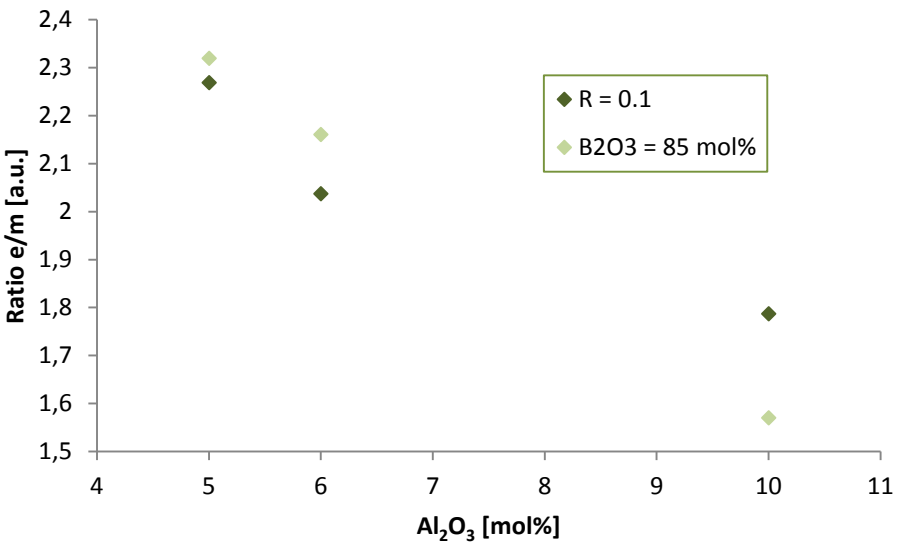

Figure 48: e/m ratio for the ternary glass samples with different Al_2O_3 content and either constant B_2O_3 amount or constant R-values (Na_2O/B_2O_3).

Since a lower e/m value means a more symmetric surrounding [1], the diagrams show that higher Na_2O amounts mean less symmetry around the Eu^{3+} ion whereas more Al_2O_3 amounts lead to higher local symmetry.

5.4.2 Nephelauxetic effect

To investigate the nephelauxetic effect in the binary and ternary glass samples the positions of the $^7F_0 \rightarrow {}^5D_0$ transition were analysed. The recorded transmission spectra were converted to absorbance spectra, smoothed ("Savitzky-Golay "method) and baseline corrected with the *OriginLab software*. The results are shown in the following figures.

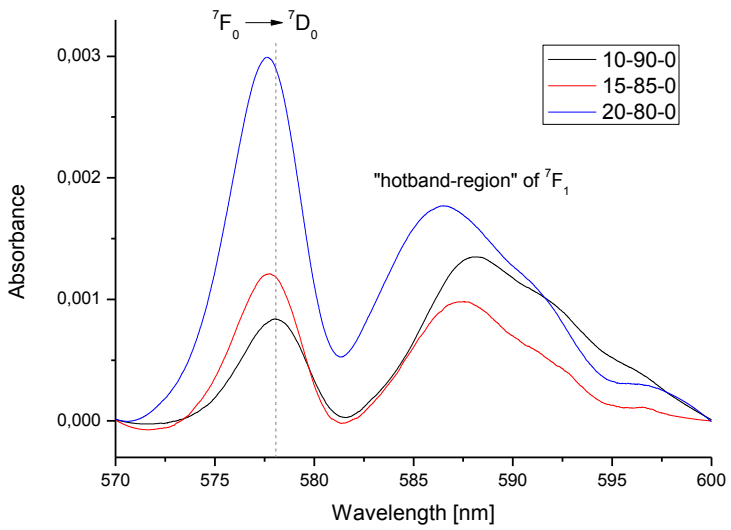

Figure 49: Absorbance spectra of three binary glass samples with a Na_2O amount of 10 mol%, 15 mol% and 20 mol%.

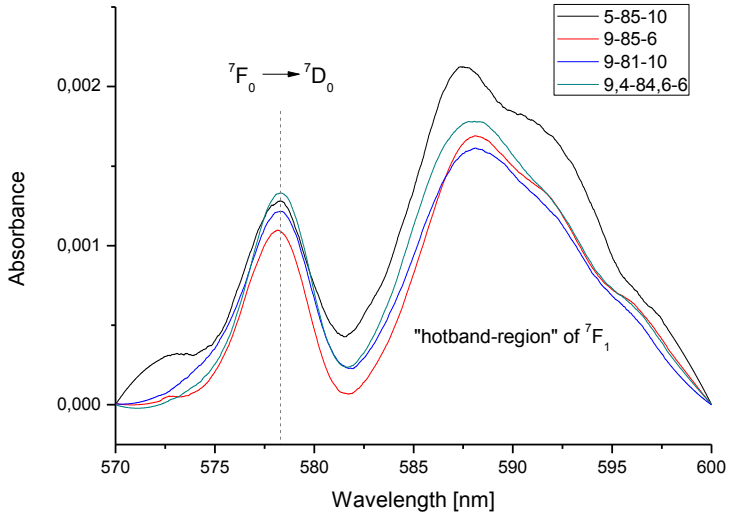

Figure 50: Absorbance spectra of four binary glass samples with an Al_2O_3 amount of 6 mol% and 10 mol% for either a constant B_2O_3 amount or a constant R-value (= Na_2O/B_2O_3).

From the spectra it can be seen that there is a shift of the $^7F_0 \rightarrow {}^5D_0$ transition to lower wavelengths and therefore to higher energies with increasing modifier amount for binary glasses, whereas there is no shift recognizable for the ternary glass samples. A lower energy of the 0 → 0 transition indicates a higher nephelauxetic effect with decreasing modifier amount. As a consequence the results show that there is a higher tendency towards

covalent interactions between the ligands and the Eu^{3+} ion with lower modifier amount in the binary glasses. This also means that the covalent character of the interaction seems to be favoured by polyborate groupings with high amount of BO_3 – units. The reason for the absence of a shift of the transition peaks in the ternary glass samples might be the more rigid structure of the network compared to binary glasses. [29,33]

5.5 Reabsorption mechanism

For one of the first experiments in this thesis emission spectra with different delay times were recorded (see section 4.2.1 table 7) to demonstrate the difference in the decay times for the emission of the Eu^{2+} and the Eu^{3+} ions. Hence either the integrated Eu^{2+} peaks or the integrated Eu^{3+} peaks were plotted versus the delay time. Then these curves were exponentially fitted (via *OriginLab software*) to determine the decay times (see Figure 51 and Figure 52).

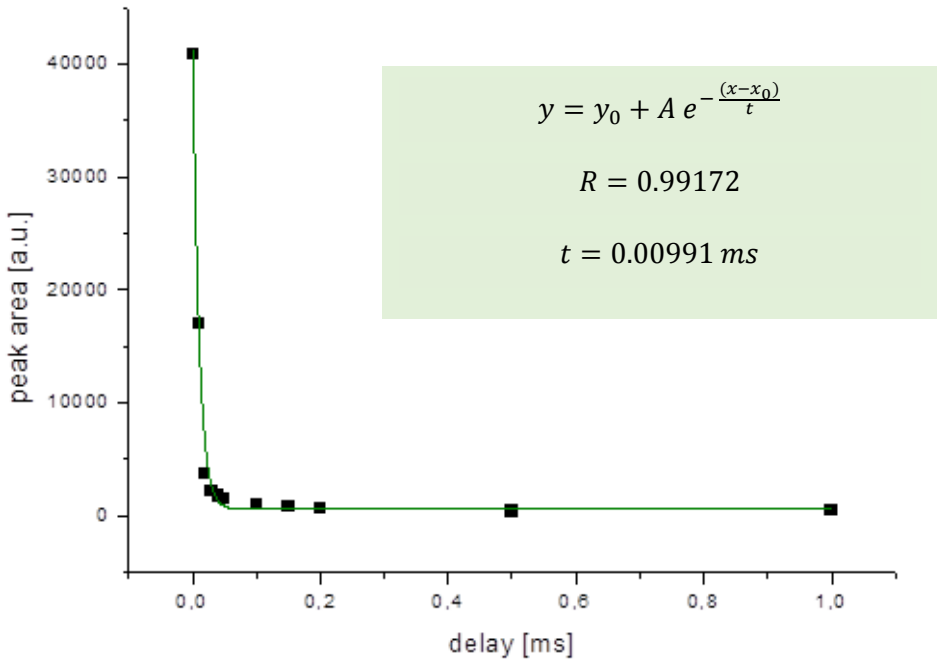

Figure 51: Plot of the integrated Eu^{2+} emission peaks measured at different delay times. The exponential curve for the fit and the calculated decay time are shown in the green box.

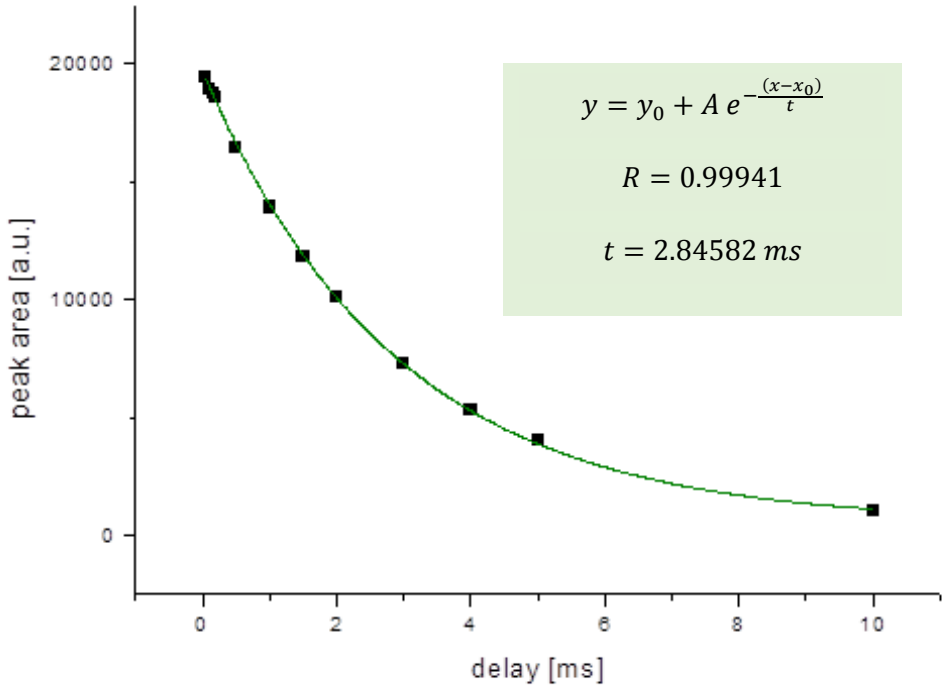

Figure 52: Plot of the integrated Eu^{3+} emission peaks measured at different delay times. The exponential curve for the fit and the calculated decay time are shown in the green box.

The curve of the Eu^{3+} emission had to be modified to get the right decay time, because the emission peaks first increase from 0.0 ms until 0.05 ms which is shown in the insert in Figure 53. The peak area only starts to decrease when the emission of Eu^{2+} is going to zero, which correlates to a delay time of 0.1 ms (see Figure 51). This fact delivered evidence that some kind of energy transfer takes place between the two Europium species in the prepared glass samples.

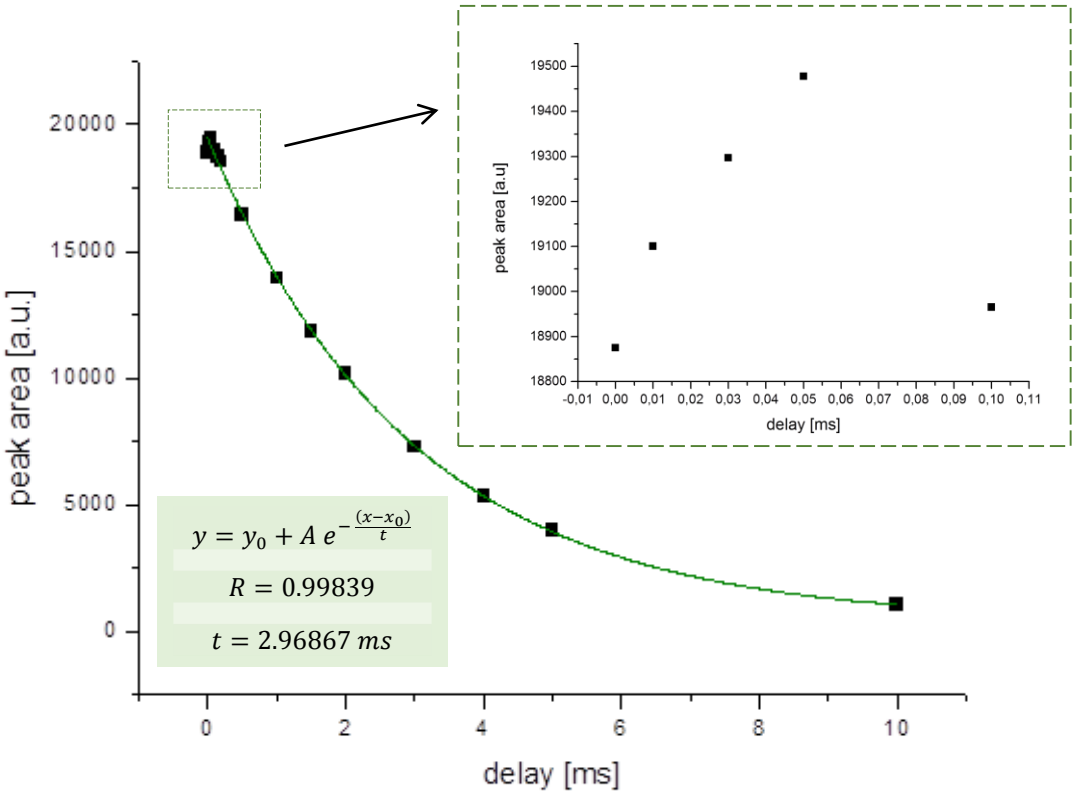

Figure 53: Plot of the integrated Eu^{3+} emission peaks measured at different delay times, including all measured values. The increment shows the peak areas for the delay times 0.0 ms, 0.01 ms, 0.03 ms, 0.05 ms and 0.1 ms. The exponential curve for the fit and the calculated decay time are shown in the green box.

During the investigations to elucidate the "self-reduction" mechanism an interesting phenomenon in the emission spectra was observed. In every emission peak of the Eu^{2+} ion a dip at the same wavelength was visible. Comparing these dips with the excitation spectrum of Eu^{3+} emission showed that the wavelength of the dip in the Eu^{2+} spectrum corresponds exactly to the maximum in the excitation spectrum of Eu^{3+}.

The emission spectra for all prepared glass series with different compositions and the related excitation spectrum of the Eu^{3+} emission are shown in Figure 54, Figure 55 and Figure 56.

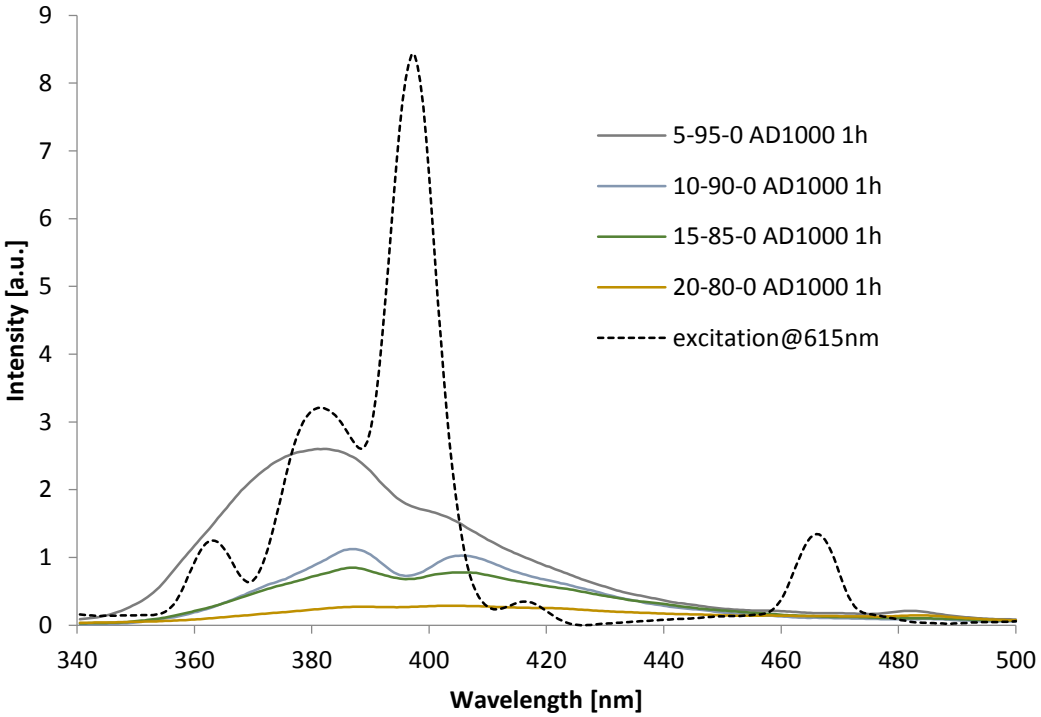

Figure 54: Emission spectra of the samples with different modifier content (solid lines) compared with the excitation spectrum at the maximum wavelength of the Eu^{3+}emission (dashed line). The excitation wavelength was 254 nm and the emission wavelength 615 nm.

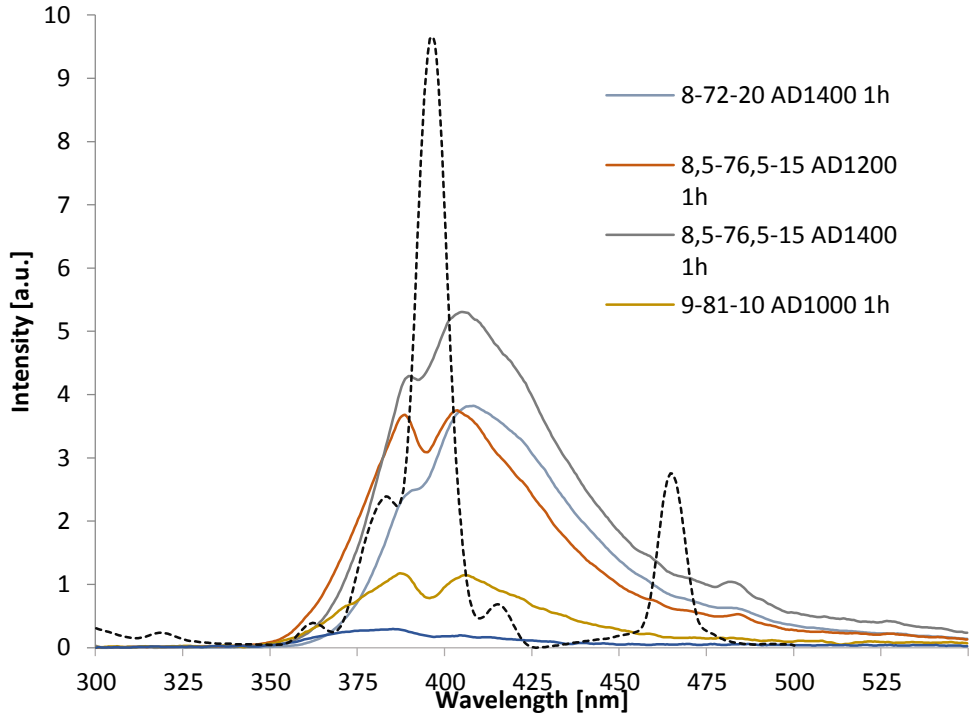

Figure 55: Emission spectra of the samples with different Al_2O_3 content (solid lines) compared with the excitation spectrum at the maximum wavelength of the Eu^{3+}emission (dashed line). The excitation wavelength was 254 nm and the emission wavelength 615 nm.

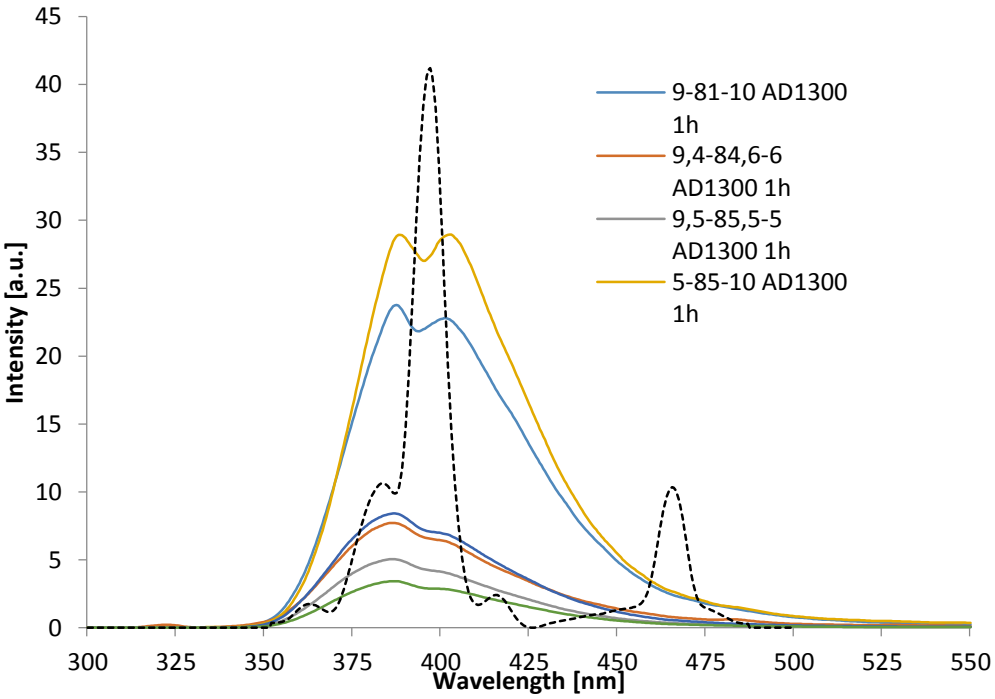

Figure 56: Emission spectra of the samples with different Al_2O_3 content and either constant B_2O_3 amount or constant R-value (=Na_2O/B_2O_3) (solid lines) compared with the excitation spectrum at the maximum wavelength of the Eu^{3+}emission (dashed line). The excitation wavelength was 320 nm and the emission wavelength 615 nm.

This indicates that a reabsorption mechanism takes place in the glass. When Eu^{2+} gets excited and relaxes to the ground state, part of the energy of the relaxation causes emission and the other part of the energy gets absorbed by the Eu^{3+} ion which gets excited and also relaxes radiative to the ground state. [40-44]

To proof the theory of the reabsorption mechanism luminescence spectra were recorded at wavelengths were only Eu^{2+} gets excited and Eu^{3+} does not. The excitation wavelength was chosen from the excitation spectra in Figure 57.

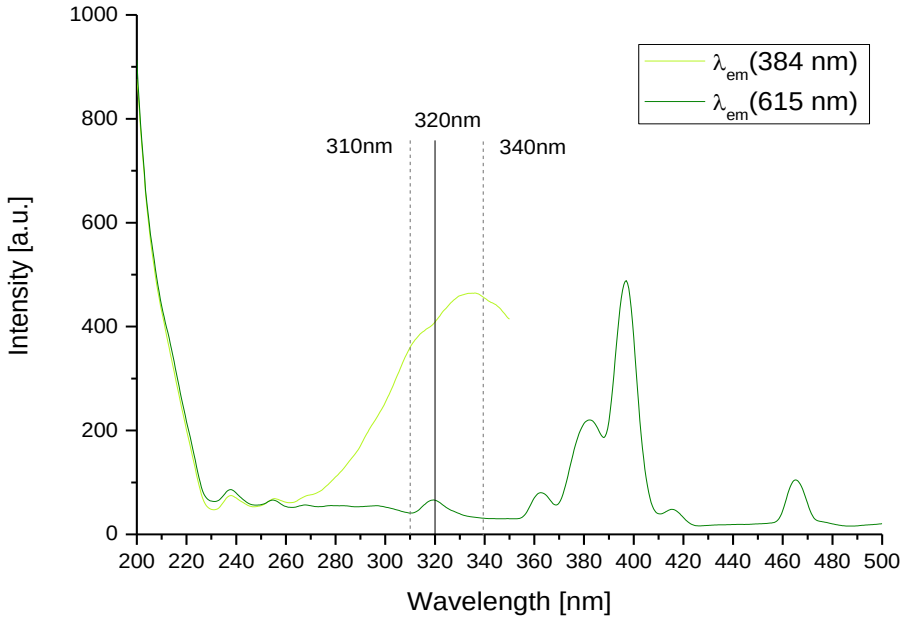

Figure 57: Comparison of the excitation spectra at the maximum of the Eu^{2+} emission (384 nm) and the Eu^{3+} emission (615 nm). The solid line marks the wavelength were both ions get excited and the dashed lines indicate were only Eu^{2+} gets excited. The excitation spectra of the glass 9-81-10 AD1000 2h were randomly picked from all excitation spectra recorded.

According to the excitation spectra the wavelengths 310 nm and 340 nm were picked for the emission spectra. The result in Figure 58 demonstrates clearly that the reabsorption process took place in the measured sample because an obvious Eu^{3+} peak is visible although only Eu^{2+} got excited. Therefore the energy must be provided from the Eu^{2+} ion while relaxing to the ground state.

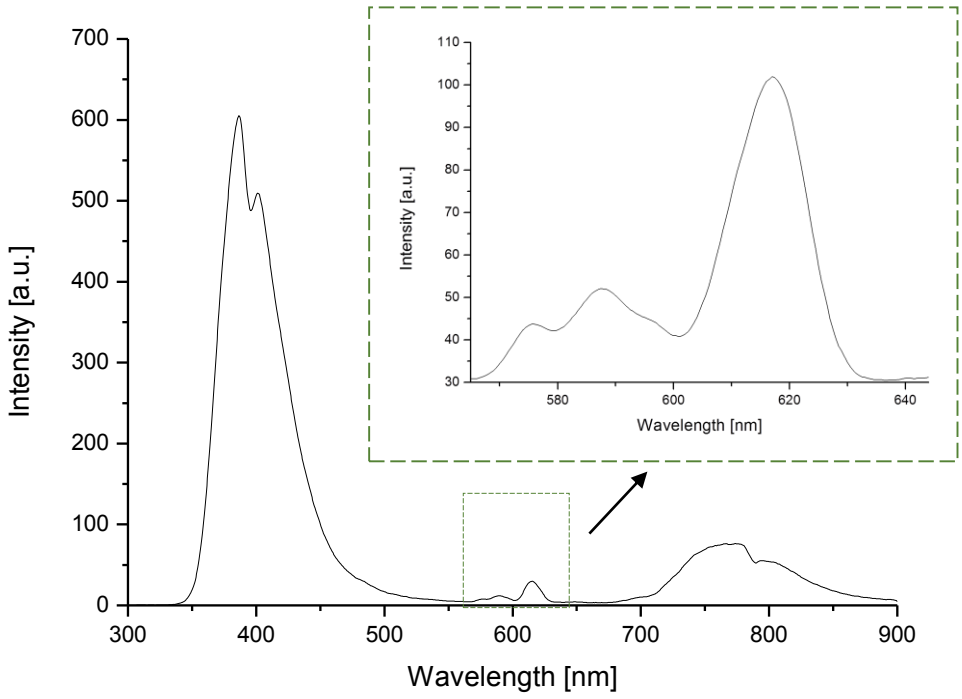

Figure 58: Emission spectrum of sample 9-81-10 AD1000 1h at an excitation wavelength of 310 nm. The increment shows the magnification of the Eu^{3+} peak. The dip in the Eu^{2+} peak is also visible.

The emission spectrum with an excitation wavelength of 340 nm also delivers evidence for a reabsorption mechanism but as the cut-off filter at 350 nm was not good enough to cut off all the excitation light a filter at 390 nm had to be used. This caused a virtual shift of the emission peak and a vanishing of the dip in the emission peak and is therefore not presented in this thesis.

5.6 Discussion

To elucidate the reason for the “self-reduction” mechanism in the investigated glass samples two main theories were considered as useful due to several references. [1-4,20,24,25] The first theory is based on the concept of the optical basicity by Duffy [45] the second theory involves the varying substructures in the glass according to the compositional change (see section 2). [20,21,25,46-48]

5.6.1 Optical basicity

One explanation for the "self-reduction" mechanism is the altered optical basicity of a glass system due to its composition. The theory claims that the higher the optical basicity of the glass the lower the reduction probability, because a higher basicity favours a higher positively charged ion. The concept of the optical basicity by Duffy considers the basicity as the electron donor power of the glass based on the concept of the Lewis acids and bases. An electron donation to an ion affects the optical spectra of the metal ions introduced into an oxidic medium and the optical basicity can be measured from the ratio of the red-shift via equation 1. Duffy investigated Tl^{+} and Pb^{2+} ions in sodium-borate-glasses (SBG) and in a CaO surrounding. Due to the higher electron donation power of CaO compared to the SBG the probe ions experience a higher red shift in the spectra than due to the lower electron donation power of the SBG. [45]

$$\Lambda = \frac{\upsilon_f - \upsilon}{\upsilon_f - \upsilon_{O^{2-}}} \qquad \textit{Equation 1}$$

Λ … *optical basicity*

υ … $UV\ absorption\ maximum$

υ_f … $^1S_0 \rightarrow {}^3P_1\ frequency\ in\ the\ gas\ phase$

$\upsilon_{O^{2-}}$ … $^1S_0 \rightarrow {}^3P_1\ frequency\ in\ CaO$

The optical basicity can directly be calculated from the UV absorption maximum with established values for υ_f and υ_{O2-}. [45]

For this study the theoretical optical basicity Λ_{th} of glass systems has been used to calculate the optical basicity in respect to the stoichiometry of the glass. It represents the average electron donor power of the medium. [45]

$$\Lambda_{th} = \chi_{AO_{a/2}} \Lambda\left(AO_{a/2}\right) + \chi_{BO_{b/2}} \Lambda\left(BO_{b/2}\right) + \cdots \qquad \textit{Equation 2}$$

$\Lambda\left(XO_{x/2}\right)$ … $optical\ basicity\ of\ oxides$

$\chi_{AO_{a/2}}$ … $equivalent\ fractions\ (proportion\ of\ oxygen\ atoms)$

An example for better understanding is shown below for the sample $10Na_2O - 90B_2O_3 - 0Al_2O_3$ [in mol%]:

$$\Lambda_{th} = \frac{10}{280} * 1.15 + \frac{270}{280} * 0.42 = 0.446$$

The values for the optical basicities were extracted from table 2 in paper [45].

Figure 59 compares the reduction probability and the optical basicity versus the modifier content in the glass.

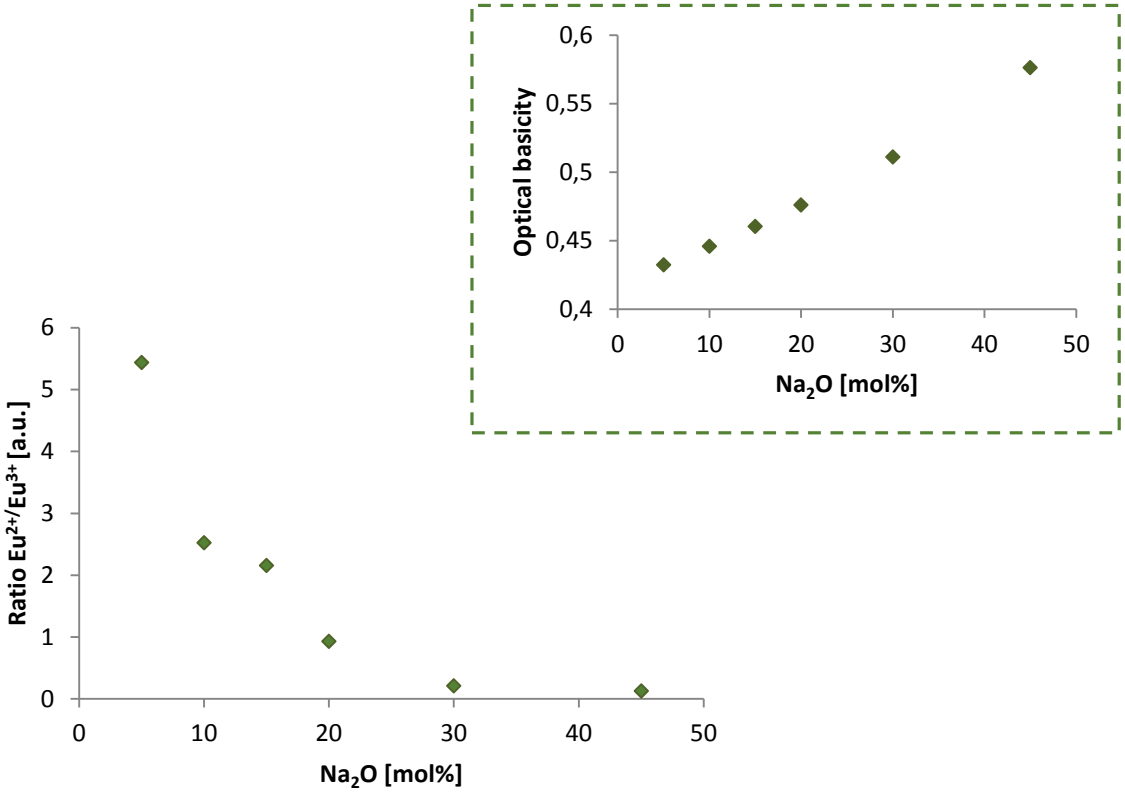

Figure 59: Ratio of the integrated Eu^{2+} peak and the integrated Eu^{3+} peak for the glass samples with different Na_2O content (5 mol%, 10 mol%, 15 mol%, 20 mol%, 30 mol% and 45 mol% Na_2O). All glasses were melted at 1000 °C for 1 hour and were quenched on air with no further heat treatment. The peaks correspond to the original emission spectra without normalized Eu^{3+} peak. The increment shows the optical basicity in dependence of the Na_2O content.

For the binary glass samples the theory that higher Na_2O content leads to an increase in the optical basicity and a decrease in the reduction probability in the glass could be more or less confirmed if one takes into account that there is a deviation from the linear Λ_{th} values to the experimental values for SBGs, which is assigned to the different types of sites in SBG. [45]

For the ternary glass samples, however, the trend only fits for the glass compositions with constant B_2O_3 content [4] while the samples with constant R-value exhibit a different correlation as shown in Figure 60.

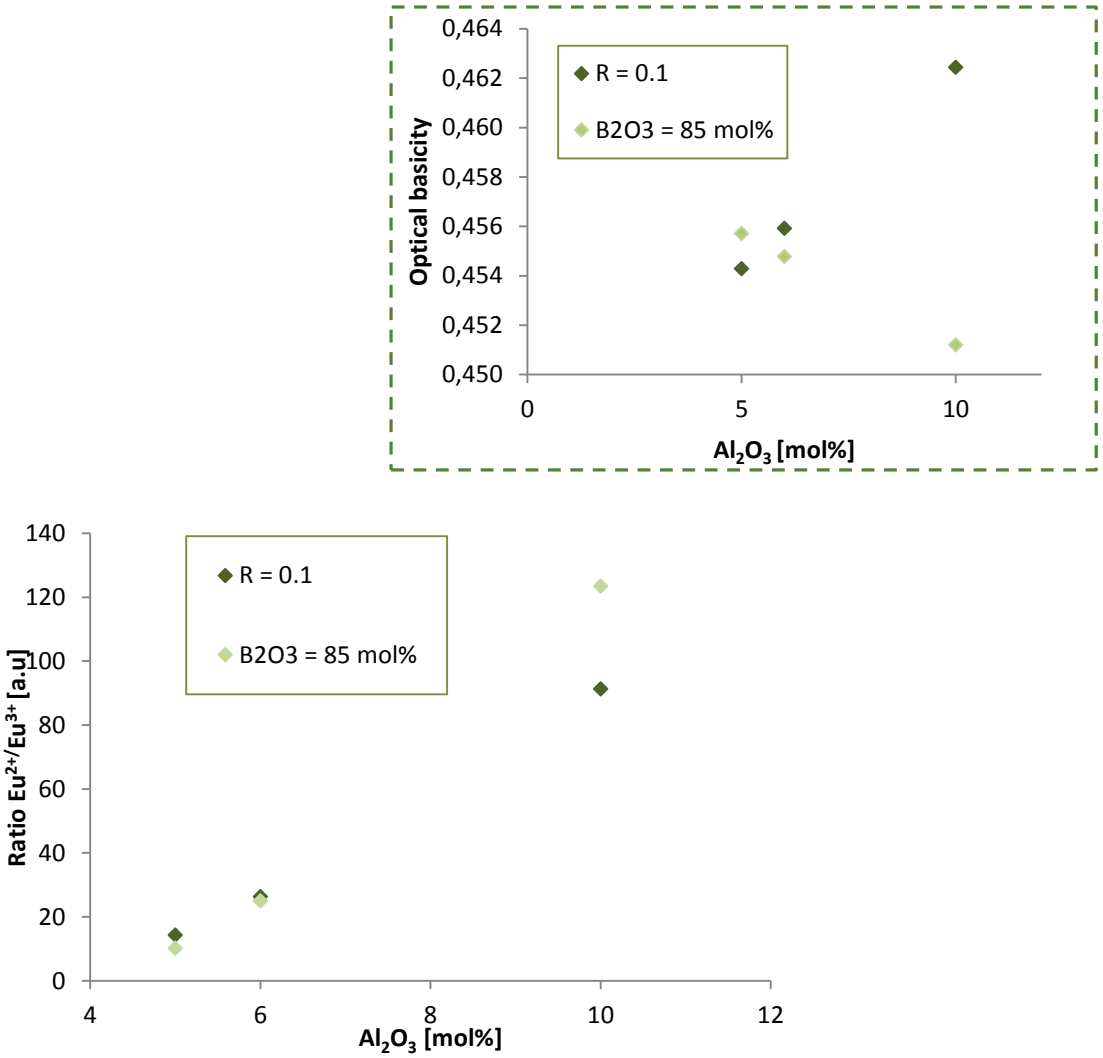

Figure 60: Ratio of the integrated Eu^{2+} peak and the integrated Eu^{3+} peak for the glass samples with different Al_2O_3 content (5 mol%, 6 mol% and 10 mol%) and either constant B_2O_3 amount or constant R-value (Na_2O/B_2O_3). Samples melted for 1 h at 1300 °C , quenched on air with no further heat-treatment. The peaks correspond to the original emission spectra without normalized Eu^{3+} peak. The increment shows the optical basicity in dependence of the Al_2O_3 content.

As for the ternary glass samples the trends run opposite for the two glass series, the optical basicity cannot be the only explanation for the reduction phenomenon in the glass. Therefore the second theory had to be examined closer.

5.6.2 Glass structure

As described in section 2 various models and literature exist on the structure of sodium-borate glasses. But to calculate the amount of BO_4-units in the prepared glass samples the equation proposed by Doweidar and co-workers [24] who referred to Kim and Bray [49] was used.

$$N_{4(B)} = (1 - 0.031\ y)M \qquad \textit{Equation 3}$$

$y \ldots Al_2\ O_3\ [mol\%]$

$M \ldots\ Na_2O/B_2O_3$

(M-value also written as R-value in this thesis)

Corresponding to this equation the following graphs were drawn and compared to the reduction probability in the investigated glass samples.

Additionally the e/m ratios are shown which indicate that the difference in symmetry also seems to depend on the ratio of BO_4/BO_3-units.

Binary glass

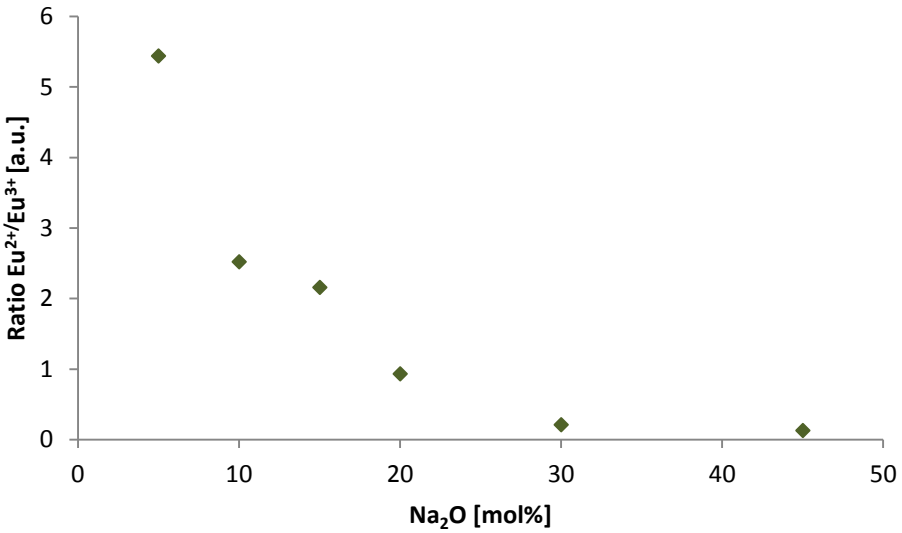

Figure 61: Ratio of the integrated Eu^{2+} peak and the integrated Eu^{3+} peak for the glass samples with different Na_2O content (5 mol%, 10 mol%, 15 mol%, 20 mol%, 30 mol% and 45 mol% Na_2O). All glasses were melted at 1000 °C for 1 hour and were quenched on air with no further heat treatment. The peaks correspond to the original emission spectra without normalized Eu^{3+} peak.

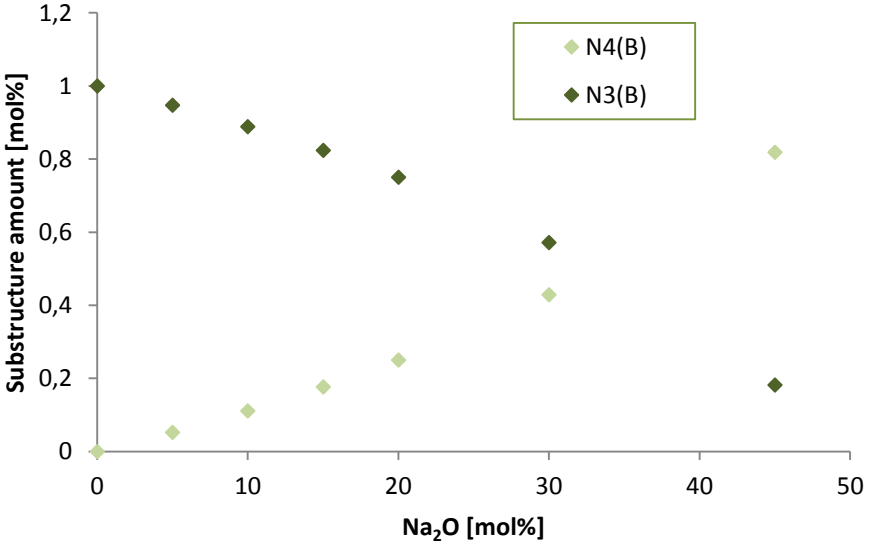

Figure 62: Amount of the BO_3- and BO_4-units as a function of the Na_2O content. Values were calculated with equation 3.

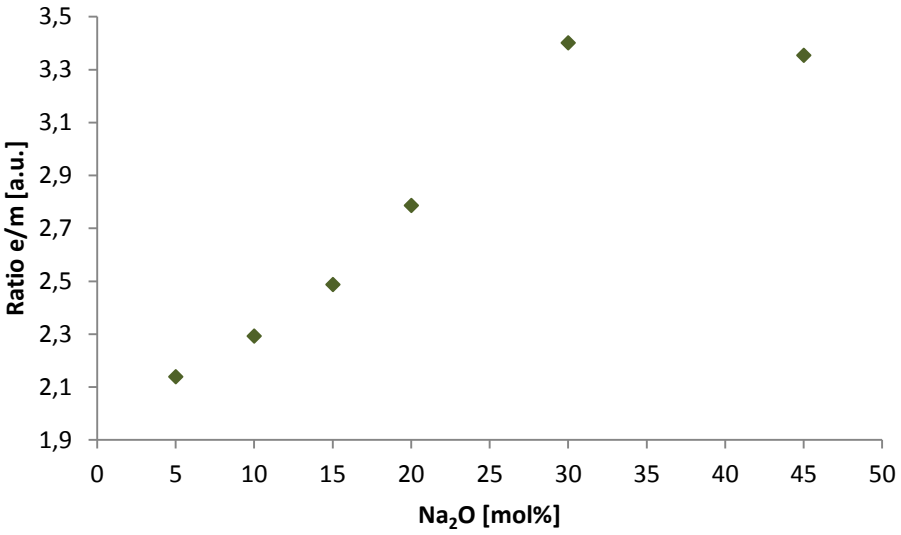

Figure 63: e/m ratio for the binary glass samples with different Na_2O amount.

Ternary glass

The ternary glass samples were plotted differently to demonstrate the influence of the structure more clearly.

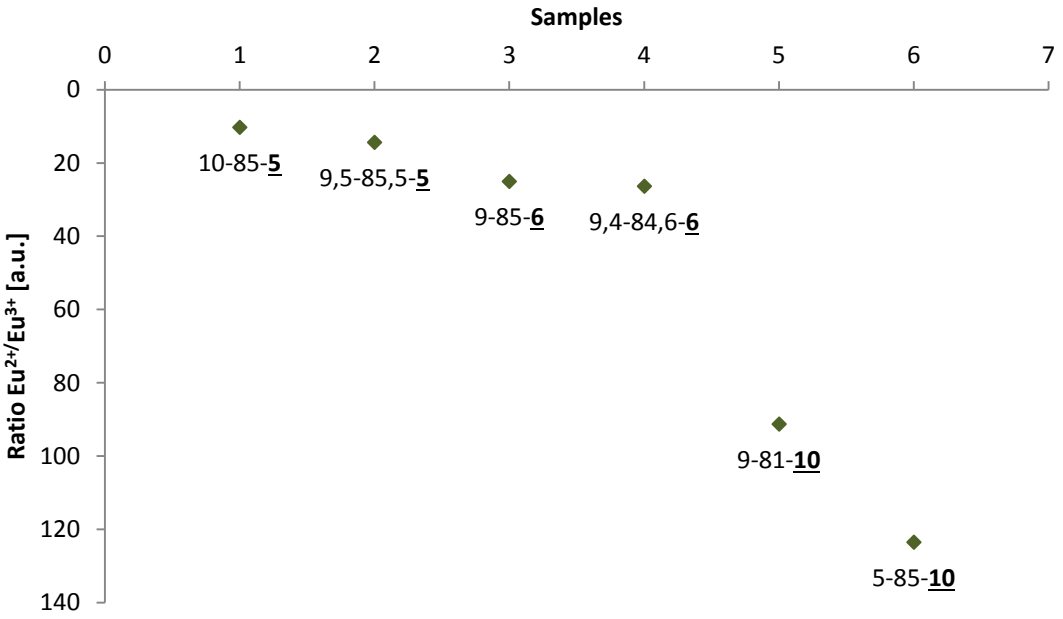

Figure 64: Ratio of the integrated Eu^{2+} peak and the integrated Eu^{3+} peak for the glass samples with different Al_2O_3 amount (5 mol%, 6 mol% and 10 mol%) and either constant R-value (Na_2O/B_2O_3) or constant B_2O_3 amount. The melting temperature was 1300 °C and the melting time 1 hour. All samples were quenched on air and had no further heat-treatment. The peaks correspond to the original emission spectrum (excitation wavelength: 320 nm) without normalized Eu^{3+} peak.

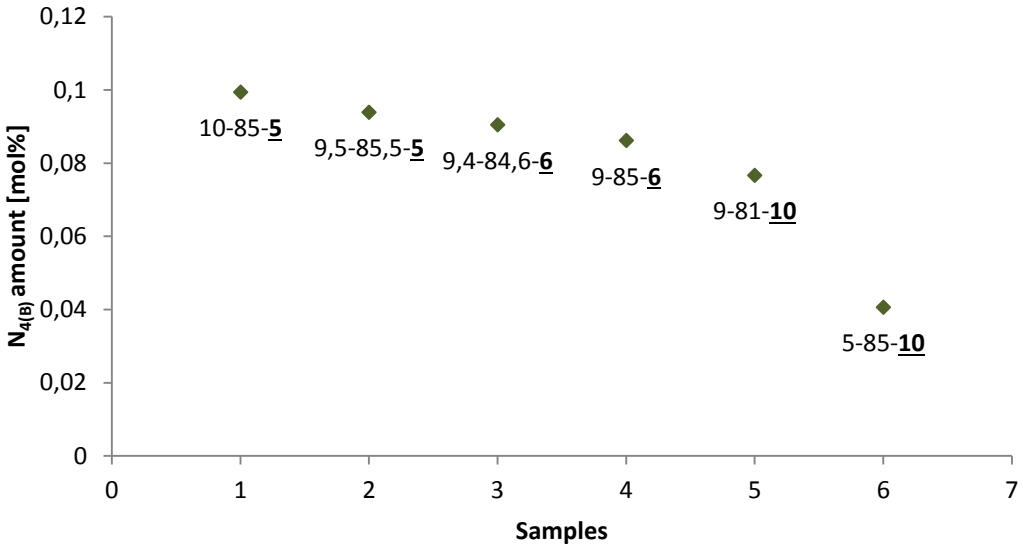

Figure 65: Amount of the BO_4- units as a function of the Al_2O_3 content. Values were calculated with equation 3.

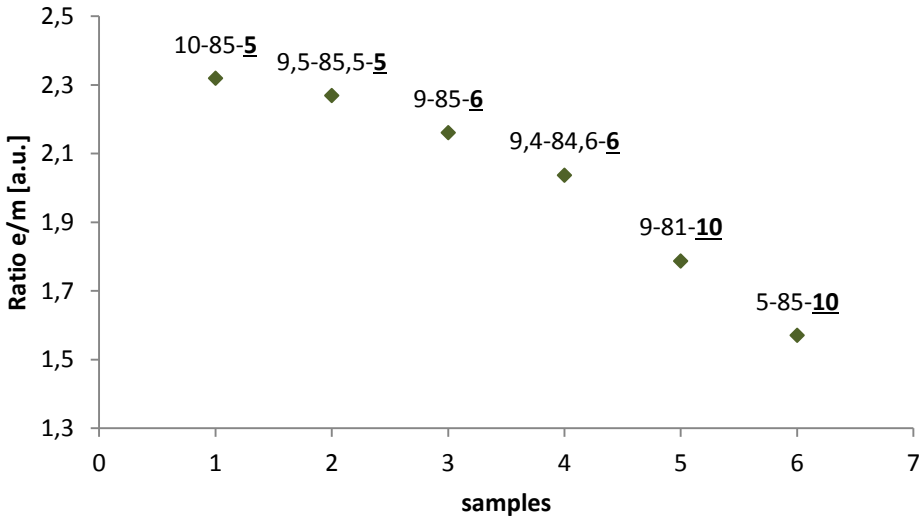

Figure 66: e/m ratio for ternary glass samples with different Al_2O_3 amount.

Comparison of all these trends makes it likely that the probability of the "self-reduction" process depends strongly on the structural changes in the glass. This means that the higher the amount of BO_3-units the higher the probability of a reduction of the ion. It also can be shown that BO_3-units create a more symmetric surrounding of the Eu^{3+} ion. This can be explained by the fact, that the NBOs of the BO_3-units are easier to direct to a symmetric surrounding than the more rigid BO_4 structure. The different possible explanations why the BO_3-units favour the reduction of the ions from Eu^{3+} to Eu^{2+} are discussed in the next section.

5.7 “Self-reduction” mechanism

Three main issues were considered to find a possible explanation for the “self-reduction” mechanism: The structure dependence, the influences of the preparation conditions and the lack of reproducibility.

As for the **structure dependence** two possible mechanisms were found which could explain the “self-reduction”.

One explanation includes ***NBOs*** which can only be formed by BO_3 - units in the glass. If in two neighboring sites two NBOs recombine with each other (four NBOs in total), four bridging BO_3-units are formed by releasing one oxygen molecule. The oxidation reaction of the oxygen ions to the evaporating oxygen molecule is linked to the reduction of four Europium ions.

Mechanism

$$4\ B\emptyset_2O^- + 4\ Eu^{3+} \rightarrow 4\ B\emptyset_3 + 4\ Eu^{2+} + O_2$$

Redox - Reaction

$$2\ O^{2-} \rightarrow O_2 + 4\ e^- \quad \text{(Oxidation)}$$

$$4\ Eu^{3+} + 4\ e^- \rightarrow 4\ Eu^{2+} \quad \text{(Reduction)}$$

The driving force for this mechanism may be the higher stability of the glass system due to the reduction of dangling bonds, the reduced sterical hindrance of the negative charged dangling bonds and the gain of energy due to the formation of the new bonds. But it also has to be considered that the positively charged sodium ions are no longer compensated in the glass because of the reduction of negatively charged NBOs and that the Krogh-Moe model predicts NBO - formation for binary glass not until a Na_2O content of 30 mol% is reached.

The second explanation comprises ***defects*** which occur in all real systems. These defects involve oxygen vacancies due to the lack of oxygen incorporation in the subunits of the glass. This means that either an oxygen atom of the modifier had not been incorporated correctly

into the glass or that oxygen evaporated during the heating and therefore there is a lack of oxygen in the system. [50-59]

This lack of oxygen plays a more important role if it occurs in BO_3- units than in BO_4-units because BO_4-units simply form BO_3-units ($B\emptyset_4 \rightarrow B\emptyset_3$) which do not change the stability significantly in glass systems. But if an oxygen atom is missing in a BO_3 unit ($B\emptyset_3 \rightarrow B\emptyset_2^+$) a positively charged boron ion is formed and then the system is not stable anymore and there have to be ways to compensate the oxygen loss.

Hypothetically possible reactions for these defect bindings are listed below. Except for the first reaction (defect ion and a NBO in the neighbourhood) every reaction needs oxygen to "repair" the binding. Since only one oxygen atom is necessary, the second oxygen (if the oxygen is derived from molecular oxygen of the atmosphere) reacts with another oxygen atom to form molecular oxygen again. The oxidation of the oxygen ions to molecular oxygen is then combined with a reduction of four Europium ions.

Mechanisms

$$B\emptyset_2^+ + B\emptyset_2O^- \rightarrow 2\ B\emptyset_3$$

$$B\emptyset_2^+ + B\emptyset_2^+ + 3\ O^{2-} + 4\ Eu^{3+} \rightarrow 2\ B\emptyset_3 + O_2 + 4\ Eu^{2+}$$

$$B\emptyset_2^+ + 3\ O^{2-} + 4\ Eu^{3+} \rightarrow B\emptyset_2O^- + O_2 + 4\ Eu^{2+}$$

$$B\emptyset_2^+ + B\emptyset_3 + 3\ O^{2-} + 4\ Eu^{3+} \rightarrow B\emptyset_3 + B\emptyset_4 + O_2 + 4\ Eu^{2+}$$

Redox - Reaction

$$2\ O^{2-} \rightarrow O_2 + 4\ e^- \quad \text{(Oxidation)}$$

$$4\ Eu^{3+} + 4\ e^- \rightarrow 4\ Eu^{2+} \quad \text{(Reduction)}$$

The driving force for this process is a gain in stability due to "repair" of the missing bond.

However, it is difficult to explain the **influence of the preparation conditions** consistent with these two theories.

One problem evolves from the contradiction between the results for the difference in the cooling rate (air and ice) and the time dependence. The results indicate that a higher cooling rate means less reduction in the glass. A possible explanation could be that the glass does not have enough time for the rearrangement. But this would also lead to a higher reduction probability with longer melting times, which is not the case because the results indicate a lower probability with increasing melting times.

The results of the post-heat-treatment of the samples are factored out because they show a "re-oxidation" of the Europium ions to Eu^{3+} after the reduction took place in the glass. Also the temperature dependence could not be discussed because no significant results were achieved.

The **lack of reproducibility** could already be seen from the measurements of the time and the temperature dependence. Additionally emission spectra (see Figure 67) of all prepared glass samples with the composition 10-90-0 AD1000 with a melting time of 1 hour were recorded with exactly the same parameters to check for the reproducibility. It was expected that all spectra would show the same characteristics.

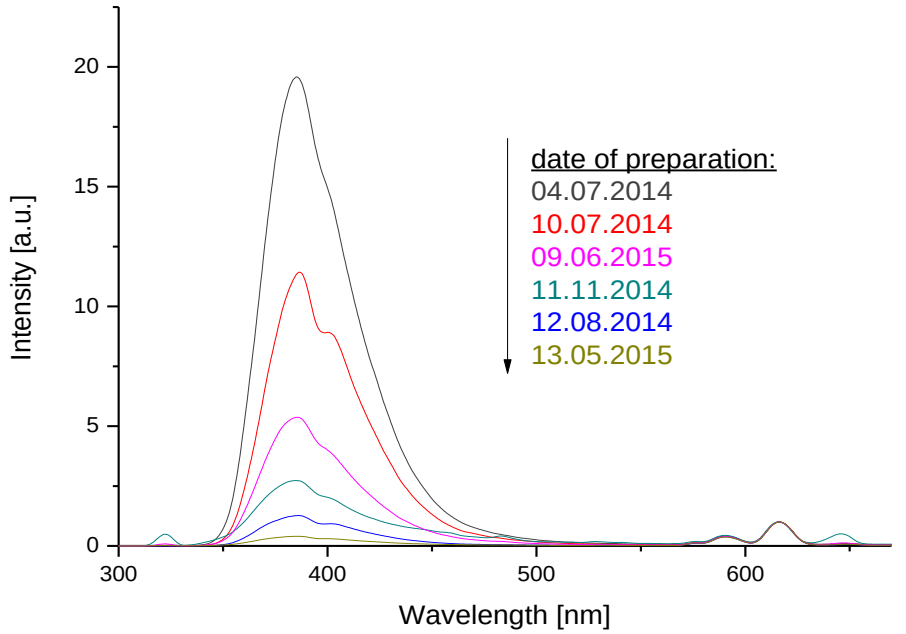

Figure 67: Emission spectra of the samples 10-90-0 AD1000 with a melting time of 1 h, prepared on different dates. The excitation wavelength was 320 nm. All spectra were normalized to the value 1 for the Eu^{3+} maximum.

The comparison of the spectra shows that the reproducibility is not even guaranteed if the composition, the preparation conditions and the measurement parameters are the same. This could be explained by both mechanisms. The probability that two NBOs recombine may depend on the statistical distribution of the NBOs in different sites. As for the defect theory the probability of the recombination reactions depends on many factors. Except for pure borate glass there are no compositions where only BO_3-units are created and therefore it cannot be predicted if the oxygen vacancy appears in a BO_4- or in a BO_3-unit. Additionally there may be at least one reaction where the “repair” of the binding does not lead to a reduction. As there are many other factors it is obvious that it is difficult to predict the reduction probability considering defects as initiating step. Another explanation for the missing reproducibility may be chemical composition deviations.

6 Conclusion and Outlook

The spectroscopic analysis of the Europium doped binary sodiumborate glasses and ternary sodium boroaluminate glasses with luminescence and absorption spectroscopy showed, that the preparation conditions as well as the composition of the glasses have significant influence on the “self-reduction” mechanism.

The investigation of the preparation conditions revealed that the variation of some parameters, e.g., melting time or cooling rate causes a change of the reduction probability in the glass. The obtained spectra indicated that the longer the melting time, the lower the reduction probability of Europium in the glasses. Experiments with different quenching methods (cooling on air and cooling on ice) made a comparison of different cooling rates possible. This led to the conclusion that faster cooling rates lower the reduction probability of the Europium ions. The experiments with different thermal post-treatment procedures showed that a subsequent annealing in the oven leads to an increase of Eu^{3+} ions. A possible explanation could be a “re-oxidation” of the ions in the glass when treated at temperatures in the range of the glass transition. A dependence on the melting temperature could not be proven in this thesis but there are reasons to suppose that there is a tendency towards higher reduction probability with lower temperature.

It is known, that the properties of binary sodiumborate and ternary sodium boroaluminate glasses change significant with a small change in composition. [15] In this thesis it could be seen, that there was also a significant change in the reduction probability in the glasses with changing composition. One explanation is the varying optical basicity of the glass for different compositions. While the trends for the binary glasses were in rather good agreement with this theory, experiments with ternary glass series showed that this theory could not be the only explanation, since most of the results deviated from the predicted trends. This led to the second explanation, involving the structural changes as a consequence of the compositional variation in the glass. Therefore the spectroscopic data from the experiments were compared to the structural information taken from literature. [20,21,24,25]

For both glass families (binary and ternary) it could be seen that a high amount of BO_3-units in the glass leads to a high reduction probability of the Europium ions. In the binary glasses

an addition of modifier leads to a transformation of BO_3-units to BO_4-units whereas in the ternary glasses the addition of Al_2O_3 leads to a higher amount of BO_3-units since the modifier is first consumed for the formation of AlO_4-units and the transformation of BO_3-units to BO_4-units only takes place if there is residual modifier left. [20,21,24,25] Apart from the calculation of the amount of BO_3-units in the glass samples, the BO_3/BO_4 ratio could also be estimated from the e/m - ratio and the according change of symmetry of the surrounding of the Europium ion.

Since for both glass families the same trend was found it is concluded that the main influence on the reduction probability for different compositions results from the structural changes in the glass matrix.

The exact mechanism for the “self-reduction” involving BO_3-units could not be elucidated completely in the frame of this thesis, but there two possible mechanisms are proposed: The involvement of NBOs, which can only be formed in BO_3-units, on the one hand and defects in the glass as driving force for the reduction on the other hand. However, none of these two theories could explain all phenomena found in this thesis consistently and it is therefore still not clear how the “self-reduction” mechanism works. But in any case it could be shown that for the mechanism the BO_3-units play an important role (composition dependence) and that it is rather likely that the reduction involves the formation of molecular oxygen (redox-couple). The results of this thesis also indicate that it is difficult to achieve a controlled reduction of the Europium ions in the glass samples without using a reducing atmosphere, as the reproducibility of the experiments could not be guaranteed.

For further investigations the exact chemical composition of the prepared and measured glass samples needs to be analyzed and measurement of the actual amount of BO_3/BO_4 - units compared to the calculated ones could also help to give information about the mechanism.

7 References

[1] Jiao, Q., Yu, X., Xu, X., Zhou, D., & Qiu, J. (2013). Phenomenon of Eu^{3+} self-reduction induced by B_2O_3 configuration structure in sodiumborate glasses. *Journal of Applied Physics*, *114*(4), 043107.

[2] Wang, C., Peng, M., Jiang, N., Jiang, X., Zhao, C., & Qiu, J. (2007). Tuning the Eu luminescence in glass materials synthesized in air by adjusting glass compositions. *Materials Letters*, *61*(17), 3608–3611.

[3] Zeng, H., Yang, Y., Lin, Z., Liang, X., Yuan, S., Chen, G., & Sun, L. (2011). The effect of B_2O_3 on the luminescent properties of Eu ion-doped aluminoborosilicate glasses. *Journal of Non-Crystalline Solids*, *357*(11-13), 2328–2331.

[4] Jiao, Q., Yu, X., Xu, X., Zhou, D., & Qiu, J. (2013). Relationship between Eu^{3+} reduction and glass polymeric structure in Al_2O_3 - modified borate glasses under air atmosphere. *Journal of Solid State Chemistry*, *202*, 65–69.

[5] Lv, T.-S., Xu, X.-H., Zhou, D.-C., Yu, H.-L., Qiu, J.-B. (2014). Efficient multi-wavelength-driven spectral conversion from ultraviolett to visible in transparent borosilicate glasses. *Ceramics International, 40*(8), Part A, 12367-12373.

[6] Liu, S., Zhao, G., Ruan, W., Yao, Z., Xie, T., Jin, J., Yin, H., Wang, J., & Han, G. (2008). Reduction of Eu^{3+} to Eu^{2+} in Aluminoborosilicate Glasses Prepared in Air. *Journal of the American Ceramic Society*, *91*(8), 2740–2742.

[7] Peng, M., & Hong, G. (2007). Reduction from Eu^{3+} to Eu^{2+} in $BaAl_2O_4$:Eu phosphor prepared in an oxidizing atmosphere and luminescent properties of $BaAl_2O_4$:Eu. *Journal of Luminescence*, *127*(2), 735–740

[8] Peng, M., Pei, Z., Hong, G., & Su, Q. (2003). Study on the reduction of $Eu^{3+}\rightarrow Eu^{2+}$ in $Sr_4Al_{14}O_{25}$: Eu prepared in air atmosphere. *Chemical Physics Letters*, *371*(1-2), 1–6.

[9] Fu, H., Qiao, X., Cui, S., Luo, Q., Qian, J., Fan, X., & Zhang, X. (2012). Tunable white light emission from glass-ceramics containing Eu^{2+}, Tb^{3+}, Eu^{3+} co-doped $SrLaF_5$ nanocrystals. *Materials Letters*, *71*, 15–17.

[10] Liu, Z., Chen, Q., Dai, N., Yu, Y., Yang, L., & Li, J. (2012). Tunable white light emitting glass suitable for long-wavelength ultraviolet excitation. *Journal of Non-Crystalline Solids, 358*, 3289-3293.

[11] Liu, J., Liang, K., Wu, Z.-C., Mei, Y.-M., Kuang, S.-P., & Li, D.-X. (2014). The reduction of Eu^{3+} to Eu^{2+} in a new orange–red emission Sr3P4O13: Eu phosphor prepared in air and its photoluminescence properties. *Ceramics International, 40*, 8827-8831.

[12] Zhang, J.-C., Long, Y.-Z., Zhang, H.-D., Sun, B., Han, W.-P., & Sun, X.-Y. (2014). Eu^{2+}/Eu^{3+}-emission-ratio-tunable $CaZr(PO_4)_2$:Eu phosphors synthesized in air atmosphere for potential white light-emitting deep UV LEDs. *Journal of Materials Chemistry C, 2*, 312.

[13] Riedel, E.; Anorganische Chemie. 6, 756ff, de Gruyter, Berlin, New York, 2004.

[14] Gatterer, K.; Scriptum: Solid State Spectroscopy. CHE.578., SS2013.

[15] Varshneya, A. K.; Fundamentals of Inorganic Glasses. Academic Press, Boston, San Diego, New York, London, Sydney, Tokyo, Toronto, 1994.

[16] García Solé, J., Bausá, L.E. & Jaque, D.; An Introduction to the Optical Spectroscopy of Inorganic Solids. 200ff, John Wiley & Sons, Ltd, England, 2005.

[17] Riedel, E.; Anorganische Chemie. 6, 538ff, de Gruyter, Berlin, New York, 2004.

[18] Varshneya, A. K.; Fundamentals of Inorganic Glasses. 30, Academic Press, Boston, San Diego, New York, London, Sydney, Tokyo, Toronto, 1994.

[19] Gatterer, K.; Habilitation treatise: Optical Spectroscopy of Rare-Earth Doped Oxide Glasses. 6ff, Faculty of Science and Technology, University of Technology, Graz, 1998.

[20] Kamitsos, E. I., & Chryssikos, G. D. (1991). Borate glass structure by Raman and infrared spectroscopies. *Journal of Molecular Structure*, *247*, 1–16.

[21] Bray, P.J., & O'Keefe, J.G. (1963). Nuclear magnetic resonance investigations of the structure of alkali borate glasses. *Physics and Chemistry of Glasses, 4*, 37.

[22] Gatterer, K.; Habilitation treatise: Optical Spectroscopy of Rare-Earth Doped Oxide Glasses. 13ff, Faculty of Science and Technology, University of Technology, Graz, 1998.

[23] Kuppinger, C.M., & Shelby, J.E. (1985). Viscosity and Thermal Expansion of Mixed-Alkali Sodium-Potassium Borate Glasses. *Journal of the American Ceramic Society,* 68, 463.

[24] Doweidar, H., Moustafa, Y. M., Abd El-Maksoud, S., & Silim, H. (2001). Properties of $Na_2O–Al_2O_3–B_2O_3$ glasses. *Materials Science and Engineering: A*, *301*(2), 207–212.

[25] Gresch, R., Müller-Warmuth, W., & Dutz, H. (1976). ^{11}B and ^{27}Al NMR studies of glasses in the system Na_2O-B_2O_3-Al_2O_3 (“NABAL”). *Journal of Non-Crystalline Solids, 21*, 31–40.

[26] Riedel, E.; Anorganische Chemie. 6, 652ff, de Gruyter, Berlin, New York, 2004.

[27] Hölsä, J. (2009). Persistent luminescence beats the afterglow: 400 years of persistent luminescence. *The Electrochemical Scociety Interface,* 42-45.

[28] Nazarov, M. & Noh, D.Y.; New Generation of Europium and Terbium Activated Phosphors from syntheses to application. 115ff, Pan Stanford Publishing, Singapore, 2012.

[29] Gatterer, K.; Habilitation treatise: Optical Spectroscopy of Rare-Earth Doped Oxide Glasses. 25ff, Faculty of Science and Technology, University of Technology, Graz, 1998.

[30] Judd, B.R., & Jørgensen, C.K. (1964). Hypersensitive pseudoquadruploe transition in lanthanindes. *Molecular Physics, 8,* 281.

[31] Gatterer, K.; Habilitation treatise: Optical Spectroscopy of Rare-Earth Doped Oxide Glasses. 28, Faculty of Science and Technology, University of Technology, Graz, 1998.

[32] Jørgensen, C.K. (1962). The Nephelauxetic Series. *Progress in Inorganic Chem*istry, *4*, 73.

[33] Gatterer, K., Pucker, G., & Fritzer, H.P. (1997). Structural information in the optical spectra of Eu^{3+} doped glasses from the ternary system Na_2O-B_2O_3-SiO_2. *Physics and Chemistry of Glasses, 38*(6), 293-299.

[34] Nelson, C., Furukawa, T., & White, W.B. (1983). Transition metal ions in glasses: Network modifiers or quasi-molecular complexes?. *Materials Research Bulletin, 18*, 959

[35] Sheng, K. C., & Korenowski, G. M. (1988). Laser-Induced Optical Emission Studies of Eu^{3+} Sites in Polycrystalline Powders of Monoclinic and Body-Centered Cubic Eu_20_3. *Journal of Physical Chemistry*, *1*(92), 50–56.

[36] Piskernik, M.; Project Lab Surface and Interface Technologies: Das Phänomen der Selbstreduktion von Eu^{3+} durch die Variierung des Borat-Gehaltes in Natriumboratglas. Institute of Physical and Theoretical Chemistry, University of Technology, Graz, 2014.

[37] LS55 User's Guide. 163ff, Perkin Elmer, Inc., United Kingdom, 2007.

[38] Hofer, J.; Diploma thesis: Fluorescence- and Reflection Spectroscopy of Industrially Relevant Minerals for Automatic Sensor Based Sorting Applications. Institute of Physical and Theoretical Chemistry, University of Technology, Graz, 2012.

[39] Hardware Guide: High-Performance Lambda Spectrometers, 27ff, Perkin Elmer, Inc., United Kingdom, 2011.

[40] Jun-Gill, K., Min-Kook, N., & Youngku, S. (2000). Luminescence from KCl co-doped with Eu^{2+} and Eu^{3+} ions. *J. Phys.: Condensed Matter*, *12*, 199–203.

[41] Jun-Gill, K., Jung, J.-S., Hong, J.-P., Won, S.-J., Sohn, Y., & Rhee, C. K. (2001). Spectral holes and induced luminescence in KCl co-doped with Eu^{2+} and Eu^{3+} ions. *J. Phys.: Condensed Matter*, *13*, 2835-2843.

[42] Kang, J.-G., Hong, J.-P., Won, S.-J., & Kim, C.-O. (2003). Photophysics of RbCl co-doped with Eu^{2+} and Eu^{3+} , *Journal of Physics and Chemistry of Solids 64*, 631–639.

[43] Biswas, K., Sontakke, A. D., Sen, R., & Annapurna, K. (2012). Luminescence properties of dual valence Eu doped nano-crystalline BaF_2 embedded glass-ceramics and observation of $Eu^{2+} \rightarrow Eu^{3+}$ energy transfer. *Journal of Fluorescence*, *22*(2), 745–752.

[44] Dai, W. B. (2014). Mechanism of the reduction and energy transfer between Eu^{2+} and Eu^{3+} in Eu-doped $CaAl_2Si_2O_8$ materials prepared in air. *Journal of Materials Chemistry C*, *2*, 3951.

[45] Duffy, J. A. (1993). A review of optical basicity and its applications to oxidic systems. *Geochimica et Cosmochimica Acta*, *57*(16), 3961–3970.

[46] Nassar, A.M., & Adawai, M.A. (1982). The Role , *21*, 31–40. The role of Al^{3+} ions in alumino borate glasses as revealed by molar volume, refractive index and microhardness, *Journal of Non-Crystalline Solids, 50,* 155-161

[47] Bunker, B. C., Kirkpatrick, R. J., & Brow, R. K. (1991). Local Structure of Alkaline-Earth Boroaluminate Crystals and Glasses: I, Crystal Chemical Concepts-Structural Predictions and Comparisons to Known Crystal Structures. *Journal of the American Ceramic Society*, *74*(6), 1425–1429.

[48] Bunker, B. C., Kirkpatrick, R. J., Brow, R. K., Turner, G. L., & Nelson, C. (1991). Local Structure of Alkaline-Earth Boroaluminate Crystals and Glasses: II, ^{11}B and ^{27}Al MAS NMR Spectroscopy of Alkaline-Earth Boroaluminate Glasses. *Journal of the American Ceramic Society*, *74*(6), 1430–1438.

[49] Kim, K.S., Bray, P.J. (1974). *Physics and Chemistry of Glasses, 15*, 47.

[50] Rao, K.J.; Structural Chemistry of Glasses. 1, Elsevier, Amsterdam, Boston, London, New York, Oxford, Paris, San Diego, San Francisco, Singapore, Sydney, Tokyo, 2002.

[51] Griscom, D. L. (1974). E.S.R. studies of radiation damage and structure in oxide glasses not containing transition group ions: A contemporary overview with illustrations from the alkali borate system. *Journal of Non-Crystalline Solids*, *13*(2), 251–285.

[52] Möncke, D., & Ehrt, L. (2004). Irradiation induced defects in glasses resulting in the photoionization of polyvalent dopants. *Optical Materials*, *25*, 425-437.

[53] Liang, H., Hanzawa, H., Horikawa, T., & Machida, K. (2008). Optical hole burning properties of europium-doped calcium bromide-based aluminoborate glasses. *Journal of Alloys and Compounds*, *457*(1-2), L6–L8.

[54] Machida, K., Ueda, D., Inoue, S., & Adachi, G. (1999). Structural modification-induced valence change of the europium ion doped in Barium Octaborate. *Electrochemical and Solid-State Letters*, *2*(11), 597-599.

[55] Hao, J., Gao, J., & Cocivera, M. (2003). Tuning of the blue emission from europium-doped alkaline earth chloroborate thin films activated in air. *Applied Physics Letters*, *82*(17), 2778-2780.

[56] Tikhomirov, V. K., Seddon, A. B., Furniss, D., & Ferrari, M. (2003). Intrinsic defects and glass stability in Er^{3+} doped TeO_2 glasses and the implications for Er^{3+}-doped tellurite fiber amplifiers. *Journal of Non-Crystalline Solids*, *326-327*, 296–300.

[57] Kawazoe, H. (1985). Effect of modes of glass-formation on structure of intrinsic or photon induced defects centered on III, IV or V cations in oxide glasses. *Journal of Non-Crystalline Solids*, *71*(1-3), 231–243.

[58] Kordas, G., Weeks, R. A., & Kinser, D. L. (1983). The influence of fusion temperature on the defect center concentration of GeO_2 glass. *Journal of Applied Physics*, *54*(9), 5394.

[59] Griscom, D.L. (1971). ESR studies of an intrinsic trapped-electron center in x-irradiated alkali borate glasses. *The Journal of Chemical Physics, 55*(3), 1113-1122.

8 List of Figures

Figure 1: Differences and similarities between crystal structure (left) and glass structure (right). [19] _____ *11*

Figure 2: Possible actions of the modifier (M_2O) in a glass network. Adopted from [19]. ___ *12*

Figure 3: Schematical drawing of polyborate groupings from left to right: boroxol ring, diborate and pentaborate. Adapted from [20,22]. _____ *13*

Figure 4: Polyborate subunits BO_3 (planar) and BO_4 (tetrahedral). _____ *14*

Figure 5: Predicted Krogh-Moe model (dashed line) and experimental data (solid line) for the structural dependence of the binary glasses on the alkali amount in mol%. [22,23] _____ *14*

Figure 6: Orbital graph of the $4f^6$ configuration of Eu^{3+}. _____ *19*

Figure 7: Emission spectra of Eu^{2+} (dashed line) and of Eu^{3+} (solid line). The spectra were recorded after excitation with 396 nm and have been arbitrarily picked from the produced glass samples. _____ *20*

Figure 8: Splitting of the 5d-energy levels of the Eu^{2+} ion with increasing crystal field strength Δ and its according emission (from left to right: UV, blue, green, red), adapted from [27]. _ *21*

Figure 9: Dieke diagram [26] with magnification of the Eu^{3+} ion and some important emission transitions, adapted from [29]. _____ *24*

Figure 10: Schematical drawing of the different possible incorporations of RE ions into a glass network. I) molecular complex, II) quasi-molecular complex, III) network modifier and IV) network former. Adopted from [29,34]. _____ *25*

Figure 11: Absorbance spectrum of crystalline Eu_2O_3 with magnification of the $^7F_0 \rightarrow {}^5D_0$ transition. _____ *27*

Figure 12: Absorbance spectrum of Eu_2O_3 incorporated in a ternary glass sample (9,4-84,6-6 AD1300) with magnification of the $^7F_0 \rightarrow {}^5D_0$ transition. _____ *28*

Figure 13: Picture of the oven with magnifications of the crucible and the copper mould. __ *31*

Figure 14: Ternary phase diagram with all glass sample compositions prepared in this thesis. _____ *34*

Figure 15: Picture of the LS55 with magnification of the specimen holder. _____ *35*

Figure 16: Screenshot of the manual control window of the LS55. _____ *36*

Figure 17: Picture of the L950 with the integrating sphere detector. The details show the opened sample chamber and a magnification of the specimen holder. _____ *41*
Figure 18: Screenshot of the control window of the L950. _____ *42*
Figure 19: Photos of the pure borate glass (0-100-0 AD1300) [left] and the crystals on the crucible for the ternary glass 8.5-76.5-15 AD1400 [right]. _____ *44*
Figure 20: XRD spectra of the samples 0-100-0 (left) and 1-99-0 (right). _____ *44*
Figure 21: XRD spectrum of the needles of the sample 8.5-76.5-15 AD1400 and a simulation of the crystal structure (red spheres: Oxygen, green spheres: Aluminium and orange spheres: Boron). _____ *45*
Figure 22: Glass samples with the composition 10-90-0 AD1000 and a melting time of 1 h, prepared with different quenching methods and post-treatments, photographed in daylight. The different preparation methods were, from left to right: AD, AA, AC, ID, IA, and IC. ____ *46*
Figure 23: Glass samples with the composition 10-90-0 AD1000 and a melting time of 1 h, prepared with different quenching methods and post-treatments, photographed under UV light with a wavelength of 365 nm. The different preparation methods were, from left to right: AD, AA, AC, ID, IA, and IC. _____ *46*
Figure 24: Glass samples with the composition 10-90-0 AD1000 and a melting time of 1 h, prepared with different quenching methods and post-treatments, photographed under UV light with a wavelength of 254 nm. The different preparation methods were, from left to right: AD, AA, AC, ID, IA, and IC. _____ *46*
Figure 25: Emission spectra of the samples 10-90-0, melted at 1000 °C with different quenching methods and post-treatments. The excitation wavelength was 320 nm. All spectra were normalized to the value 1 for the Eu^{3+} *maximum at 615 nm.* _____ *47*
Figure 26: Ratio of the integrated Eu^{2+} *peak and the integrated* Eu^{3+} *peak for the glass composition 10-90-0, melted at 1000 °C with different quenching methods and post-treatments. The peaks were integrated in the original emission spectra (excitation wavelength: 320 nm) without normalized* Eu^{3+} *peak.* _____ *48*
Figure 27: Emission spectra of the samples 10-90-0 AD1000 with melting times of 45 min, 1 h, 1 h 15 min and 2 h. The excitation wavelength was 254 nm. All spectra were normalized to the value 1 for the Eu^{3+} *maximum.* _____ *49*

Figure 28: Glass samples with the composition 10-90-0 AD1000 prepared with different melting times, photographed at daylight. Melting times were, from left to right: 30 min, 1h, 1 h 15 min, 1 h 30 min, 1 h 45 min and 2 h. _____ *49*

Figure 29: Glass samples with the composition 10-90-0 AD1000 prepared with different melting times, photographed under UV light with a wavelength of 365 nm. Melting times were, from left to right: 30 min, 1h, 1 h 15 min, 1 h 30 min, 1 h 45 min and 2 h. _____ *49*

Figure 30: Glass samples with the composition 10-90-0 AD1000 prepared with different melting times, photographed under UV light with a wavelength of 254 nm. Melting times were, from left to right: 30 min, 1h, 1 h 15 min, 1 h 30 min, 1 h 45 min and 2 h. _____ *50*

Figure 31: Emission spectra of the samples 10-90-0 AD1000 with melting times of 30 min, 1 h, 1 h 15 min, 1 h 30 min, 1 h 15 min and 2 h. The excitation wavelength was 320 nm. All spectra were normalized to the value 1 for the Eu^{3+} *maximum.* _____ *50*

Figure 32: Ratio of the integrated Eu^{2+} *peak and the integrated* Eu^{3+} *peak for the glass samples 10-90-0 AD1000 with melting times of 45 min, 1 h, 1 h 15 min and 2 h (2nd series) and melting times of 30 min, 1 h, 1 h 15 min, 1 h 30 min, 1 h 15 min and 2 h (3rd series). The peaks correspond to the original emission spectra without normalized* Eu^{3+} *peak.*_____ *51*

Figure 33: Ratio of the integrated Eu^{2+} *peak and the integrated* Eu^{3+} *peak for the glass samples 10-90-0 AD1000 and AD1300 with a melting time of 1 h. The peaks correspond to the original emission spectra without normalized* Eu^{3+} *peak.*_____ *51*

Figure 34: Glass samples with different amount of Na_2O*, melted at 1000 °C* for 1 h and quenched on air with no further heat treatment, photographed in daylight. The compositions were, from left to right: 0-100-0, 5-95-0, 10-90-0, 15-85-0, 20-80-0, 30-70-0 and 45-55-0. *0-100-0: after 1 h increase to 1200°C for 1 h.* _____ *52*

Figure 35: Glass samples with different amount of Na_2O*, melted at 1000 °C* for 1 h and quenched on air with no further heat treatment, photographed under UV light at a wavelength of 365 nm. The compositions were, from left to right: 0-100-0, 5-95-0, 10-90-0, 15-85-0, 20-80-0, 30-70-0 and 45-55-0. *0-100-0: after 1 h increase to 1200°C for 1 h.*____ *52*

Figure 36: Glass samples with different amount of Na_2O*, melted at 1000 °C* for 1 h and quenched on air with no further heat treatment, photographed under UV light at a wavelength of 254 nm. The compositions were, from left to right: 0-100-0, 5-95-0, 10-90-0, 15-85-0, 20-80-0, 30-70-0 and 45-55-0. *0-100-0: after 1 h increase to 1200°C for 1 h.*____ *52*

Figure 37: Emission spectra of the samples with different modifier content (5 mol%, 10 mol%, 15 mol%, 20 mol%, 30 mol% and 45 mol% Na_2O). All samples were melted at 1000 °C for 1 hour and were quenched on air with no further heat treatment. The excitation wavelength was 254 nm. All spectra were normalized to the value 1 for the Eu^{3+} maximum. _____ 53

Figure 38: Glass samples photographed in daylight. Top - from left to right: 10-90-0 AD1000 2 h, 9-81-10 AD1000 2 h, 8.5-76.5-15 AD1200 2 h and 8-72-20 AD1400 1 h 30 min. Bottom - from left to right: 10-90-0 AD1000 1 h, 9-81-10 AD1000 1 h, 8.5-76.5-15 AD1200 1 h, 8.5-76.5-15 AD1400 1 h and 8-72-20 AD1400 1 h. _____ 53

Figure 39: Glass samples photographed under UV light at a wavelength of 365 nm. Top - from left to right: 10-90-0 AD1000 2 h, 9-81-10 AD1000 2 h, 8.5-76.5-15 AD1200 2 h and 8-72-20 AD1400 1 h 30 min. Bottom - from left to right: 10-90-0 AD1000 1 h, 9-81-10 AD1000 1 h, 8.5-76.5-15 AD1200 1 h, 8.5-76.5-15 AD1400 1 h and 8-72-20 AD1400 1 h._____ 54

Figure 40: Glass samples photographed under UV light at a wavelength of 254 nm. Top - from left to right: 10-90-0 AD1000 2 h, 9-81-10 AD1000 2 h, 8.5-76.5-15 AD1200 2 h and 8-72-20 AD1400 1 h 30 min. Bottom - from left to right: 10-90-0 AD1000 1 h, 9-81-10 AD1000 1 h, 8.5-76.5-15 AD1200 1 h, 8.5-76.5-15 AD1400 1 h and 8-72-20 AD1400 1 h._____ 54

Figure 41: Emission spectra of the samples with different Al_2O_3 content (0 mol%, 10 mol%, 15 mol% and 20 mol%). The samples were melted for 1 hour and the melting temperatures varied with composition. The excitation wavelength was 254 nm. All spectra were normalized to the value 1 for the Eu^{3+} maximum. _____ 55

Figure 42: Glass samples with the following compositions, melted at 1300 °C for 1 h and quenched on air with no further heat treatment, were photographed in daylight. Top - from left to right: 9.5-85.5-5, 9.4-84.6-6 and 9-81-10. Bottom - from left to right: 10-85-5, 9-85-6 and 5-85-10. _____ 55

Figure 43: Glass samples with the following compositions, melted at 1300 °C for 1 h and quenched on air with no further heat treatment, were photographed under UV light at a wavelength of 365 nm. Top - from left to right: 9.5-85.5-5, 9.4-84.6-6 and 9-81-10. Bottom - from left to right: 10-85-5, 9-85-6 and 5-85-10._____ 56

Figure 44: Glass samples with the following compositions, melted at 1300 °C for 1 h and quenched on air with no further heat treatment, were photographed under UV light at a

wavelength of 254 nm. Top - from left to right: 9.5-85.5-5, 9.4-84.6-6 and 9-81-10. Bottom - from left to right: 10-85-5, 9-85-6 and 5-85-10. _____ *56*

Figure 45: Emission spectra of the samples with different Al_2O_3 content (5 mol%, 6 mol% and 10 mol%) and either constant B_2O_3 amount or constant R-value (Na_2O/B_2O_3). The samples were melted for 1 hour at 1300 °C, quenched on air with no further heat-treatment. The excitation wavelength was 320 nm. All spectra were normalized to the value 1 for the Eu^{3+} maximum. _____ *57*

Figure 46: Ratio of the integrated Eu^{2+} peak and the integrated Eu^{3+} peak for the glass samples with different Al_2O_3 amount (5 mol%, 6 mol% and 10 mol%) and either constant R-value (Na_2O/B_2O_3) or constant B_2O_3 amount. The samples were melted for 1h at 1300 °C, quenched on air with no further heat-treatment. The peaks correspond to the original emission spectra (excitation wavelength: 320 nm) without normalized Eu^{3+} peak. _____ *57*

Figure 47: e/m ratio for the binary glass samples with different Na_2O amount. _____ *58*

Figure 48: e/m ratio for the ternary glass samples with different Al_2O_3 content and either constant B_2O_3 amount or constant R-values (Na_2O/B_2O_3). _____ *59*

Figure 49: Absorbance spectra of three binary glass samples with a Na_2O amount of 10 mol%, 15 mol% and 20 mol%. _____ *60*

Figure 50: Absorbance spectra of four binary glass samples with an Al_2O_3 amount of 6 mol% and 10 mol% for either a constant B_2O_3 amount or a constant R-value (= Na_2O/B_2O_3). ____ *60*

Figure 51: Plot of the integrated Eu^{2+} emission peaks measured at different delay times. The exponential curve for the fit and the calculated decay time are shown in the green box. ___ *61*

Figure 52: Plot of the integrated Eu^{3+} emission peaks measured at different delay times. The exponential curve for the fit and the calculated decay time are shown in the green box. ___ *62*

Figure 53: Plot of the integrated Eu^{3+} emission peaks measured at different delay times, including all measured values. The increment shows the peak areas for the delay times 0.0 ms, 0.01 ms, 0.03 ms, 0.05 ms and 0.1 ms. The exponential curve for the fit and the calculated decay time are shown in the green box. _____ *63*

Figure 54: Emission spectra of the samples with different modifier content (solid lines) compared with the excitation spectrum at the maximum wavelength of the Eu^{3+}emission (dashed line). The excitation wavelength was 254 nm and the emission wavelength 615 nm. _____ *64*

Figure 55: Emission spectra of the samples with different Al_2O_3 content (solid lines) compared with the excitation spectrum at the maximum wavelength of the Eu^{3+}emission (dashed line). The excitation wavelength was 254 nm and the emission wavelength 615 nm. _____ *64*

Figure 56: Emission spectra of the samples with different Al_2O_3 content and either constant B_2O_3 amount or constant R-value (=Na_2O/B_2O_3) (solid lines) compared with the excitation spectrum at the maximum wavelength of the Eu^{3+}emission (dashed line). The excitation wavelength was 320 nm and the emission wavelength 615 nm. _____ *65*

Figure 57: Comparison of the excitation spectra at the maximum of the Eu^{2+} emission (384 nm) and the Eu^{3+} emission (615 nm). The solid line marks the wavelength were both ions get excited and the dashed lines indicate were only Eu^{2+} gets excited. The excitation spectra of the glass 9-81-10 AD1000 2h were randomly picked from all excitation spectra recorded. _ *66*

Figure 58: Emission spectrum of sample 9-81-10 AD1000 1h at an excitation wavelength of 310 nm. The increment shows the magnification of the Eu^{3+} peak. The dip in the Eu^{2+} peak is also visible. _____ *67*

Figure 59: Ratio of the integrated Eu^{2+} peak and the integrated Eu^{3+} peak for the glass samples with different Na_2O content (5 mol%, 10 mol%, 15 mol%, 20 mol%, 30 mol% and 45 mol% Na_2O). All glasses were melted at 1000 °C for 1 hour and were quenched on air with no further heat treatment. The peaks correspond to the original emission spectra without normalized Eu^{3+} peak. The increment shows the optical basicity in dependence of the Na_2O content. _____ *69*

Figure 60: Ratio of the integrated Eu^{2+} peak and the integrated Eu^{3+} peak for the glass samples with different Al_2O_3 content (5 mol%, 6 mol% and 10 mol%) and either constant B_2O_3 amount or constant R-value (Na_2O/B_2O_3). Samples melted for 1 h at 1300 °C , quenched on air with no further heat-treatment. The peaks correspond to the original emission spectra without normalized Eu^{3+} peak. The increment shows the optical basicity in dependence of the Al_2O_3 content. _____ *70*

Figure 61: Ratio of the integrated Eu^{2+} peak and the integrated Eu^{3+} peak for the glass samples with different Na_2O content (5 mol%, 10 mol%, 15 mol%, 20 mol%, 30 mol% and 45 mol% Na_2O). All glasses were melted at 1000 °C for 1 hour and were quenched on air with no further heat treatment. The peaks correspond to the original emission spectra without normalized Eu^{3+} peak. _____ *72*

Figure 62: Amount of the BO_3- and BO_4-units as a function of the Na_2O content. Values were calculated with equation 3. _____ *72*
Figure 63: e/m ratio for the binary glass samples with different Na_2O amount. _____ *73*
Figure 64: Ratio of the integrated Eu^{2+} peak and the integrated Eu^{3+} peak for the glass samples with different Al_2O_3 amount (5 mol%, 6 mol% and 10 mol%) and either constant R-value (Na_2O/B_2O_3) or constant B_2O_3 amount. The melting temperature was 1300 °C and the melting time 1 hour. All samples were quenched on air and had no further heat-treatment. The peaks correspond to the original emission spectrum (excitation wavelength: 320 nm) without normalized Eu^{3+} peak. _____ *73*
Figure 65: Amount of the BO_4- units as a function of the Al_2O_3 content. Values were calculated with equation 3. _____ *74*
Figure 66: e/m ratio for ternary glass samples with different Al_2O_3 amount. _____ *74*
Figure 67: Emission spectra of the samples 10-90-0 AD1000 with a melting time of 1 h, prepared on different dates. The excitation wavelength was 320 nm. All spectra were normalized to the value 1 for the Eu^{3+} maximum. _____ *77*

9 List of Tables

Table 1: Comparison of the two Europium ions with respect to their electron configuration, transition and ground state. _____ *22*

*Table 2: Temperature program for the glass production.*_____ *31*

Table 3: Preparation parameters for the binary glass production with different modifier content. _____ *32*

Table 4: Parameters for the measurement of binary glass samples with varying modifier content. _____ *38*

Table 5: Parameters for the first measurement of the ternary glass samples with varying Al_2O_3 amount (mol%). _____ *39*

Table 6: Parameters for the second measurement of the ternary glass samples with varying Al_2O_3 amount (mol%). _____ *39*

Table 7: Parameters for the measurement for the decay time (left) and for the reabsorption mechanism (right). _____ *40*

*Table 8: Parameters and wavelength range for the measurements of some binary and ternary glass samples.*_____ *43*

Table 9: Parameters and wavelength range for the measurements of crystalline Eu_2O_3. ___ *43*

10 Appendix

I) Tables of all prepared glass samples

amount	glass samples			comments
1	0-100-0	AD1200	1 h	
1	0-100-0	AA1200	1 h	
1	1-99-0	AD1400	1 h	45 min at 1300 °C and 30 min at 1400 °C
1	1-99-0	AA1400	1 h	45 min at 1300 °C and 30 min at 1400 °C
1	5-95-0	AD1000	1 h	
1	5-95-0	AA1000	1 h	
4	10-90-0	AD1000	1 h	
4	10-90-0	AA1000	1 h	
1	10-90-0	AC1000	1 h	
1	10-90-0	ID1000	1 h	
1	10-90-0	IA1000	1 h	
1	10-90-0	IC1000	1 h	
1	10-90-0	AD1200	2 h	1 h at 1000°C and 1 h at 1200 °C
1	10-90-0	AD1200	2 h	1 h at 1000°C and 1 h at 1200 °C
1	10-90-0	AC1200	2 h	1 h at 1000°C and 1 h at 1200 °C
1	10-90-0	AD1000	15 min	
2	10-90-0	AD1000	30 min	
2	10-90-0	AD1000	45 min	
2	10-90-0	AD1000	1 h 15 min	
1	10-90-0	AD1000	1 h 30 min	
1	10-90-0	AD1000	1 h 45 min	
3	10-90-0	AD1000	2 h	
1	15-85-0	AD1000	1 h	
1	15-85-0	AA1000	1 h	
1	20-80-0	AD1000	1 h	
1	20-80-0	AA1000	1 h	
1	30-70-0	AD1000	1 h	
1	30-70-0	AA1000	1 h	
1	45-55-0	AD1000	1 h	
1	45-55-0	AA1000	1 h	
1	45-55-0	AD1000	2 h	
1	45-55-0	AD1000	3 h	

amount	glass samples			comments
2	9-81-10	AD1000	1 h	
1	9-81-10	AA1000	1 h	
1	9-81-10	AC1000	1 h	
1	9-81-10	AD1000	2 h	
1	9-81-10	AA1000	2 h	
1	9-81-10	AC1000	2 h	
1	8,5-76,5-15	AD1200	1 h	30 min at 1000 °C and 1 h at 1200 °C
1	8,5-76,5-15	AA1200	1 h	30 min at 1000 °C and 1 h at 1200 °C
1	8,5-76,5-15	AC1200	1 h	30 min at 1000 °C and 1 h at 1200 °C
1	8,5-76,5-15	AD1200	2 h	30 min at 1000 °C and 2 h at 1200 °C
1	8,5-76,5-15	AA1200	2 h	30 min at 1000 °C and 2 h at 1200 °C
1	8,5-76,5-15	AC1200	2 h	30 min at 1000 °C and 2 h at 1200 °C
1	8,5-76,5-15	AD1400	1 h	
1	8-72-20	AD1400	1 h	
1	8-72-20	AD1400	1 h	
1	8-72-20	AC1400	1 h	
1	8-72-20	AD1400	1 h 30 min	
1	8-72-20	AD1400	1 h 30 min	
1	8-72-20	AC1400	1 h 30 min	
1	5-85-10	AD1000	1 h	
1	9,5-85,5-5	AD1000	1 h	
1	9,4-84,6-6	AD1000	1 h	
1	10-85-5	AD1000	1 h	
1	9-85-6	AD1000	1 h	

Sample code:

mol% Na_2O-mol% B_2O_3-mol% Al_2O_3_quenching_post-treatment_temperature_melting time

Example: 10-90-0 AD1000 1h

The glass with the composition: 10 mol% Na_2O, 90 mol% B_2O_3, 0 mol% Al_2O_3 and 0.5 mol% Eu_2O_3 was quenched on air with no further heat treatment. It has been melted at 1000 °C for 1 hour.

II) Original sample weights

sample name	m(Na_2CO_3) [g] *c*	m(Na_2CO_3) [g] *w*	m(B_2O_3) [g] *c*	m(B_2O_3) [g] *w*	m(Al_2O_3) [g] *c*	m(Al_2O_3) [g] *w*	m(Eu_2O_3) [g] *c*	m(Eu_2O_3) [g] *w*	glass [g]
quenching method & post-treatment variation									
10-90-0	6,0036	6,0039*	35,4924	35,4925*	0	0*	0,9968	0,9962*	40
time variation 1-3									
10-90-0	6,0036	6,004	35,4924	35,495	0	0	0,9968	0,997	40
10-90-0	6,0036	6,003	35,4924	35,493	0	0	0,9968	0,997	40
10-90-0	12,7578		75,4215		0		2,1181		85
temperature variation									
10-90-0	3,7523	3,7521	22,1828	22,1825	0	0	0,623	0,6232	25
Na_2O variation									
0-100-0	0	0*	19,527	19,507*	0	0*	0,493	0,4933*	20
1-99-0	0,2975	0,2975	19,3326	19,3328	0	0	0,4936	0,4935	20
5-95-0	1,4928	1,4921*	18,6313	18,6314*	0	0*	0,4957	0,4954*	20
15-85-0	4,5273	4,5274*	16,8515	16,8514*	0	0*	0,5011	0,5013*	20
20-80-0	6,0694	6,069*	15,947	15,9477*	0	0*	0,5038	0,503*	20
30-70-0	9,2047	9,2049*	14,108	14,1081*	0	0*	0,5094	0,5093*	20
45-55-0	28,08	28,0801*	22,5436	22,5436*	0	0*	1,036	1,0361*	40
Al_2O_3 variation 1 & 2									
10-90-0	6,0037	6,005	35,4925	35,493	0	0	0,9967	0,997	40
9-81-10	5,1613	5,164	30,5128	30,512	5,5169	5,515	0,9521	0,951	40
8,5-76,5-15	4,7678	4,7684	28,1865	28,1862	8,0941	8,0822	0,9312	0,9315	40
8-72-20	4,3912	4,3931	25,9599	25,9598	10,5609	10,5609	0,9113	0,9112	40
9,5-85,5-5	1,6719	1,6711	9,8837	9,8831	0,8465	0,8468	0,2922	0,292	12
9,4-84,6-6	1,6467	1,6467	9,735	9,735	1,0112	1,0111	0,2908	0,2904	12
10-85-5	1,7608	1,7605	9,8311	9,8311	0,8469	0,8468	0,2923	0,2924	12
9-85-6	1,576	1,576	9,777	9,7771	1,0107	1,0105	0,2907	0,2908	12
5-85-10	0,8567	0,8559	9,5663	9,5628	1,6483	1,646	0,2845	0,2847	12
9-81-10	1,5484	1,5472	9,1538	9,1545	1,6551	1,6561	0,2856	0,2858	12

c… calculated *w… weighed* **weighed by Gössler Ines Anna*

III) Measurement parameters: preparatory studies

quenching method & post-treatment variation

sample name(s): 10-90-0 **AD**1000 1h, 10-90-0 **AA**1000 1h, 10-90-0 **AC**1000 1h

10-90-0 **ID**1000 1h, 10-90-0 **IA**1000 1h, 10-90-0 **IC**1000 1h

fixed parameters: method – gate [ms] – delay [ms]:

phosphorescence - 0.4 - 0.0

varied parameters: λ_{exc} [nm] - detector gain [V] - $slit_{em}$ [nm]/ $slit_{exc}$ [nm]:

254 – 775 – 7/7

320 – 720 – 7/6

366 – 775 – 7/7

396 – 10/8

396 – 775 – 7/7

time variation

sample name(s): 10-90-0 AD1000 **15min**, 10-90-0 AD1000 **30min**, 10-90-0 AD1000 **45min**, 10-90-0 AD1000 **1h**, 10-90-0 AD1000 **1h15min**, 10-90-0 AD1000 **1h30min**, 10-90-0 AD1000 **1h45min**, 10-90-0 AD1000 **2h**

fixed parameters: method - $slit_{em}$ [nm] - $slit_{exc}$ [nm] - gate [ms] - delay [ms]:

phosphorescence - 7- 7 -0.4 - 0.0

varied parameters: λ_{exc} [nm] -detector gain [V]:

254 – 775

320 – 775

366 – 10/8

396 – 10/8

IV) Measurement conditions – XRD

Sample 0-100-0

Dataset Name	GAT_P0
File name	P:\ROENTGEN\XRD\GATTERER\GAT_P0.RAW
Comment	Scan Mode: Continuous scan mode
Measurement Date / Time	05.05.2015 08:57:32
Raw Data Origin	BRUKER-binary V4 (.RAW)
Scan Axis	Gonio
Start Position [°2Th.]	10,0000
End Position [°2Th.]	100,0000
Step Size [°2Th.]	0,0200
Scan Step Time [s]	191,0000
Measurement Temperature [°C]	25,00
Anode Material	Cu
K-Alpha1 [Å]	1,54060
K-Alpha2 [Å]	1,54443
K-Beta [Å]	1,39225
K-A2 / K-A1 Ratio	0,50000
Generator Settings	40 mA, 40 kV
Diffractometer Type	Theta/Theta

Sample 1-99-0

Dataset Name	GAT_P1
File name	P:\ROENTGEN\XRD\GATTERER\GAT_P1.RAW
Comment	Scan Mode: Continuous scan mode
Measurement Date / Time	05.05.2015 10:25:12
Raw Data Origin	BRUKER-binary V4 (.RAW)
Scan Axis	Gonio
Start Position [°2Th.]	10,0000
End Position [°2Th.]	100,0000
Step Size [°2Th.]	0,0200
Scan Step Time [s]	382,0000
Measurement Temperature [°C]	25,00
Anode Material	Cu
K-Alpha1 [Å]	1,54060
K-Alpha2 [Å]	1,54443
K-Beta [Å]	1,39225
K-A2 / K-A1 Ratio	0,50000
Generator Settings	40 mA, 40 kV
Diffractometer Type	Theta/Theta

Sample 8.5-76.5-15

Dataset Name	GATT20814
File name	P:\ROENTGEN\XRD\FAM\gatt14\GATT20814.raw
Comment	Scan Mode: Continuous scan mode
Measurement Date / Time	20.08.2014 15:10:40
Raw Data Origin	BRUKER-binary V4 (.RAW)
Scan Axis	Gonio
Start Position [°2Th.]	10,0000
End Position [°2Th.]	100,0000
Step Size [°2Th.]	0,0200
Scan Step Time [s]	382,0000
Scan Type	Pre-set time
Measurement Temperature [°C]	25,00
Anode Material	Cu
K-Alpha1 [Å]	1,54060
K-Alpha2 [Å]	1,54443
K-Beta [Å]	1,39225
K-A2 / K-A1 Ratio	0,50000
Generator Settings	40 mA, 40 kV
Diffractometer Type	Theta/Theta